Charge-Carrier Transport in Amorphous Organic Semiconductors

by

Benjie N. Limketkai

Submitted to the Department of Electrical Engineering and Computer Science

in partial fulfillment of the requirements for the degree of

Doctor of Philosophy

at the

MASSACHUSETTS INSTITUTE OF TECHNOLOGY

February 2008

© 2008 Massachusetts Institute of Technology. All rights reserved.

Signature of Author ....
Department of Electrical Engineer and Computer Science
January 11, 2008

Certified by ....
Marc A. Baldo
Professor of Electrical Engineering and Computer Science
Thesis Supervisor

Accepted by ....
Terry P. Orlando
Professor of Electrical Engineer and Computer Science
Chairman, Department Committee on Graduate Students

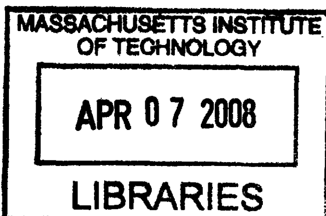

ARCHIVES

TABLE OF CONTENTS

Chapter 1 -- Introduction 7
1.1 Introduction 7
1.2 Charge-Carrier Transport in Organic Semiconductors 8
Chapter 2 – Localization and Transition Rates: From Microscopic to Macroscopic Models 11
2.1 Introduction 11
2.2 Density of States in Disordered Solids 11
2.2.1 Localized Band-tail States 11
2.2.2 Mott Transition 12
2.2.3 Anderson Transition 12
2.3 Localization and Hopping in Organic Semiconductors 13
2.3.1 Localization Due to Physical Disorder 13
2.3.2 Localization Due to Polarization 14
2.3.3 Hopping Activation Energy 15
2.4 Polaron Hopping and Marcus Electron Transfer 16
2.5 Non-Polaron Hopping Transport in Disordered Solids 16
2.5.1 Introduction 16
2.5.2 Master Equation of Hopping Kinetics 17
2.5.3 Resistor Network Models 18
2.5.4 Variable-Range Hopping (VRH) 20
2.5.5 Percolation Theory 21
2.5.6 Transport Energy Level Concept 26
Chapter 3 – Trapped-Charge-Limited Transport in Organic Semiconductors 29
3.1 Introduction 29
3.2 Transport in Organic Molecular Crystals 30
3.3 Trap-Free Space Charge Limited (SCL) Conduction 30
3.4 Trapped Charge Limited (TCL) Conduction 32
3.4.1 Introduction 32
3.4.2 Single Energy Level Trap 32
3.4.3 Exponential Distribution of Trap States 33
3.4.4 Gaussian Distribution of Trap States 34
Chapter 4 – Bulk-limited Transport in Amorphous Organic Semiconductors 35
4.1 Introduction 35
4.2 Time-of-Flight Measurement of Charge-Carrier Mobility 35
4.3 Temperature and Electric Field Dependences of Mobility 36
4.3.1 Introduction 36
4.3.2 Mobility Measurements 37
4.3.3 'Poole-Frenkel' Electric Field Dependence of Mobility 38
4.4 Models to Explain Temperature and Electric Field Dependences of Mobility ... 40
4.4.1 The Gaussian Disorder Model (GDM) 40
4.4.2 The Correlated Disorder Model (CDM) 42
4.4.3 Small Polaron Model 44
4.5 Charge-Carrier Density Dependence of Mobility 45
4.6 Models to Explain Charge-Carrier Density Dependence of Mobility 48

4.7 Model to Explain Combined Temperature, Field, and Density Dependences of Mobility 49
4.8 Doping Dependence of Mobility 50
4.9 Bulk-limited Current Conduction in Organic Semiconductors using Modified Temperature, Field, Density-Dependent Mobility Expression 52
4.9.1 Field-Dependent Mobility in SCLC 52
4.9.2 Charge-density Dependent Mobility in SCLC 53
4.9.3 Field and Charge-density Dependent Mobility in SCLC 54
Chapter 5 – Percolation Model for Bulk-limited Transport in Amorphous Organic Semiconductors 55
5.1 Introduction 55
5.2 Theory 56
5.2.1 Background 56
5.2.2 Zero-Field Limit 57
5.2.3 Zero-Temperature Limit 59
5.2.4 Non-Zero Temperature and Electric Field 60
5.3 Experiment 61
5.4 Conclusion 64
5.5 Discussion 65
Chapter 6 – Injection-limited Transport in Amorphous Organic Semiconductors 67
6.1 Introduction 67
6.2 Modeling Localization and Disorder for Injection 67
6.3 Interfacial Trap Model for Charge Injection 70
6.3.1 Introduction 70
6.3.2 Metal-Organic Interface 71
6.3.3 Interface Roughness and Polarization 72
6.3.4 Calculation of Current 76
6.3.5 Current-Voltage Measurements 78
6.3.6 Discussion 84
6.3.7 Conclusion 87
6.4 Injection and/or Bulk Limited Conduction 87
Chapter 7 – Cathode-Doping of Organic Semiconductors 89
7.1 Introduction 89
7.2 Experimental Results 93
7.3 Discussion 95
7.3.1 Cathode Metal Forms Interface Traps 95
7.3.2 Effect of Cathode-doped Charge on *J*-*V* Characteristics 96
7.4 Conclusion 99
Chapter 8 – Conclusion 100
8.1 Summary and Future Work 100
References 101

Charge-Carrier Transport in Amorphous Organic Semiconductors

by Benjie N. Limketkai

Submitted to the Department of Electrical Engineering and Computer Science
on January 11, 2008
in partial fulfillment of the requirements for the degree of
Doctor of Philosophy

Abstract

Since the first reports of efficient luminescence and absorption in organic semiconductors, organic light-emitting devices (OLEDs) and photovoltaics (OPVs) have attracted increasing interest. Organic semiconductors have proven to be a promising material set for novel optical and/or electrical devices. Not only do they have the advantage of tunable properties using chemistry, but organic semiconductors hold the potential of being fabricated cheaply with low temperature deposition on flexible plastic substrates, ink jet printing, or roll-to-roll manufacturing. These fabrication techniques are possible because organic semiconductors are composed of molecules weakly held together by van der Waals forces rather than covalent bonds. Van der Waals bonding eliminates the danger of dangling bond traps in amorphous or polycrystalline inorganic films, but results in narrower electronic bandwidths. Combined with spatial and energetic disorder due to weak intermolecular interactions, the small bandwidth leads to localization of charge carriers and electron-hole pairs, called excitons.

Thus, the charge-carrier mobility in organic semiconductors is generally much smaller than in their covalently-bonded, highly-ordered crystalline semiconductor counterparts. Indeed, one major barrier to the use of organic semiconductors is their poor charge transport characteristics. Yet this major component of the operation of disordered organic semiconductor devices remains incompletely understood.

This thesis analyzes charge transport and injection in organic semiconductor materials. A first-principles analytic theory that explains the current-voltage characteristics and charge-carrier mobility for different metal contacts and organic semiconductor materials over a wide range of temperatures, carrier densities, and electric field strengths will be developed. Most significantly, the theory will enable predictive models of organic semiconductor devices based on physical material parameters that may be determined by experimental measurements or quantum chemical simulations. Understanding charge transport and injection through these materials is crucial to enable the rational design for organic device applications, and also contributes to the general knowledge of the physics of materials characterized by charge localization and energetic disorder.

Thesis Supervisor: Marc A. Baldo
Title: Professor of Electrical Engineering

Acknowledgements

First and foremost, I give praise and thanks to the Lord God Almighty, for He is good; His love endures forever. In His great mercy and unfailing love, grace and peace has been given to us through faith in Christ Jesus. This faith is more precious than anything. The Lord is my strength and shield. My heart trusts in Him, and I am helped. My heart leaps for joy, and I am grateful and give thanks to Him forever...

I want to acknowledge my thesis supervisor, Professor Marc Baldo, for his guidance and instruction in conducting scientific research. I thank the Lord, for Marc helped me a lot to better understand the overall process of research and communication. I am thankful to both Marc and Professor Terry Orlando for supporting me in my graduate studies. Aside from being on my thesis committee, Professor Orlando was also my course advisor. He was always very friendly and taught and advised students very well. I want to thank Professor Vladimir Bulovic, who was on my thesis committee, for his motivating enthusiasm in our work and research in the field of organic semiconductors.

I thank Luke Theogarajan for being like a science mentor, who answered all sorts of questions ranging from physics to chemistry to circuits. The Lord blessed him with much knowledge in many different topics. I also want to acknowledge Kaveh Milaninia and Mihai Bora for all the helpful discussions during lunch and our coffee/tea breaks after lunch. Kaveh is a fabrication and experimentalist guru who provided technical advice and help. Mihai is analytic in everything, and so it was always insightful to talk to him, even about random things. And for all their help in various aspects of graduate school and lab work, I'd like to thank everybody else in the Soft Semiconductor group: Kemal Celebi, Mike Currie, Shlomy Goffri, Tim Heidel, Priya Jadhav, Jiye Lee, Jon Mapel, Carlijn Mulder, and Evan Moran. I also want to acknowledge the people in Professor Bulovic's LOOE (Laboratory of Organic Optoelectronics) group for all their help and for the collaboration between our two groups.

I want to thank Lakshminarayan Srinivasan for all the helpful discussions. And, I am thankful to my wife Lily, my parents, Benito and Thanh-Nhan Lim, and my siblings, Berkeley, Brian, Benson, and Benhan, for all their support in everything.

Chapter 1 – Introduction

1.1 Introduction

Organic semiconductors possess advantages over conventional inorganic semiconductors in certain large area applications, particularly in optoelectronic devices such as displays and solar cells. Yield concerns typically prohibit the fabrication of large area electronics on crystalline inorganic semiconductors. Polycrystalline and amorphous inorganic semiconductors possess defects at boundaries between crystalline grains. Defects degrade the electronic and optical properties and may be sources of instability if there are dangling bonds. In contrast, organic semiconductor devices exhibit good optical properties even when fabricated by low temperature deposition on flexible plastic substrates, ink jet printing, or roll-to-roll manufacturing.[1] These inexpensive fabrication techniques are possible because of the fundamental nature of the solid-state organic material, which is made up of isolated, individual molecules held together by weak van der Waals bonds. Unlike their inorganic counterparts, molecular solids are atomically ordered – there are no dangling bonds. But the weak intermolecular bonds exacerbate intermolecular disorder that acts to localize electronic states. Importantly, this preserves the optical properties of individual molecules in the solid state.

Electronic devices based on organic semiconductors, such as organic light-emitting diodes (OLED), photovoltaics (OPV), and thin film transistors (OTFT) have attracted considerable interest recently. But perhaps the first commercial use of organic semiconductors was their application as photoconductors on photocopier and laser printer drums. In early photocopiers, amorphous Selenium (*a*-Se) was used as the photoconductive material. Organic semiconductors were later used because they are non-toxic, inexpensive to coat on the drum, and have an easily controllable spectral response. But it was soon evident that that charge transport in organic semiconductors could not be explained by conventional models. The charge carrier mobility in organic semiconductors varies by orders of magnitude with changes in charge density, electric field or temperature. This realization initiated the field of charge transport in organic semiconductors. In the 1970's, work focused on photoconductive materials such as the

archetype molecularly-doped polymer: a donor-acceptor blend consisting of donor polyvinylcarbazole (PVK) and acceptor trinitrofluorenone (TNF). These disordered molecular-doped polymer films, used for xerography, were the first type of structures used for studying hopping transport in disordered organic systems.[2, 3] Although the early studies made significant progress, predictive models of the charge carrier mobility remained a distant goal – a situation that has continued to the present day.

1.2 Charge-Carrier Transport in Organic Semiconductors

Bulk organic semiconductors are macroscopic assemblies of molecules or polymer chains. The constituent molecular components are weakly held together by van der Waals forces. Consequently, they have narrower electronic bandwidths, and their charge carriers and electron-hole pairs, called excitons, are localized to a few molecules. Organic semiconductors are often highly disordered (both spatially and energetically), especially in the amorphous state, and hence, their charge-carrier mobility is smaller than their covalently-bonded, highly-ordered crystalline semiconductor counterparts. Due to the poor mobility, applications for organic semiconductors tend to exploit properties other than electrical conduction, such as strong optical properties and the feasibility of large-area fabrication.

A comparison of van der Waals bonded molecular crystals and covalent atomic crystals is shown in the table below, after Silinsh and Capek.[4]

Molecular Crystals	Covalent Crystals
Weak van der Waals intermolecular interactions ~10^{-3} – 10^{-2} eV	Strong covalently bonded interatomic interactions ~2 – 4 eV
Charge-carrier and exciton localization	Charge-carrier and exciton delocalization
Charge-carrier and exciton energies determined by many electron interactions (*e.g.*, polarization)	Single electron approximation
Charge-carriers and excitons treated as polaronic quasi particles	Charge-carriers are free electrons and holes
Low charge-carrier mobility ($\mu \approx 1$ cm^2/Vs); small mean free path (on the order of lattice constant) at room temperature	High charge-carrier mobility; long mean free path (100 – 1000 times lattice constant)
Large effective mass of charge-carriers (100 – 1000 times bigger than electron	Small effective mass (less than mass of electron)

mass)	
Hopping-type charge transport	Band-type charge transport
Frenkel excitons	Wannier excitons
Low melting and sublimination temperatures; low mechanical strength; high compressibility;	High melting and sublimination temperatures; high mechanical strength; low compressibility;

Table 1-1:[4] Comparison of properties of molecular and covalent crystals. After Silinsh and Capek (1994).[4]

Even though organic semiconductors are typically found in applications that do not require good electronic properties such as high charge carrier mobility, it is important to understand charge transport in organic semiconductors because it typically dominates the behavior of organic semiconductor devices. Models to explain current-voltage characteristics in organic semiconductor devices traditionally assume that conduction is either limited by injection or transport in the bulk.

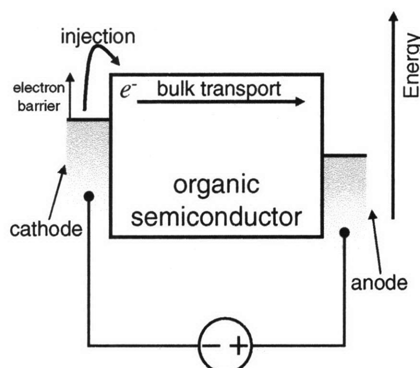

Figure 1-1: Total current is from the charge injection rate from metal contacts into organic semiconductor and the subsequent bulk transit to the other contact. Most models assume current is dominated by one of these two mechanisms.

Injection-limited models have conventionally been described under a tunneling[5, 6] or Richardson-Schottky thermionic emission[5] approach. Both models have been successfully employed for inorganic semiconductors. Tunneling and thermionic emission models have been applied analytically[7] and using Monte Carlo simulations[8, 9] to describe injection current in organic semiconductors.

Bulk transport models are based on the drift equation, $J = qn\mu F$, where $\mu = \mu(n, F, T)$. A space-charge limited current (SCLC) model for a perfect insulator with no intrinsic carriers or traps and a constant charge-carrier mobility obeys the Mott-Gurney equation.[10] One set of bulk-limited models concentrates on the charge-carrier density (*n*) dependence of the charge-carrier mobility. One type of '*n*-model' is the trap-charge limited conduction (TCLC) model,[11] which is a modification of the SCLC to include a trap distribution. A charge-density dependence arises because as the charge concentration is increased, the traps fill up to increase the density of available charge in the conduction band that can participate in current motion. A second set of bulk-limited models, the '*F*-models', seek to interpret experimental data in terms of an electric-field dependent charge-carrier mobility. Experimental studies of charge transport in organic semiconductors have observed that the electric field dependence of mobility follows an approximate Poole-Frenkel form, $\log\mu \sim \sqrt{F}$.[3] Experiments support both models.[12] However, it is difficult to explain the temperature, field, and charge density dependence of mobility with a unified theory.

To summarize, charge-carrier transport in organic semiconductors is still not fully understood. A comprehensive explanation for mobility and current-voltage characteristics is needed to optimize general device performance. Not only is a theory for charge transport in organic semiconductors essential to the rational design of these type of devices, it will also help contribute to the general understanding of the physics of materials characterized by charge localization and energetic disorder. This thesis will present a first-principles analytic theory that will give a unified description of the temperature, field, charge density, and material properties dependences of charge transport in solid-state organic semiconductors that can be successfully compared to experiment.

Chapter 2 – Localization and Transition Rates: From Microscopic to Macroscopic Models

2.1 Introduction

This chapter begins by defining charge carrier localization and we discuss its causes. Then, we discuss microscopic transition rates for charge-carriers moving within an organic semiconductor material lattice. A macroscopic resistor network[13] for current transport is then modeled based on the microscopic behavior.

2.2 Density of States in Disordered Solids

2.2.1 Localized Band-tail States

To describe the density of states in disordered solids, a simple model is used with the following Hamiltonian:[14, 15]

$$H = \sum_{j} E_j \left|\phi_j\right\rangle\left\langle\phi_j\right| + \sum_{j,k} \beta_{jk} \left|\phi_j\right\rangle\left\langle\phi_k\right| \tag{2.1}$$

where $\left|\phi_j\right\rangle$ is the electronic wavefunction at site j, E_j is the energy of site j, and β_{jk} is the interaction energy between sites j and k. In an ideal crystalline solid, where all the site energies are equal, the Hamiltonian describes a single band with abrupt band edges and bandwidth determined by the interaction energy β.[15] In a disordered solid, disorder can be modeled by assigning random site energies from a probability distribution function (assigning random values for the diagonal elements, E_j; hence, the name diagonal disorder). With the inclusion of disorder, the resulting DOS broadens and gains smooth band-tails at the band edges. The band-tail density of states for a d-dimensional disordered solid will be an exponential, $g(E) = A\exp\left[B\left(\pm\left(E_0^{\pm} - E\right)^{-d/2}\right)\right]$, for a probability distribution function, $P(E_j) = \frac{1}{2}\left[\delta(E_j - E_A) + \delta(E_j - E_B)\right]$.[14] This distribution function represents a uniformly random two-component (A,B) alloy (compositional disorder), where E_A and E_B are the ground state energies of the alloy

components A and B, respectively. An Anderson disorder model of a uniform probability distribution function, $P(E_j) = \frac{1}{W}\theta\left(\frac{W}{2} - |E_j|\right)$, where W is the width of the distribution and θ is a step function, also yields an exponential band-tail.[14] This probability distribution function could represent uniformly varying site energies arising from lattice disorder (structural disorder), where the range of perturbed energies is modeled to be limited by width W. Therefore, an exponential is commonly used to describe the band-tail distribution in disordered materials. Gaussians are also commonly used to represent random disorder.[3] Unfortunately, the actual density of states in organic semiconductors is difficult to measure. Exponential models of the density of states are commonly employed in analytic models, whereas Gaussian densities of states are more common in numerical models. In both cases, however, the width of the distribution is typically a fit parameter, and it is not certain whether the shape of the distribution is significant within the operating range of most organic semiconductor devices. Nevertheless, accurate measurements of the density of states remain an important unsolved problem for organic semiconductors.

2.2.2 Mott Transition

Various types of distribution functions modeling diagonal disorder in solids result in a band with band-tails. For charges in the middle of the band far above the band-tail states, the effect of disorder will be weak, and their electronic wavefunctions will not decay such that they are localized within a region of space. The states in the middle of the band are extended,[14] and the states in the band-tails are localized. Mott[16] introduced the concept of mobility edge, the energy level position that separates the localized states from the extended states. If the Fermi energy is below the mobility edge, the dc conductivity at $T = 0$ is zero. Once the Fermi energy passes the mobility edge, Mott[16] predicted a transition from an insulating to a metallic state (metal-insulator transition).

2.2.3 Anderson Transition

As the disorder is increased, the extended states near the band edge will start to localize and the mobility edges will move further up into the band. Once the disorder is

strong enough such that its width W exceeds the extended states bandwidth, the entire band will be localized. This transition from a metallic to an insulating system by increasing disorder is called an Anderson[17] transition. Amorphous organic semiconductors are believed to have large enough disorder that all the states are localized.

2.3 Localization and Hopping in Organic Semiconductors

2.3.1 Localization Due to Physical Disorder

Organic semiconductor films possess various morphologies that all have some degree of disorder, with amorphous films being the most disordered and molecular crystals the most ordered. All organic semiconductors are characterized by weak van der Waals bonding, which gives them weak intermolecular interactions. This weak coupling of molecules results in weak interaction energy β to give narrow electronic bandwidths. For disordered amorphous films, where there is weak conformational, morphological, and molecular order, there will be dispersion in energy levels of the constituent organic molecules. This statistical variation of width W in the energy level distribution of the molecules will overcome the already narrow electronic bands to create Anderson charge localization.[17]

There are several possible physical causes for the energetic disorder in bulk amorphous films. One source is the random orientation of molecular dipoles in spatially and geometrically disordered molecular films. The energy of a charged molecule in a lattice of polar molecules will be affected by the surrounding dipole interactions. In a physically disordered lattice, the polar molecules are randomly oriented, and charges on different molecule locations will see different surrounding dipole orientations, and consequently have different energies.

Following the work of Young,[18] consider a charge sitting on a site in a simple cubic lattice with lattice spacing a_0. The site energies around the charge are located at $a_0\mathbf{n}$, where $\mathbf{n} = i\mathbf{i} + j\mathbf{j} + k\mathbf{k}$ and $\mathbf{i}$, $\mathbf{j}$, and $\mathbf{k}$ are the unit lattice vectors. Each lattice point has a probability f of having a point dipole p. The energy contributed from the dipole on lattice point n is:[1]

$$e_n = -\frac{qp}{4\pi\varepsilon a_0^2}\frac{\hat{\mathbf{n}}\cdot\hat{\mathbf{p}}}{n^2} \tag{2.2}$$

The total energy affecting a charge by the surrounding dipoles is $E = \sum_n e_n$. Assuming that the average energy from the dipole interactions is zero, the variance in energy with isotropic and uncorrelated dipole moments is:[1]

$$\langle E^2 \rangle = \sum_{n,n'} \langle e_n e_{n'} \rangle = \sum_n \langle e_n^2 \rangle = \sum_n \frac{q^2 p^2}{16\pi^2 \varepsilon^2 a_0^4} \frac{\langle (\hat{\mathbf{n}}\cdot\hat{\mathbf{p}})^2 \rangle}{n^4} f \tag{2.3}$$

The variance in the energetic dipole disorder is then:[18]

$$\sigma^2 = \frac{1}{3} f \frac{q^2 p^2}{16\pi^2 \varepsilon^2 a_0^4} \sum_n \frac{1}{n^4} \approx \frac{1}{3} f \frac{q^2 p^2}{16\pi^2 \varepsilon^2 a_0^4} (16.5323) \tag{2.4}$$

For Alq_3 with a dipole moment of p = 5.3 Debye, the standard deviation of the dipole disorder is σ = 0.13 eV. This disorder width W of 0.13 eV will be sufficient to create localization. The higher order moments make minor corrections but the second order moment is dominant, giving an approximate Gaussian distribution of energy states due to dipole moment disorder.[18] The higher order moments do affect the tail of the distribution and a simple Gaussian DOS may not be accurate in heavily dipolar amorphous materials.[18-22]

2.3.2 Localization Due to Polarization

However, localization does not only occur due to the physical disorder that is present in amorphous films but it can also manifest itself even in well-ordered molecular crystals due to polarization. According to the Born-Oppenheimer approximation, the electronic wavefunction responds instantaneously to changes in nuclear coordinates. Therefore, any nuclear rearrangement due to polarization or temperature must be considered because it affects the electronic wavefunction. The localization time is defined as the length of time a charge resides at a particular site. It is dependent on the physical disorder, average interaction energy β, and other parameters that may influence a charge to hop out of a site, such as the electric field and temperature. Anderson[17] concluded that at zero applied electric field and zero temperature, if the localization condition is satisfied, the charge will remain at the lattice site for infinite time. The different polarization

effects (electronic, molecular, lattice polarization) will influence charge hopping if they occur on times scales shorter than the localization time of the charge.[4] The electronic polarization time is significant because the rearrangement of the electronic wavefunctions is relatively instantaneous. The molecular and lattice polarization occurs on much slower time scales and are comparable to localization time of the carriers if the interaction energy $\beta < 0.1$ eV.[1]

The polarization effects can overcome the weak intermolecular energy to distort the molecular lattice. This rearrangement of the surrounding molecules lowers the energy of the charged molecule. The energy required to remove this excess charge will then exceed the nearest neighbor interaction energy, which leads to self-trapping, or self-localization.[4, 23] If these molecular conformation energy changes are a significant contribution to the total activation energy barrier for escape, then not only should the single carrier be considered in a model of charge transport but the surrounding polarized molecules must be considered as well. The motion of the charge and its surrounding polarization is then treated as a quasi-particle known as a polaron.[1]

2.3.3 Hopping Activation Energy

The effect of localization is that the mean free path of charges is typically of the order of the spacing between adjacent molecular sites, and charges moving through the disordered lattice are scattered at each molecular site.[4] The charge transport mechanism is therefore hopping of charge carriers from one localized state to another within a lattice of molecular sites. Hopping transport is a thermally activated process, where the activation energy, or energy difference of the charge at the initial and final localized state, is determined by two factors. The first is the statistical variation in site energies due to the physical disorder of the organic material, where there is variation in lattice energy contribution to each site because of intermolecular spacing disorder. The second is intramolecular conformational energy changes due to polarization of a charge to the surrounding molecules.[3] If localization is dominated by molecular conformational changes, then charge transfer is thermally activated with an activation energy that is dependent on the active molecular deformations. These models are known as polaron

models. Often, however, energetic disorder is more important in creating localization, and many models only consider static energetic disorder influence on activation energy.

2.4 Polaron Hopping and Marcus Electron Transfer

The charge and its associated polarization cloud are collectively called a polaron, and the properties of this quasi-particle polaron are conserved as the polaron moves through the lattice. The size of the polarization cloud is dependent on the strength of localization and interaction energy. Holstein[24, 25] considered the motion of a polaron in a lattice where the intermolecular overlap between sites is on the order of or less than the activation energy required for a charge to move to another lattice site. This small-polaron model[24-26] is analogous to Marcus theory[27, 28] of charge transfer between adjacent donor and acceptor molecules. Marcus theory deals with the charge transfer mechanism in solution, where reorganization energy comes from the rearrangement of molecular geometry (intramolecular vibration) and polarization of the surrounding molecules in solution (reorientation of dipoles in the solvent) upon addition or removal of an electron to a molecule.[27] A parallel can be formed for charge transfer in the solid-state, where the reorganization energy mainly comes from vibrational relaxation and not rotation of solvent dipoles. Small-polaron models are based on coupling of the charge with low-frequency phonon modes, with a reorganization energy calculated to be twice that of the polaron binding energy.[24-26]

Nuclear rearrangement limits the rate of polaron hopping since from the Born-Oppenheimer approximation, electronic changes is much faster than molecular rearrangement. Consequently, charge transfer first requires the surrounding molecules to relax to the optimal nuclear arrangement and form an activated complex.

2.5 Non-Polaron Hopping Transport in Disordered Solids

2.5.1 Introduction

Transport in disordered organic semiconductors, and disordered solids in general, is characterized by charge localization and a hopping transport mechanism. Hopping conduction was first applied to describe the anomalous behavior of transport observed in

doped semiconductors at sufficiently low temperatures. One of the first observations was made by Hung and Gliessman[29] who measured the Hall coefficient and resistivity of different Germanium samples with different kinds of impurities and concentrations from room temperature down to liquid helium temperatures. According to conventional impurity semiconductor conduction theory, as temperature is reduced, the concentration of the electrons in the conduction band (or holes in the valence band) should decrease, and the resistivity and Hall coefficient should increase. However, Hung and Gliessman[29] found that the resistivity saturates and the Hall coefficient reached a maximum at low temperatures. These anomalies led them to conclude that a different mechanism of conduction was taking place at low temperatures.

For low doping concentrations, there is weak overlap and impurity states are localized. At low temperatures, there will be little thermal excitation to the bands and most charges will be localized to the impurity states. In this case, band current becomes negligible, and tunneling conduction of electrons in localized impurity donor states in the gap becomes the predominant process. This phonon-assisted tunneling conduction process was suggested by Mott[30] and Conwell.[31]

2.5.2 Master Equation of Hopping Kinetics

In the regime where the hopping mechanism is predominant, transport is determined by charge-carriers moving from one localized state to another. The hopping motion of charge-carriers can be described by the kinetic master equation:[32, 33]

$$\frac{\partial P_i(t)}{\partial t} = \sum_{j \neq i} \left[W_{ji} P_j(t)\left(1 - P_i(t)\right) - W_{ij} P_i(t)\left(1 - P_j(t)\right) \right] \tag{2.5}$$

where $P_i(t)$ is the occupational probability of site i at time t and W_{ij} is the transition rate from site i to site j. Often times, under the condition that the system is close to equilibrium, a linearization can be made to the master equation. Several approaches to solve the master equation include the resistor network method,[13] percolation theory,[34] effective medium theory,[35] the continuous-time-random-walk (CTRW) method,[36] and the Green function method.[32] Vissenberg presents and discusses these methods used to solve the linearized master equation.[33]

2.5.3 Resistor Network Models

Miller and Abrahams[13] developed a model that reduces the incoherent hopping transitions in a disordered lattice to a random resistor network. Their[13] proposed network is used to calculate the hopping conductivity G in semiconductors in the presence of a weak external field. In this hopping transport, the electronic states are localized with the wavefunctions decaying like $\exp\left[-\alpha\left|\mathbf{r}-\mathbf{R}_i\right|\right]$ (α is the inverse localization length, $\mathbf{R}_j$ is the spatial position of a site j) and the energy difference between pairs of sites is $\Delta E=\left|E_i-E_j\right|\gg\beta_{ij}$ (β_{ij} is interaction energy between sites i and j; E_i and E_j is the energy of sites i and j, respectively). A linearization can be applied for weak-field transition rates, $\Gamma_{ij}-\Gamma_{ji}\propto G_{ij}\left(\mu_i-\mu_j\right)$ (G_{ij} is related to transition rate Γ_{ij} from site i to site j; μ_i and μ_j is the potential at sites i and j, respectively). From detailed balance of rates, the transition rates in the low-field regime is:[13]

$$\begin{aligned}\Gamma_{ij}&\propto\exp\left[-2\alpha\left|\mathbf{R}_j-\mathbf{R}_i\right|\right]\exp\left[-\Delta E/kT\right],\ \Delta E>0\ \textbf{(upward hops)}\\ \Gamma_{ij}&\propto\exp\left[-2\alpha\left|\mathbf{R}_j-\mathbf{R}_i\right|\right],\ \Delta E<0\ \textbf{(downward hops)}\end{aligned} \tag{2.6}$$

Note that using Miller-Abraham rates assumes that the electron-phonon coupling is weak enough to have polaronic effects be negligible compared to static disorder in the hopping process. The activation energy ΔE will be only dependent on the site energy differences (caused by static disorder) and not on molecular conformation energies required to form activated complexes for charge transfer.

From the master equation (Eq. (2.5)), the net steady-state current flow from site i to site j is:[33, 37]

$$I_{ij}=q\left[W_{ij}P_i\left(1-P_j\right)-W_{ji}P_j\left(1-P_i\right)\right] \tag{2.7}$$

The occupational probabilities of sites is given by the Fermi-Dirac statistics:

$$P_i=\frac{1}{1+\exp\left[\left(E_i-\mu_i\right)/kT\right]} \tag{2.8}$$

where μ_i is the non-equilibrium quasi-electrochemical potential at site i. At equilibrium, the electrochemical potential is given by $\mu_i=\mu-q\mathbf{F}\cdot\mathbf{r}_i$, where μ is the chemical potential, $\mathbf{F}$ is the applied electric field vector, and $\mathbf{r}_i$ is the position vector of site i. The

non-equilibrium quasi-electrochemical potential deviates from a well-defined equilibrium electrochemical potential as the temperature is reduced, disorder increases, and the applied electric field increases.[37] Using Miller-Abrahams hopping rates (Eq. (2.6)), the net current flow in Eq. (2.7) will be:[33, 37]

$$I_{ij} = qv_0 \frac{e^{-2\alpha r_{ij}} e^{\frac{-|E_j - E_i|}{2kT}} \left(e^{(E_i - E_j)/2kT} e^{(E_j - \mu_j)/kT} - e^{(E_j - E_i)/2kT} e^{(E_i - \mu_i)/kT} \right)}{e^{(E_i - \mu_i)/2kT} e^{(E_j - \mu_j)/2kT} \left(e^{-(E_i - \mu_i)/2kT} + e^{(E_i - \mu_i)/2kT} \right) \left(e^{-(E_j - \mu_j)/2kT} + e^{(E_j - \mu_j)/2kT} \right)} \tag{2.9}$$

where the absolute value in the exponential in the numerator comes from the dependence on the energy difference between sites *i* and *j*. Eq. (2.9) can be rewritten as:[33, 37]

$$I_{ij} = qv_0 \frac{\exp\left[-2\alpha r_{ij}\right] \exp\left[-|E_j - E_i|/2kT\right] \sinh\left[(\mu_i - \mu_j)/2kT\right]}{2\cosh\left[(E_i - \mu_i)/2kT\right] \cosh\left[(E_j - \mu_j)/2kT\right]} \tag{2.10}$$

For small deviations from equilibrium (deviations of non-equilibrium quasi-electrochemical potential from equilibrium electrochemical potential), the net current can be linearized:[33, 37]

$$\begin{aligned} I_{ij} &= G_{ij}\left(\mu_i - \mu_j\right) \\ &= \frac{qv_0}{4kT} \frac{\exp\left[-2\alpha r_{ij}\right] \exp\left[-|E_j - E_i|/2kT\right]}{\cosh\left[(E_i - \mu_i)/2kT\right] \cosh\left[(E_j - \mu_j)/2kT\right]} \left(\mu_i - \mu_j\right) \end{aligned} \tag{2.11}$$

where the approximation $\sinh\left[(\mu_i - \mu_j)/2kT\right] \approx (\mu_i - \mu_j)/2kT$ is used. The net current between the two sites has been linearized to an ohmic current through a resistor with conductance G_{ij}. Therefore, the hopping conduction between sites in a disordered lattice can now be treated with a random resistor network. The disordered hopping conductivity can be found by calculating the conductivity of a random resistor network.

To calculate the conductivity of their network, Miller and Abrahams assumed that the statistical distribution of resistances in the network of localized impurity states only depends on the intersite distances, and not the individual site energies. However, it was later argued that in calculating the total conductivity of their resistor network, the transport paths in their reduced network may not always represent the true paths carrying most of the current.[38] Since Miller-Abrahams assumed nearest neighbor hops, the pathway of nearest neighbor hops may reach a site that is isolated far away from any

nearby sites. This difficult path will have little current; and most charges will rather go through a non-nearest neighbor path that is more optimal.

2.5.4 Variable-Range Hopping (VRH)

The assumption of nearest-neighbor hops may be incorrect for low enough temperatures where the thermally-activated hopping rates become much smaller than the spatial tunneling rates. If there is a continuum of localized states, carriers will be able to choose sites with more favorable energies closer to the Fermi level. Mott pointed out that if the activation energy to a nearest neighbor site was large, a more favorable hop might be to a site farther away with a lower activation energy. This tradeoff of energy and distance for the optimal jump depends on the respective transition rates (energy-dependent hops and spatial-dependent tunneling rates). Since the energy-dependent transition is thermally-activated, the optimal hopping distance will depend on temperature. This mechanism of hopping conduction is called variable-range hopping (VRH).[39]

Mott proposed that variable-range hopping conductivity is determined by optimal hops that maximizes the transition rates over energy and space. Within a sphere of radius R (the average hopping distance), a charge-carrier at the Fermi level will have at least one available site to hop to that has an energy within an average range, ΔE:[33]

$$1 = \frac{4\pi R^3}{3} g(E_F)\Delta E \Leftrightarrow \Delta E = \frac{3}{4\pi R^3 g(E_F)} \tag{2.12}$$

where a uniform density of states is assumed in the vicinity of the Fermi energy, $g(E) = g(E_F)$. The conductance can then be written as (using Miller-Abrahams rates):[33]

$$G = G_0 \exp\left[-2\alpha R - \frac{3}{4\pi R^3 g(E_F) kT}\right] \tag{2.13}$$

Maximizing the conductance, the optimal mean hopping distance is:[33]

$$R = \left[\frac{9}{8\pi\alpha kT g(E_F)}\right]^{1/4} \tag{2.14}$$

This leads to an optimized hopping rate that is proportional to $\exp\left[1/T^{1/4}\right]$. In general, the temperature dependence of the hopping conductivity is:[33, 38]

$$\sigma = \sigma_0 \exp\left[-\left(\frac{T_1}{T} \right)^{\alpha} \right] \qquad (2.15)$$

where $\alpha = 1/(d+1)$ for a uniform DOS in a d-dimensional system. In general, depending on the DOS and the dimension of the system, the power exponent α in Eq. (2.15) can vary from 0 (hopping dominated by spatial dependent transitions) to 1 (hopping dominated by temperature dependent transitions).[33]

For, a three-dimensional variable-range hopping system in a uniform DOS (uniform around the Fermi energy), the log of the conductivity should scale as $T^{-1/4}$. The temperature parameter T_1 in Eq. (2.15) is given by:[33, 38]

$$T_1 = \frac{C\alpha^3}{kg(E_F)} \qquad (2.16)$$

where C is a dimensionless parameter. The temperature dependence of the conductivity of amorphous germanium from 60K to 300K was found to be consistent with Mott's formula.[40-44] Similar temperature dependences were well-described by Mott's formula for amorphous silicon and carbon.[42] Mott VRH theory predicts a temperature dependence of conductivity transition from $T^{-1/4}$ to $T^{-1/3}$ with a dimensionality change from 3D to 2D hopping.

2.5.5 Percolation Theory

The Miller-Abrahams network model was independently modified with percolation theory by Ambegaokar *et al.*,[34] Shklovskii and Efros,[45] and Pollak.[46] Vissenberg and Matters[47] later applied percolation theory to successfully describe transport in amorphous organic semiconductor thin-film transistors. Percolation paths are the most optimal paths for current and these paths determine the hopping conductivity of disordered solids. Percolation theory is based on the principle that the disordered hopping conductivity is not determined by the rate of average hops, but it is limited by the rate of the most difficult hops (lowest conductance) in the most conductive path. A review on applications of percolation theory is given by Sahimi.[38]

In percolation theory, the random resistor network is first viewed as a system made up of individual disconnected clusters, whose average size is dependent on a

reference conductance G. For a given reference conductance G, all conductive pathways between sites with $G_{ij} \leq G$ are removed from the network, which leaves a collection of spatially disconnected clusters of high conductivity, $G_{ij} \geq G$. As this threshold reference conductance G is decreased, the size of these isolated clusters increases. The critical percolation conductance is defined as the maximum reference conductance $G = G_c$ at the point when percolation first occurs; meaning, a continuous, infinite cluster (cluster that spans the whole system) first forms. This infinite cluster will be composed of clusters that are all connected by critical conductive links with conductance G_c. From percolation theory, the conductivity is limited by these links, and the total conductance of the system is then equal to G_c. To determine the threshold for percolation, the average number of bonds per site is calculated. A bond is defined as a link between two sites which have a conductance $G_{ij} > G$. As the reference conductance G decreases, the average number of bonds per site B increases. A large average number of bonds per site indicates a large average size of a cluster (collection of sites with $G_{ij} > G$). Therefore, it is assumed that once the average number of bonds per site B reaches some critical bond number B_c, the average cluster sizes will be large enough such that they all touch and form a continuous pathway that spans the whole disordered system (form an infinte cluster). Vissenberg and Matters[47] set the critical bond number to $B_c \simeq 2.8$, which was calculated for a three-dimensional amorphous system.[38, 48]

Assuming near equilibrium and describing the transition rates with Miller-Abrahams hopping rates, from Eq. (2.11), the conductance between sites i and j is given by:[33, 37]

$$G_{ij} = \frac{q\nu_0}{4kT} \frac{\exp\left[-2\alpha r_{ij}\right]\exp\left[-\left|E_j - E_i\right|/2kT\right]}{\cosh\left[\left(E_i - \mu_i\right)/2kT\right]\cosh\left[\left(E_j - \mu_j\right)/2kT\right]} \tag{2.17}$$

where μ_i and μ_j are the quasi-electrochemical potentials that deviate from the equilibrium electrochemical potentials, $\mu - q\mathbf{F}\cdot\mathbf{r}$, where μ is the chemical potential, **F** is the applied field, and **r** is the position of the sites. If the most relevant hops in the critical infinite cluster-binding links involve site energies that are high above the quasi-

electrochemical potential ($E_i - \mu_i \gg kT$), the conductance in Eq. (2.17) for small applied electric fields can be approximated in the zero-field limit as:[33, 47]

$$G_{ij} \approx \frac{qV_0}{kT}\exp\left[-2\alpha r_{ij}\right]\exp\left[-\frac{|E_j - E_i| + |E_i - E_F| + |E_j - E_F|}{2kT}\right] \tag{2.18}$$

where E_F is the Fermi energy (or chemical potential μ). In this case, the conductance between sites can be written as:[33, 47]

$$G = G_0 \exp\left[-s_{ij}\right] \tag{2.19}$$

with $G_0 = qV_0/kT$ and:[33, 47]

$$s_{ij} = 2\alpha r_{ij} + \frac{|E_j - E_i| + |E_i - E_F| + |E_j - E_F|}{2kT} \tag{2.20}$$

The conductance G_{ij} between sites i and j is now related to s_{ij}. At the first formation of an infinite cluster, the clusters (collection of sites with $s_{ij} < s_c$) will all bond at the critical conducting link s_c. The conductivity of the disordered system is therefore $\sigma = \sigma_0 \exp[-s_c]$, where s_c is the critical exponent of the critical conductance when percolation first occurs (when $B = B_c$).

The average number of bonds B is equal to the density of bonds, N_b, divided by the density of sites that form bonds, N_s, in the material. At the percolation threshold, when $B = B_c$, the density of bonds is given by:[47]

$$N_b = \int d^3 r_{ij} \int dE_i \int dE_j g(E_i) g(E_j) \theta(s_c - s_{ij}) \tag{2.21}$$

where r_{ij} is integrated in three dimensions over the entire material, $g(E)$ is the DOS in the material, and θ is the Heaviside unit step function. The density of sites that form bonds at the percolation threshold ($B = B_c$) is given by:[47]

$$N_s = \int dE g(E) \theta(s_c kT - |E - E_F|) \tag{2.22}$$

Note that $E_{max} = E_F + s_c kT$ is the maximum energy that participates in bond formation. The maximum energy is obtained in the limit of $r_{ij} \to 0$. The maximum distance between sites that can still form bonds is $r_{max} = s_c/2\alpha$ (only downward hops occur between

maximally separated bonded sites). Vissenberg and Matters assumed an exponential DOS in their material (amorphous organic semiconductors):[47]

$$g(E)=\begin{cases}\frac{N_0}{kT_0}\exp[E/kT_0], & -\infty<E\le 0\\ 0 & , \quad E>0\end{cases} \tag{2.23}$$

where N_0 is the total density of states (molecular density) per unit volume and T_0 is a characteristic temperature that determines the width of the exponential distribution. They defined a charge-carrier occupation δ, which, for low enough temperatures ($T<T_0$) and charge-carrier concentrations ($|E_F|\gg kT_0$), is given by :[47]

$$\delta=\frac{1}{N_0}\int dEg(E)f(E,E_F)\simeq\exp\left[\frac{E_F}{kT_0}\right]\Gamma\left(1-\frac{T}{T_0}\right)\Gamma\left(1+\frac{T}{T_0}\right) \tag{2.24}$$

where $f(E,E_F)$ is the Fermi-Dirac distribution with Fermi energy E_F, and $\Gamma(z)\equiv\int_0^\infty dy\exp[-y]y^{z-1}$.

Substituting Eqs. (2.20) and (2.23) into Eqs. (2.21) and (2.22), Vissenberg and Matters obtained:[47]

$$B_c=\frac{N_b}{N_s}\approx\pi N_0\left(\frac{T_0}{2\alpha T}\right)^3\exp\left[\frac{E_F+s_ckT}{kT_0}\right] \tag{2.25}$$

where they assumed that most of the hops take place at the tail of the distribution ($|E_F|\gg kT_0$) and that the maximum energy hop forming a bond is large ($s_ckT\gg kT_0$). They remarked that their result in Eq. (2.25) is up to a numerical factor in agreement with previous results[49-51] that employed different approaches for variable-range hopping (VRH) in an exponential band-tail.

Using Eq. (2.25), the conductivity of the disordered system is given by: [47]

$$\sigma=\sigma_0e^{-s_c}=\sigma_0\left[\left(\frac{T_0}{2\alpha T}\right)^3\frac{\pi N_0\delta}{B_c\Gamma(1-T/T_0)\Gamma(1+T/T_0)}\right]^{T_0/T} \tag{2.26}$$

Vissenberg and Matters[47] noted that their conductivity expression (Eq. (2.26)) has an Arrhenius-like temperature dependence, $\sigma\propto\exp[-E_A/kT]$, with an activation energy E_A

that has a weak (logarithmic) temperature dependence. Recall earlier that the temperature dependence of a general hopping conductivity can be described with:[38]

$$\sigma(T) \propto \exp\left[-\left(\frac{T_1}{T}\right)^{\alpha}\right] \tag{2.27}$$

Depending on the DOS and the dimension of the system, the power exponent α in Eq. (2.27) can vary from 0 (hopping dominated by spatial dependent transitions) to 1 (hopping dominated by temperature dependent transitions).[33]

In regards to Eq. (2.27), the temperature dependence ($\alpha \approx 1$) is different from Mott's law for 3D VRH in a constant DOS ($\alpha = 1/4$). Vissenberg and Matters[47] rationalized that for a constant DOS, hopping high in energy or over large distances play an equal role (however, the spatial dependence is slightly more important since $\alpha = 1/4$ is closer to 0), whereas for an exponential DOS (where there are increasingly more available states at higher energies), the thermally-activated transition plays a stronger role than the spatial-dependent transition (hence, α close to 1). They further pointed out that it has been previously shown that hopping charges in an exponential DOS can be described as charge motion that is dominated by thermal-activation from the Fermi level to a particular transport energy level.[52] The Arrhenius activation energy is then simply the difference between the transport energy level and the Fermi level. Note that for very low temperatures ($s_c kT < kT_0$), approximations used to obtain Eq. (2.26) are no longer valid. In this regime, charges will mainly hop near the Fermi energy. The conductivity should transition to VRH near the Fermi energy in an approximately constant DOS (small deviation in energy from Fermi level in exponential DOS).

For very low temperatures, the maximum energy of a site forming a bond ($E_{\max} = E_F + s_c kT$) is only a small fluctuation about the Fermi energy E_F that is smaller than the width of the exponential DOS ($s_c kT \ll kT_0$). Therefore, most of the charge-carriers participating in bond formations are at sites with energies near the Fermi energy and the distribution of these energies (DOS) is approximately constant. The expression for the critical bond number (Eq. (2.25)) is generalized:[33]

$$B_c \approx \pi N_0 \left(\frac{T_0}{2\alpha T}\right)^3 \left[\frac{\sinh(2s_c T/T_0) + 6 s_c T/T_0}{\sinh(s_c T/T_0)} - 8\right] \exp\left[\frac{E_F}{kT_0}\right] \tag{2.28}$$

Note that for $s_c kT \gg kT_0$, the generalized critical bond number expression (Eq. (2.28)) reduces to Eq. (2.25).[33] However, for very low temperatures ($s_c kT \ll kT_0$), the following conductivity expression is obtained:[33]

$$\sigma = \sigma_0 e^{-s_c} = \sigma_0 \exp\left[-\left(5\frac{(2\alpha)^3 T_0 B_c \Gamma(1-T/T_0)\Gamma(1+T/T_0)}{\pi T N_0 \delta} \right)^{1/4} \right] \tag{2.29}$$

The low-temperature conductivity expression in Eq. (2.29) obeys Mott's 3D variable-range hopping law in a constant DOS, $\sigma \sim \exp\left[-(T_1/T)^{1/4}\right]$ (see Eq. (2.15)).[33] Mott's law for 3D VRH in uniform DOS is Eq. (2.15) with $\alpha = 1/4$ and $T_1 = C\alpha^3/kN$ (C is a dimensionless parameter; N is density of states). However, Vissenberg[33] remarks that from Eq. (2.29):[33]

$$T_1 = \left(\frac{40B_c}{\pi} \right) \frac{\alpha^3}{k} \frac{kT_0 \Gamma(1-T/T_0)\Gamma(1+T/T_0)}{T\delta N_0} \tag{2.30}$$

Therefore, unlike VRH in a constant DOS (where $T_1 = C\alpha^3/kN$), the region in the exponential DOS approximated as constant $N = N_0\left(T\delta/kT_0\Gamma(1-T/T_0)\Gamma(1+T/T_0)\right)$ will be dependent on temperature and charge-carrier concentration.[33]

2.5.6 Transport Energy Level Concept

To simplify the hopping problem theoretically, the mobility-determining hops are assumed to be the multiple carrier hops around a single critical transport energy level within the distribution of localized states.[53] The importance of a particular energy level in the carrier hop dynamics was recognized by Grünewald and Thomas,[50] who described an activation energy of conductivity in *a*-Si with a variable-range hopping (VRH) model in an exponential band tail. Monroe also developed a transport energy level concept for an exponential density of band-tail states.[52] Baranovskii *et al.*[53] studied this transport energy level and found that it is the important energy level that dominates the steady-state and transient hopping transport phenomena in both equilibrium and non-equilibrium conditions. This transport level is the optimal energy for hops, and most hopping events are within its vicinity.

Carrier hopping between localized states is determined by a spatial-dependent tunneling transition rate and energy-dependent Boltzmann rate (see Eq. (2.6) for Miller-Abraham rates). Charges in the shallow states can easily hop upwards in energy but they also have a large number of neighboring sites where they can hop down in energy as well. In a distribution that decreases rapidly with energy, such as an exponential or Gaussian DOS, as charges move to lower trap states, hopping downwards in energy becomes slower because the number of nearby states that are lower in energy decreases dramatically. At this point, the charges will have to hop to closer sites that are higher in energy. Therefore, charges in deep states will mostly be dominated by thermal excitations to higher energies. As charges move up in energy, the hopping down process starts competing as the number of available states lower in energy increases. Whether thermal excitations or downward hops dominate is governed by the competition between the spatial-dependent and energy-dependent transition rates. The energy level at which the thermal excitation begins to dominate is called the transport energy, E_t.[52] Above this level, substantial number of carriers hop downwards (the fastest rate is hops down to states near E_t); and below, most hop upwards (fastest rate is to states near E_t). The position of this transport energy level is a function of the density of states (transport energy will be higher for steeper DOS) and the temperature. As temperature is decreased, the energy-dependent Boltzmann transition rates will decrease, and the transport level will move lower in energy. The transport energy is similar to the mobility edge in that charges are thermally activated to this energy level and higher, and the current is mainly carried by charges in the these transport states. Hopping upward and downward events in the vicinity of the transport energy level is similar to a multiple-trapping mechanism where the transport energy is the mobility edge. Experimental observations showing evidence of a disordered hopping mechanism and an existence of well-defined activation energies can be justified with the transport energy level concept. Conduction is either dominated by thermal activation to the band edge or by charge hopping within the band-tail states with a transport energy level.

The transport energy level model was developed considering an exponential band-tail, however, Baranovskii *et al.*[54] showed that a transport energy level also existed for density of localized states of the form, $g(E) \sim \exp\left[-(E/E_0)^{\lambda}\right]$, with $\lambda = 2$ and $\lambda = 1/2$.

Since a transport energy level existed for both these DOS, it should also exist for any intermediate DOS from $\lambda = 2$ to $\lambda = 1/2$.[54] Therefore, amorphous materials containing these types of DOS may be theoretically analyzed with the notion of a transport energy level. Baranovskii and co-workers[54-57] used the transport energy level concept to derive the mobility in a Gaussian DOS representing disordered amorphous organic semiconductors.

Chapter 3 – Trapped-Charge-Limited Transport in Organic Semiconductors

3.1 Introduction

This chapter looks at the macroscopic models for charge transport in relatively ordered organic materials. Models to explain charge transport in organic semiconductor devices traditionally fall into two regimes of operation. One is injection-limited transport which supposes that the injection barrier between the electrode and organic is the main bottleneck for charges to move from one electrode to the other. In this case, the induced current from an applied voltage is rate limited by the properties of the metal/organic interface, *i.e.* the interface barrier height, interfacial doping, cathode material, interfacial morphology, and etc. The other is a bulk-limited transport model that assumes that the injection barrier is sufficiently low and that the main bottleneck for transport is the organic layer itself. In this case, the charge injection rate across the metal/organic interface is high enough to supply the bulk with an infinite reservoir of carriers. The induced current from an applied voltage is rate limited by the bulk properties of the organic semiconductor, *i.e.* the trap states in the bulk, the mobility, morphology of organic layer, and etc.

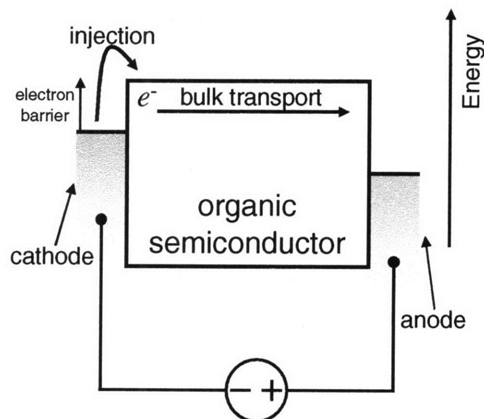

Figure 3-1: Total current is from the charge injection rate from metal contacts into organic semiconductor and the subsequent bulk transit to the other contact. Most models assume current is dominated by one of these two mechanisms.

3.2 Transport in Organic Molecular Crystals

Organic molecular crystals first surfaced as an interest with the evidence of electroluminescence of anthracene crystals.[58, 59] Since molecular crystals cannot be easily grown into thin films, the molecular crystal layers are relatively thick and transport are usually limited by the bulk properties of these materials.

Molecular crystals are ordered van der Waals bonded molecules. Similar to covalent bonded inorganic semiconductors, they may be highly ordered with good electrical properties. But similar to other van der Waals bonded solids, they have relatively narrow bandwidths. Molecular crystals are believed to possess some characteristics of both delocalized band transport and localized hopping.[1] Since molecular crystals are somewhat well-ordered, the physical disorder should not play a significant role in charge localization. Therefore, if localized charge hopping is believed to operate in organic molecular crystals, the cause should be polaronic effects. When employing band transport models for molecular crystals, the single electron approximation is used; whereas, for more disordered transport, polaron effects that comprises the charge and its associated electronic and molecular polarization clouds are considered.

The charge-carrier mobility in crystalline naphthalene is observed to increase with decreasing temperature.[60] This is consistent with band transport because if transport were from thermally-activated hopping, the mobility would increase with temperature. The temperature dependence of charge carrier mobility follows a power-law behavior, but deviates at higher temperatures, suggesting a transition to polaronic effects.[60] Some research has been done in employing a combination of these two types of transports for organic molecular crystals.[1]

3.3 Trap-Free Space Charge Limited (SCL) Conduction

Organic semiconductors have a relatively low density of free carriers (compared to semiconductors that have narrower bandgaps to allow relatively high density of carriers in the bands at room temperature). In an undoped organic semiconductor, all the charges that carry current must be injected. This charge is uncompensated and gives the organic semiconductor a net charge, known as space charge. Space-charge models for

trap-free insulators, and trapped-charge models with the presence of traps have been applied to describe current in these materials.[61-65]

One of the most important models for transport in molecular crystals (wide bandgap, insulator crystals) is the space-charge limited current (SCLC) model.[10] Assuming that the current is bulk-limited (the injection contact does not limit the current flow into the bulk) and the current density is determined by the drift current for large enough fields and mobility (diffusive process can be neglected; diffusion is usually significant only near the contact):

$$J = q\mu nF - qD\frac{dn}{dx} \simeq q\mu nF \tag{3.1}$$

where μ is the mobility ($v = \mu F$ is the drift velocity of the charge-carriers), n the charge density, and F the applied electric field. When a voltage is applied across a material, an electric field is established, causing injected space-charge and thermally-excited charges present in the conduction band to flow from one contact to the other. If current from the injected charge density is comparable to the intrinsic charge density, the semiconductor will no longer be quasi-neutral. For large enough biases, most of the charges contributing to current will be injected space-charge.

A pure molecular crystal will have no intrinsic charges and therefore, the charge density n that contributes to current (in Eq. (3.1)) are all uncompensated charges injected from the contacts. Therefore, the cross-over voltage for pure molecular crystals is very small, and the current–voltage curve is practically all in the space-charge-limited current regime. The electric field from the injected space charge is given from Poisson's equation:

$$\nabla F = \frac{qn}{\varepsilon} \tag{3.2}$$

where ε is the dielectric constant of the molecular crystal. Solving Eqs. (3.1) and (3.2) simultaneously for one dimension and constant mobility, the trap-free space-charge-limited current is obtained (Mott-Gurney law, Child's Law, SCLC square-law):[10, 66]

$$J_{SCL} = \frac{9}{8}\varepsilon\mu\frac{V^2}{d^3} \tag{3.3}$$

From Eq. (3.3), space-charge limited current gives a slope of 2 on a log J – log V plot.

3.4 Trapped Charge Limited (TCL) Conduction

3.4.1 Introduction

For a crystalline semiconductor with no traps in the SCLC regime, the injected space charge will propagate freely with the semiconductor mobility μ_0. This is the case for a trap-free solid. However, if there are traps in the bandgap, some of the injected carriers will be lost to these traps and only the fraction of them that remain in the conduction (or valence) band will conduct.[64, 65, 67] Since plots of the current-voltage characteristics of organic semiconductor molecular crystals on log-log scales gave slopes much larger than 2,[68] it has been proposed that the cause for these high slopes was due to additional trap states that are present in molecular crystals. These trap states will be more predominant in polycrystalline and amorphous molecular solids.

The trap-charged limited current (TCLC) model assumes current is from the motion of drifting carriers trapped and thermally released by localized trap states in the bandgap, and that the frequency of these trapping events is significant enough to limit the conduction. If there is a sufficient density of deep traps, the presence of these traps can have a controlling effect on the mobility. The TCLC model[10, 11, 65] is a modification of the SCLC model that includes a trap distribution. Note that as higher voltages are applied, the quasi-Fermi level will move closer to the conduction (or valence) band. At the point where the level passes the energy levels of the traps, the traps will be full and all further injected charge will be free. The conduction will then transition to the trap-free limit.[65]

3.4.2 Single Energy Level Trap

A trap state can originate from an impurity or defect. For single energy level trap states at E_T, with density N_T, the density of trapped charges is:[1]

$$n_T = N_T e^{-(E_T - E_F)/kT} \tag{3.4}$$

where E_F is the quasi Fermi level at an applied bias. The density of charges in the conduction band (or transport energy level) that contribute to the charge motion is:[1]

$$n_0 = N_C e^{-(E_C - E_F)/kT} \tag{3.5}$$

For current that is dominated by injected charges, the current-voltage characteristics can be described by the equation:[10]

$$J = \left(\frac{\theta}{\theta+1}\right)\frac{9}{8}\varepsilon\mu\frac{V^2}{d^3} \tag{3.6}$$

where $\theta \equiv n_0/n_T$. The current expression in Eq. (3.6) still has a power-law slope of 2, but a distribution of trap state energies can yield slopes larger than 2.

3.4.3 Exponential Distribution of Trap States

A distribution of trap states can result from random disorder in the organic semiconductor. For a distribution of trap states described by an exponential distribution:[1]

$$g(E) = \frac{N_T}{E_T}e^{E/E_T},\ E<0 \tag{3.7}$$

where N_T is the density of trap states and E_T is the characteristic width of the trap distribution. The density of trapped charges is:[1]

$$n_T \approx \int_{-\infty}^{0} g(E)f(E)dE \approx \frac{N_T}{E_T}\int_{-\infty}^{E_F} e^{E/E_T}dE = N_T e^{E_F/E_T} \tag{3.8}$$

The density of charges in the conduction band ($E_C = 0$) is:[1]

$$n_0 = N_C f(E_C) \approx N_C e^{E_F/kT} = N_C\left(\frac{n_T}{N_T}\right)^{E_T/kT} \tag{3.9}$$

Assuming only the charges in the conduction band dominate current, we obtain:[1]

$$J = qn_0\mu F \tag{3.10}$$

Assuming $n_T \gg n_0$, the trap-charge limited current (TCLC) density as a function of voltage is:[1]

$$J_{TCL} = qN_C\mu\left(\frac{\varepsilon}{qN_T}\frac{m}{m+1}\right)^m\left(\frac{2m+1}{m+1}\right)^{m+1}\frac{V^{m+1}}{d^{2m+1}}, \tag{3.11}$$

where $m = E_T/kT$. From Eq. (3.11), the slope of the current-voltage characteristics on a log-log plot is m+1. Therefore, from the slopes on the log-log plots of current density versus voltage, one can extract the trap energy width E_T.

The effect of charge concentration on the mobility is implicit in the TCLC model. The TCL drift current expression is obtained by substituting Eq. (3.9) into Eq. (3.10):[1]

$$J = q\left[N_C\left(\frac{n_T}{N_T}\right)^{E_T/kT}\right]\mu F \tag{3.12}$$

where N_C is the density of states at the band edge, N_T is the total density of trap states, and n_T is the density of injected charges. Rewriting Eq. (3.12):[1]

$$J = qn_T\left[N_C\left(\frac{1}{N_T}\right)^{E_T/kT} n_T^{E_T/kT-1}\right]\mu F = qn_T\mu_{\text{eff}}F \tag{3.13}$$

An effective mobility is defined, $\mu_{\text{eff}}(n_T) = \mu(0)f(n_T)$, where $\mu(0) = \mu$ is the mobility for zero concentration. The charge-carrier concentration dependence of mobility is introduced as a mobility enhancement factor.

3.4.4 Gaussian Distribution of Trap States

Steiger *et al.*[69] have analyzed the electronic trap distributions of the amorphous electron transport material tris(8-hydroxyquinoline) aluminum (Alq_3) using fractional TSC (thermally stimulated current) and TL (thermally stimulated luminescence) techniques. The experimental results can be explained with a Gaussian distribution of trap states.[69] And it is remarked that the current-voltage relation from the SCLC model with Gaussian trap distribution has the same behavior as an exponential TCL with the power-law slope parameter given by:[69]

$$m = \left[1 + \frac{2\pi\sigma^2}{16k^2T^2}\right]^{1/2} \approx \sqrt{\frac{2\pi}{16}}\frac{\sigma}{kT}, \tag{3.14}$$

for $2\pi\sigma^2/16 \gg k^2T^2$, where σ is the standard deviation of the Gaussian trap distribution. Eq. (3.14) has the same power-law slope form as that of the exponential case, with $m = E_T/kT$. Therefore, although the form of the trap distribution will affect the shape of the *J-V* characteristics, the *J-V* curves alone are not sufficient to distinguish between an exponential and Gaussian trap distribution.

Chapter 4 – Bulk-limited Transport in Amorphous Organic Semiconductors

4.1 Introduction

This chapter discusses the phenomenological models of the temperature, electric field, and charge density dependences of the charge-carrier mobility. The mobility relation from these models can be substituted into an SCL (Eq. (3.3)) or TCL (Eq. (3.11)) model to obtain an expression for current as a function of voltage.

The relative importance of localization and polaronic effects in organic molecular crystals is still unclear. However, in amorphous organic films, Anderson localization most likely occurs because of the presence of large energy state variations and weak intermolecular interactions. Thus, the relative importance of static energetic disorder is much greater in amorphous organic semiconductors, although the contribution of molecular deformation energy (polaron effects) to the charge-carrier transport activation energy is still debated.[3, 70-72]

4.2 Time-of-Flight Measurement of Charge-Carrier Mobility

One of the most important parameters characterizing organic semiconductor devices is the charge-carrier mobility. Mobility is a metric that characterizes the overall electrical transport capability of a semiconductor. There are many experimental methods that produce mobility data,[60] either through electrical (time of flight, xerographic discharge, equilibrium carrier extraction, drift current, space-charge-limited-current, conductivity to concentration, field-effect transistor (FET), and surface acousto-electric traveling wave (SAW)) or magnetic interactions (Hall effect, magneto-resistance, and cyclotron resonance).[60] These methods listed, as applied to organic semiconductors, are elaborated and analyzed by Karl.[60] A common and convenient technique for measuring the charge-carrier mobility is by time-of-flight (TOF). An optical pulse is incident on the semiconductor, generating photo-excited carriers. A bias is applied to the semiconductor, and the transient photocurrent is measured. Depending on the applied voltage bias, either

the positive or negative carrier will be quickly swept into its respective electrode, thereby causing a large initial spike in the transient photocurrent measurement. However, the other carrier species must drift across the film. The time it takes for most of the charges to go across the film is related to the mobility:

$$v_d \equiv \mu F \Rightarrow \mu = d^2/\tau V \quad (4.1)$$

where d is the thickness of the film, τ is the transit time, V is the applied voltage, and the electric field, F, is assumed to be constant throughout the film. In order to get accurate results, the optical pulse must be relatively instantaneous. In other words, the transit time τ must be much longer than the optical pulse width by increasing the thickness of the sample film.

Unlike conventional ordered inorganic semiconductors, the carriers in disordered materials hop through a variety of paths and percolate through the sample. The dispersion in carrier velocities complicates measurements of the transit time. Following Scher and Montroll,[36] the transit time for a carrier to percolate through an amorphous film is often defined as the inflection point in the log-log plot of the photocurrent transients.

4.3 Temperature and Electric Field Dependences of Mobility

4.3.1 Introduction

Mobility in disordered organic semiconductors are many orders of magnitude smaller than crystalline organic semiconductors (typically 1 cm^2/Vs) and crystalline inorganic semiconductors (typically 10 to 1000 cm^2/Vs), and the charge-carrier mobility in disordered organic semiconductors are also observed to be field-dependent at most temperatures and fields measured. [3, 72-78] Figure 4-1 shows a typical mobility measurement for the archetypical amorphous organic semiconductor, tris(8-hydroxyquinoline) aluminum (Alq_3):

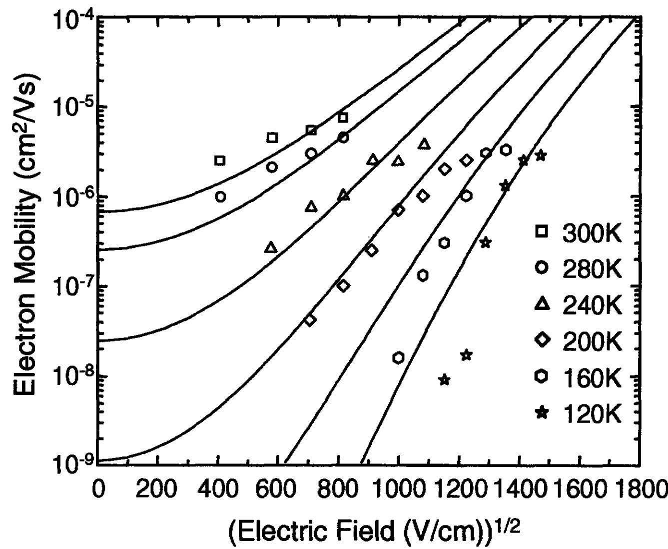

Figure 4-1: Temperature and electric field dependence of charge-carrier mobility obtained from transient electroluminescence measurements.[79] Solid lines are theoretical fits using a percolation-based bulk conduction model developed in Chapter 5. From Limketkai, Jadhav, and Baldo (2007).[80]

4.3.2 Mobility Measurements

One of the first descriptions for mobility was obtained from the observed field and temperature dependences of both electron and hole mobility in thin films of charge-transfer complexes of 2,4,7-trinitro-9-fluorenone (TNF) mixed with poly-n-vinylcarbazole (PVK). It was fit to the mobility relation by Gill:[81]

$$\mu = \mu_0 \exp\left[-\left(\Delta - \beta\sqrt{F}\right)\left(\frac{1}{kT} - \frac{1}{kT_0}\right)\right] \tag{4.2}$$

where E_0, μ_0, β, and T_0 are constants.

Gill[81] studied the mechanism of transport in molecularly-doped polymers by measuring the drift mobility in varying film compositions of PVK:TNF. The field and temperature dependences were found to be the same for practically any film composition ratio from pure polymer PVK to pure monomer TNF.[81] Varying the film composition, however, changed the measured magnitude of the drift mobility. From the variation in concentration of TNF in PVK, it was concluded that uncomplexed PVK facilitates hole transport and TNF aids electron transport.[81] The concentration dependence of mobility also suggest an intermolecular hopping mechanism.

Note that after the study of Gill,[81] similar temperature and field dependence behavior was observed for the hole mobility in other molecularly-doped polymer systems, such as in triphenylamine (TPA) doped in polycarbonate with the following expression reported by Pfister:[82]

$$\mu = \mu_0 \exp\left[\left(\frac{a}{k}\right)\left(F^n - E_0^n\right)\left(\frac{1}{T} - \frac{1}{T_0}\right)\right] \tag{4.3}$$

where a, E_0, and T_0 are constants and n is approximately equal to ½. This is identical to Gill's expression for $n = 1/2$ and $\Delta = \beta\sqrt{E_0}$.

Schein *et al.*[72] employed a graphical technique to determine the field and temperature dependence from plots of experimental data of amorphous organic solids. From the measurements of p-diethylaminobenzaldehyde-diphenyl hydrazone (DEH) doped in polycarbonate, they found that the various graphical data could be described by:[72]

$$\mu = \mu_0 \exp\left[-(T_0/T)^2\right] \exp\left[\left(\frac{\beta}{T} - \gamma\right)\sqrt{F}\right] \tag{4.4}$$

where μ_0, T_0, β, and γ are constants.

4.3.3 'Poole-Frenkel' Electric Field Dependence of Mobility

Poole-Frenkel is a limiting case of the general Onsager theory,[83] describing the dissociation of a charge pair in a Coulomb potential under an electric field. In conventional semiconductors, charges trapped at a charged defect can be detrapped by an electric field that lowers the barrier for the carrier to thermally escape the Coulomb potential. This yields the Poole-Frenkel field dependence of the drift mobility.

The potential energy seen by a hole in the presence of an applied electric field, **F**, and an electron is:[1]

$$U = -q\mathbf{F}\bullet\mathbf{R} - \frac{q^2}{4\pi\varepsilon r} \tag{4.5}$$

where ε is the permittivity of the material. The barrier lowering by an applied electric field, Δ, is obtained by finding the maximum value of U:[1]

$$\frac{dU}{dx}=0\rightarrow x=\sqrt{\frac{q}{4\pi\varepsilon F}},\Delta=\sqrt{\frac{q^3F}{\pi\varepsilon}} \tag{4.6}$$

The charge density escaping the Coulomb trap potential to participate in the drift current is:[1]

$$n=N_C\exp\left[-\frac{(q\phi_B-\Delta)}{kT}\right] \tag{4.7}$$

The total Poole-Frenkel (PF) emission current density is then:[1]

$$J_{PF}=q\mu\left(N_C\exp\left[-\frac{(q\phi_B-\Delta)}{kT}\right]\right)F=q\left(\mu\exp\left[\frac{\Delta}{kT}\right]\right)\left(N_C\exp\left[-\frac{q\phi_B}{kT}\right]\right)F \tag{4.8}$$

where original ϕ_B is the energy barrier height and N_C is the density of states at the conduction band. The mobility can then be redefined as a modified mobility:[1]

$$\mu=\mu_0\exp\left[\frac{\Delta}{kT}\right]=\mu_0\exp\left[\frac{q}{kT}\sqrt{\frac{qF}{\pi\varepsilon}}\right] \tag{4.9}$$

with a field-dependent factor that follows a $\sqrt{F}$ dependence.

This square root field dependence of mobility, frequently observed in charge transport studies of disordered organic semiconductors,[3, 73-78] is observed for mobility plots of single carrier transport. In this case, a Poole-Frenkel mechanism causing this field dependence is unsure because holes (or electrons) are the majority carriers but there are few electrons (or holes) to create Coulomb binding potentials to trap the holes (or electrons).[1]

To explain the 'Poole-Frenkel' dependence without using a Poole-Frenkel mechanism, Novikov and Vannikov[84-86] developed a model in which the transport sites are traps created by dipole moments in the polymer host matrix. Transport is then determined by the escape rate of charge carriers from these dipole traps. Based on Monte Carlo simulations, this dipole-trap model gives the mobility expression for moderately strong fields:[84]

$$\mu=\mu_0\exp\left[-\beta\left(\sqrt{F_0}-\sqrt{F}\right)\left(\frac{1}{T^2}-\frac{1}{T_0^2}\right)\right] \tag{4.10}$$

where T_0 is related to the dipole moment trap depth.

Movaghar *et al.*[87] showed that a $\log\mu \propto F^{n}$ dependence, where $0 \le n \le 0.5$, is a characteristic feature of hopping transport in a DOS manifold with n being dependent on the shape of the DOS.

4.4 Models to Explain Temperature and Electric Field Dependences of Mobility

4.4.1 The Gaussian Disorder Model (GDM)

Suppose there is diagonal disorder (variations in site energies) that creates a Gaussian distribution of LUMO energy levels of the constituent molecules in the disordered amorphous organic film:[1]

$$g(e,\sigma) = \frac{1}{\sqrt{2\pi\sigma^2}} \exp\left[-\frac{1}{2}\left(\frac{e}{\sigma}\right)^2\right] \tag{4.11}$$

where σ is the standard deviation of the dispersion in energy levels. In the Gaussian disorder model, the hopping rate of a charge from site i to site j in a lattice is assumed to follow that of Miller-Abrahams:[13]

$$\nu_{ij} = \nu_0 \exp[-2\gamma r] \begin{cases} \exp\left[-\left(E_j - E_i\right)/kT\right], & E_j > E_i \\ 1, & E_j < E_i \end{cases} \tag{4.12}$$

where γ depends on the decay rate of the localized electronic wavefunctions, and E_i and E_j are the energies of the localized state at site i and j, respectively. The total rate is composed of a spatial dependent tunneling rate in the first exponential and energy dependent Boltzmann jump rate in the second exponential.

The effect of diagonal, or energetic, disorder is to create a distribution of LUMO states such that there is an effective energy barrier for charges to thermally hop from one molecular layer to the next. The effects of off-diagonal disorder (variations in intermolecular coupling interactions) results from the dependence of the tunneling rate on the intermolecular spacing between molecules:[3]

$$\nu_{ij} \propto \nu_0 \exp\left[-2\gamma a_0 \frac{\Delta R_{ij}}{a_0}\right] \tag{4.13}$$

where a_0 is the average intermolecular spacing and ΔR_{ij} is the actual distance between sites i and j. In Monte Carlo simulations, the energies of sites i and j are randomly picked

from a Gaussian distribution (diagonal disorder). The overlap parameter $\Gamma_{ij} = 2\gamma a_0$ is also subjected to a random distribution (off-diagonal disorder). To apply this in simulation, Gaussian distributions of Γ_i and Γ_j, each with variance σ_Γ, are used to contribute to the overlap parameter Γ_{ij} with variance $\Sigma = 2\sqrt{\sigma_\Gamma}$.[3] The diagonal disorder is the spread in the distribution in site energies σ, and the off-diagonal disorder is quantified by the variance of the overlap parameter Σ, which is a convenient definition for simulation purposes.[3]

Diagonal disorder is an inhomogeneous broadening of molecular energy levels that can be caused by random internal fields from dipole interactions (excitons or permanent molecular dipole moment) and charges on other molecules. Although the diagonal disorder can be linked to some microscopic picture, modeling the effect of off-diagonal disorder as causing a Gaussian probability density of overlap parameters between sites cannot be easily rationalized from a physical picture.[3]

The GDM for molecularly-doped polymers employs a lattice of randomly positioned and assigned energy levels chosen from a Gaussian distribution. The simulations describe biased random walks of charge-carriers in the molecular lattice. From simulating the carrier dynamics in a disordered energy landscape, the mobility $\mu = v/F$ is calculated from the average carrier velocity. In the high field limit, a phenomenological mobility expression fit to the simulation plots was found:[3]

$$\mu_{GDM} = \mu_0 \exp\left[-\left(\frac{2\sigma}{3kT}\right)^2\right] \begin{cases} \exp\left[C\left(\left(\frac{\sigma}{kT}\right)^2 - \Sigma^2\right)\sqrt{F}\right], & \Sigma \geq 1.5 \\ \exp\left[C\left(\left(\frac{\sigma}{kT}\right)^2 - 2.25^2\right)\sqrt{F}\right], & \Sigma < 1.5 \end{cases} \tag{4.14}$$

where the jump rates between sites are taken to follow Miller-Abraham rates.[13] C is a constant, and σ and Σ are diagonal and off-diagonal disorder parameters, respectively. Ideally, the degree of built-in diagonal and off-diagonal disorder can be extracted from the measured temperature and field dependences of mobility of molecularly-doped polymer systems. According to Eq. (4.14), when temperature is increased such that $\hat{\sigma} \equiv \sigma/kT$ is smaller than Σ, a decreasing mobility with field should be observed. The

diagonal and off-diagonal disorders have opposite effects on the strength of the field dependence of the mobility, and pure off-diagonal disorder will yield mobility that decrease with field for the entire range of field strengths.[88]

GDM simulations have reproduced several experimentally observed data[89] and show that the experimentally observed 'Poole-Frenkel' field dependence of mobility is a signature of carrier hopping transport between disordered energy states.

4.4.2 The Correlated Disorder Model (CDM)

GDM simulations reproduced the 'Poole-Frenkel' field dependence of mobility over only a relatively narrow range of electric field strengths and only at large fields ($F > 10^5$ V/cm).[3, 19] This has led some to believe that GDM did not model disorder completely. In the GDM, the effect of disorder is modeled by two parameters, the diagonal disorder σ and off-diagonal disorder Σ. Diagonal disorder (energy variation of localized molecular states) and off-diagonal disorder (variation in intermolecular interactions) arise from random energetic interactions among molecules in the lattice. If all the energy interactions are assumed to be independent and random, the distribution of site energies should follow a Gaussian. However, it is also reasonable to assume that this same microscopic picture of random internal fields and interactions will have some correlation of energies of molecules near each other. If there is some correlation in the morphology of the material (such as tiny crystalline grains in polycrystalline films), this spatial correlation will translate to energy correlations. The question is whether these spatially correlated site energies are significant enough to affect macroscopic properties of transport, such as influencing the charge-carrier mobility.

Gartstein and Conwell[90] demonstrated that the introduction of correlation of energies of sites close together can produce 'Poole-Frenkel' behavior over a wider range of fields. This spatial correlation of energies can be justified to arise from long-range energy correlations from charge-dipole interactions[19, 21] or correlations in thermal fluctuation in molecular geometries.[91] Proper modeling of the effect of spatial disorder and its consequent result of spatial correlation in site energies is important, especially at low densities of molecular charge carriers when the spatial disorder effects is more significant.[92] Note that as the average intermolecular separation between transport sites is

increased (by decreasing the concentration of transport sites in the polymer host), the charge hopping rate will be limited by the tunneling rates. At this point, spatial disorder (which controls off-diagonal disorder in the overlap parameter that affects the tunneling rate) will be more significant than the diagonal disorder.

A possible physical origin for disorder and local correlation of site energies is dipole interactions.[18-22] In dipolar CDM, where dipole interactions is assumed to be the dominant cause for disorder and energy correlations, independent and randomly oriented dipole moments p are placed at each lattice site.[21] The energy of a charge on a site is then the sum of the dipole interactions of the surrounding lattice sites:[21]

$$U_m = -\sum_{n \neq m} \frac{q\vec{p}_n \cdot (\vec{r}_n - \vec{r}_m)}{\varepsilon |\vec{r}_n - \vec{r}_m|^3} \tag{4.15}$$

The spatial disorder is folded into the variation in the dipole moment orientations. This dipolar disorder model yields a site energy distribution that is approximately Gaussian, but unlike GDM that assumes a strict Gaussian, there will also be spatial correlations in this energy distribution from the surrounding dipoles.[18, 21]

CDM is similar to GDM in that carriers are simulated as hopping in a disordered site energies distribution. The difference is that in GDM the site energies are independently and randomly drawn from a Gaussian probability density function, whereas, in CDM, independent and random dipole moments are first assigned at each lattice site and then site energies are calculated from Eq. (4.15).[21] CDM leads to an approximate Gaussian distribution of site energies but these energies are also spatially correlated (the random energy interactions causing site energy disorder approximately independent but still has some correlations).

The mobility relation characterizing the Monte Carlo simulations in a correlated disorder model (CDM) is found for 3D charge transport under moderate fields:[21]

$$\mu_{CDM} = \mu_0 \exp\left[-\left(\frac{3\sigma}{5kT}\right)^2 + C_0 \left[\left(\frac{\sigma}{kT}\right)^{3/2} - \Gamma \right] \sqrt{\frac{qa_0F}{\sigma}} \right] \tag{4.16}$$

where C_0 = 0.78 and Γ = 2. Note that μ_0 is the zero-field mobility at $T \rightarrow \infty$. The mobility relation in Eq. (4.16) was found by fitting simulation data to a trial function:[21]

$$\mu = \mu_0 \exp\left[-A_1 \left(\frac{\sigma}{kT} \right)^n + A_2 \left(\left(\frac{\sigma}{kT} \right)^m - A_3 \right) \sqrt{\frac{qFa_0}{\sigma}} \right] \quad (4.17)$$

where A_1, A_2, A_3, n, and m are constants. The coefficient A_1 was determined from temperature dependence of simulation plots of μ at zero field, and A_2 and A_3 from temperature dependence of the slope of simulation plots of log mobility vs $\sqrt{F}$.[21] The improvement of incorporating correlation in the site energies of the localized states is the increase in the range of fields that 'Poole-Frenkel' behavior is reproduced.

For dense films of conjugated polymers, Yu *et al.*[91, 93] proposed that the dominant cause for energetic variations of localized electronics states are thermal fluctuations of the molecular geometry of the polymers. And, the intermolecular restoring force of these fluctuations leads to spatial correlations in site energies because the molecular assemblies are spatially correlated.[91, 93]

4.4.3 Small Polaron Model

The energy barrier to localized hopping are typically assumed to be either dominated by static disorder (from variations in physical structure leading to energetic and spatial disorder) or dynamic disorder (induced polaronic barrier upon adding a charge to a molecule; carrier interaction with phonons). A polaron is a quasi-particle composed of the charge and its surrounding polarization cloud. This strong charge-phonon coupling lowers the energy of the charge to create a bigger barrier for charge removal, thereby inducing self-trapping. The polarization cloud distorts the surrounding lattice molecules, and as the charge moves in the lattice, this distortion is conserved with it. Only polarization effects that are established faster than the charge localization time are part of the polaron.[1] A carrier that is confined to a single molecular site is called a 'small polaron.'[94] The associated polarization cloud is small and only extends to a few neighboring molecules.

Small polaron models employing the Marcus rate equations in small polaron hopping theory[24-26] have been used to describe the hopping mechanism of charges. Kenkre and Dunlap[95] compared the different approaches to explain transport: ordered polaronic, disordered polaronic, and disordered non-polaronic (classic GDM). Several models have been proposed that included both polaron phenomenon and energetic

disorder effects.[95-100] One approach to include both disorder and polaronic effects is to model the charge carriers as polarons moving in a disordered DOS. The inclusion of disorder can explain the observed temperature and field behavior that may otherwise be unexplained by polaronic effects alone (polarons moving in isoenergetic transport sites). The relative contribution of polaronic and disorder effects to observed macroscopic properties will vary depending on the structural properties of the disordered organic system. The activation energy barrier to localized hopping is then contributed from both static and dynamic disorder, and depending on the particular molecular system, disorder may not always be the dominant effect. The difficulty is in extracting the disorder and polaronic parameters from experimental data.

4.5 Charge-Carrier Density Dependence of Mobility

One other key dependence of mobility is the charge-carrier concentration. Tanase *et al.* studied the hole mobility of poly(2-methoxy-5-(3',7'-dimethyloctyloxy)-p-phenylene vinylene) (OC_1C_{10}-PPV) and amorphous poly(3-hexyl thiopene) (P3HT) in diodes and field-effect transistors (FET).[101] They found that the measured hole mobility in the FET architecture is orders of magnitude bigger than that measured in a diode using the same OC_1C_{10}-PPV and P3HT material.

One possible explanation for the discrepancy between diode and FET measured mobility of the same material is a possible change in charge transport parameters because of the different device architectures.[101] For example, optical properties of OC_1C_{10}-PPV indicate that the polymer chains preferentially align along the plane of the film.[101, 102] This anisotropy could yield different disorder parameters experienced by charges injected from different field directions in a diode and FET. However, Tanase *et al.*[101] found that the mobility activation energy, which is related to the disorder σ, is equal for both diode and FET (the FET activation energy was measured for different gate voltages, and then extrapolated to zero gate bias; the activation energy at zero gate bias in the FET was equal to the diode activation energy), thereby ruling out anisotropy in disorder as a cause for the differences in mobility. Therefore, they attributed the difference between the diode and FET to a dependence of mobility on charge carrier density; the higher mobility in FET is attributed to the presence of a higher concentration of charges during typical

operation in a FET compared to a diode. The carrier concentration in the accumulation channel of a FET with an applied gate bias is orders of magnitude larger than the concentration of carriers in a diode injected with an applied bias. The mobility changes in a FET and diode can be described by the charge-carrier concentration dependence.[161] The mobility in a FET is calculated by differentiating the measured channel current I_d with respect to the gate voltage V_g:[101, 103]

$$\mu_{FET}\left(V_g\right)=\frac{\partial I_d}{\partial V_g}\frac{L}{WC_iV_d} \tag{4.18}$$

where W is the channel width, L the channel length, V_d is drain voltage, and C_i is interface capacitance. For a given gate voltage, the charge-carrier concentration can be calculated. The mobility in a diode is calculated from SCLC model fits to the measured current density versus voltage (J-V) characteristics. The charge-carrier concentration in the diode is calculated from the applied voltage.

Models for diode architectures commonly explain the temperature and field-dependent mobility with hopping in a Gaussian DOS,[3] whereas in a FET, the temperature and gate-bias-dependent mobility is described with hopping in an exponential DOS.[47] To describe the experimental diode measurements, Tanase *et al.*[101] employed the CDM model:[21]

$$\mu_{CDM}=\mu_0\exp\left[-\left(\frac{3\sigma}{5kT}\right)^2+0.78\left[\left(\frac{\sigma}{kT}\right)^{3/2}-2\right]\sqrt{\frac{qa_0F}{\sigma}}\right] \tag{4.19}$$

where σ is the width of the Gaussian DOS and a_0 is the average intersite separation. To describe the experimental FET measurements, Tanase *et al.*[101] employed the percolation model of Vissenberg and Matters:[47]

$$\mu=\frac{\sigma_0}{q}\left(\frac{\left(T_0/T\right)^4\sin\left(\pi T/T_0\right)}{\left(2\alpha\right)^3B_c}\right)^{T_0/T}p^{T_0/T-1} \tag{4.20}$$

where α is the inverse decay length of localized states, B_c is the critical bond number for percolation, p is charge density, and T_0 is the width of the exponential DOS ($g(E)=N/kT_0\exp\left[E/kT_0\right],\ E\le 0$).

Tanase *et al.*[101] explained that the exponential DOS (commonly used to describe organic FET measurements), is approximately the same to a Gaussian DOS (commonly

used to describe organic diode measurements) in the energy range of the Fermi levels corresponding to the carrier concentrations in a FET during typical operation conditions.[161] Their conclusion was that there is no inherent difference in charge transport in a diode and FET; a unified theory with a temperature, field, and charge density dependent mobility should interpret the measurements in a diode and FET as simply one in the high-field, low-charge-density and the other in the low-field, high-charge-density regimes, respectively. The gate-bias dependence of mobility in FETs is strong because of the stronger dependence on charge concentration in the low-field operation.[91] The importance of the carrier density dependence to describe polymer diode and field-effect transistor measurements was explained theoretically by Yu *et al.*[91, 93]

It is difficult to separate the individual charge density and field dependences of mobility in diodes because both the electric field and charge density increase with an applied voltage. Field-effect transistors provided a system to isolate the charge density dependence of mobility, but they typically operate at much higher charge densities. To obtain lower densities in a FET, it will have to operate at lower gate biases, which will lead to drain currents that are too small to measure accurately. To obtain higher densities in diodes, the applied voltage will have to be higher, which will lead to higher fields. In the presence of high fields, it will be more difficult to differentiate between the field and density dependence of mobility in the *J-V* curves.

Electrochemical doping is another possible route to control the density in the material, but that introduces additional effects due to the added dopant impurities.[104] To solve this problem, Snaith and Gratzel[12] introduced a method to investigate the charge density dependence of mobility in the low charge density regime. Their device architecture is a hole transport material (HTM) contacted by a molecular sensitizer. Instead of a gate voltage, the hole density in the HTM is controlled by light being absorbed by dye molecules that transfer holes to the HTM and electrons to a TiO_2 layer underneath. They[12] show that increased hole density upon illumination significantly increases the hole conductivity of the material. This observed mobility enhancement at low charge densities is significant because it shows the importance of considering the charge density dependence of mobility in organic semiconductor diodes, even when the charge density may not be as big as in FETs.

4.6 Models to Explain Charge-Carrier Density Dependence of Mobility

Coehoorn *et al.*[105] provided a very thorough study of charge-carrier concentration dependence of the hopping mobility in a Gaussian DOS. They studied the concentration dependence for the regime of low-field, average intermolecular distances much larger than the decay length of the localized states, and temperatures low enough and disorder big enough such that $\sigma/kT > 1$. They analyzed several existing semianalytical models for hopping transport and modified them and applied them for Gaussian DOS. Coehoorn *et al.*[105] compared and studied the Monte Carlo simulation results of Bässler *et al.*,[3] numerical results to the master equation (Eq. (2.5)) by Pasveer *et al.*,[106] and the models of Movaghar and Schirmacher,[32] Vissenberg and Matters,[47] Arkhipov *et al.*,[107] Martens *et al.*,[108] Baranovskii *et al.*,[54, 55] Roichman *et al.*,[109, 110] and Rubel *et al.*[57]

Coehoorn *et al.* gave brief summaries of the semianalytical hopping models they compared for the study of the charge-carrier concentration dependence of mobility.[105] The Movaghar-Schirmacher[32] model utilizes a modified effective medium approximation to derive the conductivity from the master equation. Vissenberg-Matters[47] model is based on the percolation theory formalism introduced by Ambegaokar *et al.*[34] to describe hopping in an exponential DOS. The Arkhipov *et al.*[107] model suggested that the mobility can be calculated by averaging the carrier hopping rates or by using an effective transport energy level concept. Martens *et al.*[108] extended the Mott[39] variable range hopping (VRH) formalism of hopping in a uniform DOS to the case of an arbitrary DOS. They postulated that the charge concentration dependence of mobility stems from the effects of charge concentration on the DOS and delocalization. Baranovskii *et al.*[54, 55] used the transport energy level concept to derive the mobility in a Gaussian DOS. Rubel *et al.*[57] extended this model with the use of percolation theory to include more description of the dependence of mobility on the concentration of localized states *N*. Roichman *et al.*[110] used a mean medium approximation to develop a transport model that includes the charge density dependence of mobility.

Coehoorn *et al.*[105] represent results of these models in a similar form in order to make a more direct comparison. From their comparisons of the models' predicted carrier concentration dependence and numerical results of Pasveer *et al.*,[106] they proposed the following mobility expression:[105]

$$\mu(c) \cong \frac{q\nu_0}{N_t^{2/3}kT}\Phi\exp\left[-p_0 - \ln c - \left(a - \frac{E_F}{\sigma}\right)\hat{\sigma} + \frac{d}{p_0}\hat{\sigma}^2\right] \tag{4.21}$$

where N_t is total density of hopping sites, ν_0 is attempt frequency in the Miller-Abrahams rate, c is carrier concentration, and $\hat{\sigma} = \sigma/kT$ with σ as the width of the Gaussian DOS. Φ is a dimensionless function that may depend on c, $\hat{\sigma}$, and N_t/α^3, where α is the inverse of the decay length of the localized wavefunctions. E_F is the Fermi level, and how it increases in energy as carriers fill up the DOS will depend on the width of the DOS and the temperature (E_F is dependent on c and $\hat{\sigma}$). The parameters p_0, a, and d only depend on N_t/α^3. Fitting this mobility relation to results of the various models will yield different parameter values.[105] From Eq. (4.21), the concentration dependence acts to enhance the mobility, $\mu(c) \cong \mu(0) f(c, \hat{\sigma})$.

4.7 Model to Explain Combined Temperature, Field, and Density Dependences of Mobility

Pasveer *et al.*[106] proposed a unified description of the dependence of mobility on temperature, field, and charge density in disordered polymer films.[106] They used an iteration approach similar to the one suggested by Yu *et al.*[91, 93] to solve the Master equation (Eq. (2.5)) in a lattice of Gaussian distributed random site energies with Miller-Abrahams hopping rates. From fits to the numerical plots of low-field mobility versus concentration at different temperatures,[106] they obtained the following mobility relation for temperature and charge concentration:[106]

$$\begin{gathered}\mu(T,p) = \mu_0(T)\exp\left[\frac{1}{2}\left(\hat{\sigma}^2 - \hat{\sigma}\right)\left(2pa^3\right)^\delta\right], \\ \mu_0(T) = \mu_0 c_1 \exp\left[-c_2\hat{\sigma}^2\right], \\ \delta \equiv 2\frac{\ln\left(\hat{\sigma}^2 - \hat{\sigma}\right) - \ln(\ln 4)}{\hat{\sigma}^2}, \quad \mu_0 \equiv \frac{a^2\nu_0 q}{\sigma}, \quad \hat{\sigma} \equiv \frac{\sigma}{kT}\end{gathered} \tag{4.22}$$

where $c_1 = 1.8\text{x}10^{-9}$, $c_2 = 0.42$, a is the lattice spacing, σ is the width of the Gaussian distribution used to randomly assign site energies, and $p = \langle P_i \rangle / a^3$ is the density of

charge-carriers. They remarked that the parameterization is satisfactory for densities that aren't too high and will fail at densities approaching $0.5/a^3$.

From fits to numerical plots of mobility versus field at different temperatures and at low density,[106] they obtained an approximate mobility relation with decoupled field and density dependences:[106]

$$\mu(T,p,F) \approx \mu(T,p) f(T,F)$$
$$f(T,F) = \exp\left[0.44\left(\hat{\sigma}^{3/2} - 2.2\right)\left(\sqrt{1+0.8\left(\frac{qaF}{\sigma}\right)^2} - 1\right)\right] \quad (4.23)$$

Their parameterization was optimized from fits to numerical plots for low density, but is able to fit numerical plots for high density as well.[106]

4.8 Doping Dependence of Mobility

Doping a semiconductor with donor or acceptor impurities will increase the available charge-carriers to conduct current. The simplest way to model doping is to make it equivalent to just varying the concentration of charges (*e.g.*, increasing the Fermi level and density of free carriers in conduction band). These charges are not injected with the applied voltage, and hence, for a given voltage, the current density should be higher for higher dopant concentration. The specific process of doping in disordered organic semiconductors, however, will contribute other effects other than just increasing the carrier concentration.[111, 112]

To explain the doping dependence of mobility, Arkhipov and co-workers invoked a Coulombic trap effect.[104, 113, 114] They proposed that ionized dopants in disordered organic semiconductors create Coulomb potential centers that strongly interact with the charge-carriers localized at hopping sites. These interactions increase energetic disorder by creating additional deep Coulombic traps in the DOS. Therefore, although doping adds more charge-carriers into the disordered organic system to increase the Fermi level, the creation of additional deep trap states will broaden the deep tail of the DOS to counteract the shift in Fermi level. They developed an analytic model describing carrier mobility in weakly and heavily doped disordered organic semiconductors and fit experimental data of electrochemically doped polythiophenes.[104] They explained the

differences of doping dependence of mobility employing field-effect and electrochemical doping processes. The field-effect doping dependence increases monotonically with concentration because field-effect doping does not introduce ionized dopant centers to create Coulomb traps. The observed electrochemical doping dependence (decrease in mobility at low dopant levels followed by steep increase) is explained by the fact that for low dopant levels, the addition of free carriers is not enough to balance the addition of deep Coulomb traps, but eventually, for high dopant concentrations, the Coulomb traps smooth out and their activation energies decrease. Indeed, Weise *et al.*[115] conducted thermally stimulated current (TSC) measurements to probe the energetic distribution of traps for the system of 4,4',4''-tris(N-(1-naphthyl)-N-phenylamino)triphenylamine (1-NaphDATA) doped in N,N'-di(1-naphthyl)N,N'-diphenylbenzidine (α-NPD). A trap depth corresponding to the HOMO energy level difference between dopant and matrix molecules is seen for low doping concentrations.[115] However, at higher dopant concentrations, the deep traps seem to disappear in the measurements.

Martens *et al.*[108] developed a model based on a variable range hopping (VRH) theory. They proposed that the effect of increasing charge-carrier concentration is to shift the Fermi level up, increase the number of available states since DOS increases with energy, and increase the size of the localized region. The effect of doping not only increases the charge-carrier concentration but is postulated to also introduce doping-induced states near the Fermi level that will increase the conductivity. Assuming these effects are dominant, Martens *et al.*[108] derived a concentration-dependent VRH conductivity $\sigma(c)$ in a disordered system with arbitrary DOS $g(E)$ and a volume V_0 of the localized region. They fit their theory to experimental data of iron(III) chloride-doped PPV (FeCl3-doped PPV). Mott's law of 3D VRH between localized states in a constant DOS,[39] $\sigma(T)=\sigma_0 \exp\left[-(T_0/T)^{1/4}\right]$, is obeyed for low enough temperatures in doped conjugated polymers.[108] Indeed for low enough temperatures, the Martens *et al.* model retrieves Mott's expression (including concentration dependence and an exponential factor):[108]

$$\sigma=\sigma_0(c)e^{\alpha A(c)}\exp\left[-\left(T_0(c)/T\right)^{1/4}\right] \tag{4.24}$$

where c is the charge-carrier concentration, α is the inverse decay length of the localized wavefunctions, and $\sigma_0(c)$ is a concentration-dependent prefactor. The concentration affects the DOS in T_0 and the localization region size in A. Therefore, concentration dependence of mobility originates from the concentration dependence on E_F, A, T_0, and σ_0. To obtain Eq. (4.24), Martens *et al.*[108] made the approximation $g(E_F)-g(E)\approx(E-E_F)g'(E_F)$ in their general analytical result of VRH conductivity in arbitrary DOS.

4.9 Bulk-limited Current Conduction in Organic Semiconductors using Modified Temperature, Field, Density-Dependent Mobility Expression

4.9.1 Field-Dependent Mobility in SCLC

Bulk-limited current models for transport in organic semiconductors have included space-charge limited (SCL) and trapped-charge limited (TCL) models. For a prominent field and temperature dependent charge-carrier mobility,[3, 79, 116-118] as is the case for disordered organic semiconductors (see Eq. (4.2)), the SCL current is calculated using modified field-dependent charge-carrier mobility relations,[75-77, 119-122] including Poole-Frenkel, $\mu(F)=\mu(0)\exp\left[\gamma\sqrt{F}\right]$,[75, 120] and power-law, $\mu(F)=\mu(0)(F/F_0)^n$,[121] field dependences.

Blom *et al.*[75] described the hole conduction in poly(paraphenylene vinylene) (PPV) using an SCLC model with a field-dependent mobility. The SCL current density is given by:[10, 75]

$$J=q\mu(F)p(x)F(x)=q\mu(F)\left[\frac{q}{\varepsilon}\frac{dF}{dx}\right]F(x)$$
$$V=\int_0^L F(x)dx \tag{4.25}$$

where $p(x)$ is the hole density, $F(x)$ is the field as a function of x, L is the thickness of the organic semiconductor, and the mobility is taken to have the following relation:[75]

$$\mu(F)=\mu(0)\exp\left[\gamma\sqrt{F}\right]$$
$$\mu(0)=\mu_0\exp\left[-\frac{\Delta}{kT}\right] \qquad (4.26)$$
$$\gamma=B\left(\frac{1}{kT}-\frac{1}{kT_0}\right)$$

Using Eqs. (4.25) and (4.26), theoretical fits to experimental data of current density versus voltage measurements of PPV with an indium-tin oxide (ITO) anode and gold (Au) cathode were made.[75]

Campbell *et al.*[122] fit *J-V* curves using an SCLC model with modified hopping mobility of the GDM[3] relation in Eq. (4.14) and the mobility relation of Gill[81] in Eq. (4.2).

4.9.2 Charge-density Dependent Mobility in SCLC

Tanase *et al.*[123] utilized a space-charge-limited current (SCLC) model with a charge density-dependent mobility to describe the current density versus voltage (*J-V*) characteristics of OC_1C_{10}-PPV hole-only diodes. Tanase *et al.* assumed the following field-independent and density-dependent mobility relation derived from the Vissenberg-Matters[47] percolation model:[123]

$$\mu(p,T)=\mu(0,T)+\frac{\sigma_0}{q}\left(\frac{\left(\frac{T_0}{T}\right)^4\sin\left(\pi\frac{T}{T_0}\right)}{(2\alpha)^3 B_c}\right)^{T_0/T} p^{\frac{T_0}{T}-1} \qquad (4.27)$$

where p is the hole charge density, σ_0 is a conductivity prefactor, α is the inverse decay of localized states, and $B_c = 2.8$ is a critical average bond number for percolation. The first term is the hole mobility for very low charge densities; it is fit to the low bias region of the experimental *J-V* curves with the conventional SCLC model. The second term is derived from the mobility relation theoretically calculated by Vissenberg and Matters[47] for low-field, high carrier density in exponential DOS with characteristic width T_0. The justification for exponential DOS is that for high carrier densities, the Fermi level will be in the energy range of the tail of the Gaussian DOS that can be well approximated as an exponential.[101] The SCL current is given by, $J=q\mu(p)p(x)F(x)$, and is numerically

solved with Eq. (4.27) and Poisson's equation, $qp(x) = \varepsilon\, dF/dx$. Tanase *et al.*[123] were able to fit the *J-V* characteristics of OC_1C_{10}-PPV at room temperature using the SCLC model with only a density-dependent mobility.[123]

Ramachandhran *et al.*[124] derived the following analytic expression for the diode current-voltage relation using the charge-density-dependent mobility form, $\mu = an^b$, where a is a material and temperature dependent prefactor, $b = (T_0/T) - 1$, and T_0 is the width of the exponential DOS:[124]

$$J = a\varepsilon \left(\frac{\varepsilon}{q}\right)^b \frac{(b+1)^{b+1}(2b+3)^{b+2}}{(b+2)^{2b+3}} \frac{V^{b+2}}{d^{2b+3}} \tag{4.28}$$

4.9.3 Field and Charge-density Dependent Mobility in SCLC

Using their unified temperature, field, and charge density dependent mobility expression (see Eqs. (4.22) and (4.23)), Pasveer *et al.*[106] fit experimental current density-voltage characteristics for NRS-PPV and OC_1C_{10}-PPV polymer films using an SCLC model employing their mobility relation.[106] The space-charge-limited current density is calculated from:[106]

$$\begin{aligned} J &= q\mu(T, p(x), F(x))\, p(x) F(x) \\ \frac{dF}{dx} &= \frac{q}{\varepsilon} p(x) \\ V &= \int_0^L F(x)\, dx \end{aligned} \tag{4.29}$$

where L is the thickness of the polymer film. They show that by including both field and density-enhanced mobility, the current density versus voltage characteristics of polymer films can be explained with this mobility enhancement in an SCLC model.

Chapter 5 – Percolation Model for Bulk-limited Transport in Amorphous Organic Semiconductors

5.1 Introduction

Disordered organic semiconductors are comprised of molecules held together by weak van der Waals bonds. As a result, charge transport in films of organic semiconductors is dominated by disorder and localization. Initial studies of charge transport in organic semiconductors focused on the charge-carrier mobility, in particular, the field dependence that seems to follow a $\log \mu \propto \sqrt{F}$. This experimentally observed field dependence of mobility has been termed 'Poole-Frenkel' even though the source of the field dependence may not be Poole-Frenkel. Numerical simulations of charge hopping in a disordered lattice with Gaussian distributed site energies (GDM)[3] and/or spatially correlated site energies (CDM)[21] have reproduced the same observed field dependence of mobility; some of these simulations reproduced the 'Poole-Frenkel' field dependence without considering polaronic effects, suggesting that the field-dependent behavior of mobility is mainly due to static site energies disorder. Analytic theories for 1D hopping in correlated site energies have also yielded a $\log \mu \propto \sqrt{F}$ relation.[19, 91] Aside from the field dependence of mobility, the charge-carrier concentration dependence is also important. Realizing the importance for a full, unified description of mobility, Pasveer *et al.*[106] numerically solved the master equation and fit the full temperature, electric field, and concentration dependent mobility relation by parameterizing numerical plots. Although parameterizing numerical solutions and computer simulations gives a general mobility relation trend, the various parameterizations and constants introduced usually do not have an obvious physical origin (that can be extracted with measurements from independent experiments), thereby, making it difficult to link physical microscopic processes that are the predominant cause for experimentally observed macroscopic properties. Simulations of random walks of hopping carriers in a localized density of states provide useful insights on transport details (how individually varying specific input parameters on a microscopic scale will affect certain transport behaviors macroscopically; or how

invoking specific microscopic mechanisms modeled in simulations will translate into macroscopic behavior observed in simulation results), but they usually do not provide a general physical description the summarizes the dominant transport phenomenon.

In this chapter, an analytic theory for hopping transport that gives a unified description for the full temperature, electric field, and charge density dependence of the charge-carrier mobility is presented. The simple theory is verified with experimental data. An archetypical amorphous organic semiconductor, tris(8-hydroxyquinoline) aluminum (Alq_3), was chosen, where the electronic states are completely localized, and hopping transport is believed to be the dominant mechanism over the range of experimental parameters tested. Only three physical parameters (the width of the localized density of states, exponential decay length of the localized electronic wavefunctions, and maximum conductivity) are required in the analytic model to match the current density versus voltage (*J-V*) characteristics over many orders of magnitude of current from room temperature to T = 100K. The model is fit to mobility data as well, over a wide range of electric fields and temperature.

5.2 Theory

5.2.1 Background

The theory introduced in this chapter is based on a percolation model. One of the first models utilizing percolation theory to analyze the hopping conductivity in disordered systems was by Ambegaokar *et al.*[34] and later applied by Vissenberg and Matters[47] for the case of an exponential DOS to describe the charge-carrier mobility in thin-film transistors of amorphous organic semiconductors. The theory introduced in this chapter extends the percolation model presented by Vissenberg and Matters[47] to include the effects of an applied electric field. Li *et al.*[125] also employ percolation theory to study the effect of extrinsic traps on the hopping transport in organic semiconductors.

Charge-carrier hopping motion between localized states can be described by the kinetics master equation:

$$I_{ij} = q\left[W_{ij}P_i\left(1-P_j\right)-W_{ji}P_j\left(1-P_i\right)\right] \tag{5.1}$$

where I_{ij} is the net current flow of charges from donor site i to acceptor site j, W_{ij} is the hopping rate of a charge from site i to j, and P_i is the occupational probability of a charge on site i. It is assumed that one charge occupies the energy state E_i (LUMO state of organic molecule) at site i at a time.

5.2.2 Zero-Field Limit

For small electric fields, the conductance between donor and acceptor can be written as:

$$G_{da} = G_0 \exp[-s_{da}] \tag{5.2}$$

where $G_0 = q\nu_0/kT$ and from incorporating Miller-Abrahams rates (Eq. (2.6)), the following is obtained:[33, 47]

$$s_{da} = 2\alpha r_{da} + \frac{|E_d - E_F| + |E_a - E_F| + |E_d - E_a|}{2kT} \tag{5.3}$$

The average number of bonds, B, is the density of bonds divided by the density of sites that form bonds in the disordered hopping material. The density of bonds formed at the percolation threshold is given by:[47]

$$N_b = \int d^3 r_{da} \int dE_d \int dE_a g(E_d) g(E_a) \theta(s_c - s_{da}) \tag{5.4}$$

where r_{da} is integrated over the entire 3D space of the material, $g(E)$ is the density of states (DOS) of the material, θ is the Heaviside unit step function, and s_{da} is the exponent of the conductance between donor and acceptor sites, $G_{da} = G_0 \exp[-s_{da}]$. At the first instance of infinite cluster formation (first occurrence of percolation), the density of bonds satisfies the relation: $B_c = N_b/N_s$, where N_s is the density of sites forming bonds and B_c is the critical number of average bonds that corresponds to the percolation threshold. For a three-dimensional amorphous system, this critical average number of bonds is $B_c \simeq 2.8$.[38, 47, 48]

The density of states per unit energy and volume is taken to follow an exponential distribution:[11, 47]

$$g(E) = \frac{N_0}{kT_0} \exp[E/kT_0], \quad -\infty < E \le 0 \tag{5.5}$$

where N_0 is the total density of states per unit volume (molecular density in the disordered organic semiconductor material) and T_0 is the characteristic temperature that corresponds to the width of the exponential distribution. The particular choice for the DOS does not have to be an exponential, but experimental measurements of the DOS in undoped amorphous organic films using high lateral Kelvin probe force microscopy (KPFM) have shown an exponential-like tail distribution.[126] Note that the exact functional dependence of the DOS is not crucial in the results as long as it increases strongly with energy. Although, an exponential function is convenient in that the results for conductivity can be solved analytically.

The density of sites forming bonds in the infinite cluster is given by:[47]

$$N_s = \int dEg(E)\theta(s_c kT - |E - E_F|) \tag{5.6}$$

where $E_{max} = E_F + s_c kT$ is the maximum possible energy of a donor site that can form a bond to an acceptor site (a bond is defined as a link between two sites where the conductance is greater than or equal to the critical conductance, $G_{da} \geq G_c$). Only sites with energies between $s_c kT$ from the Fermi energy E_F form bonds in the infinite cluster at the percolation threshold, as calculated in Eq. (5.6).

Since the density of states $g(E)$ is assumed to increase strongly with energy, the dominant contribution to integral for the density of bonds (Eq. (5.4)) comes from high energies. Hence, the current is dominated by contributions from carriers in sites with energies approaching the maximum E_{max}. For an exponential DOS in Eq. (5.5), the dominant contribution is from E_{max}, given the condition, $|E_{max} - E_F| \gg kT_0$.

From Eq. (5.3), the critical donor energy, E_c, of a site that can participate in bond formation for a given intersite distance r_{da} is:[47]

$$E_c = E_F + (s_c - 2\alpha r_{da})kT \tag{5.7}$$

where the maximum bond energy is E_{max} (the critical donor energy taken in the limit $r_{da} \to 0$). Sites participating in longer bonds have energies less than those of sites participating in shorter bonds. For the maximum hopping distance of $r_{max} = s_c/2\alpha$, Eq. (5.7) yields $E_c = E_F$.

5.2.3 Zero-Temperature Limit

The critical donor energy given in Eq. (5.7) is in the zero-field limit ($F = 0$). In the zero-temperature limit ($T = 0$), there is no thermally-activated hopping in energy. Consequently, hopping is through tunneling and the conductivity between two sites is $G = G_0 \exp[-s_{da}]$ with $G_0 = q\nu_0$ and $s_{da} = 2\alpha r_{da}$. The critical site energy satisfies the relation:

$$f(E_c)\exp[-2\alpha r_{da}] = \exp[-s_c] \tag{5.8}$$

where $f(E)$ is the occupational probability at energy E and the acceptor sites are assumed to be approximately empty. Because there is no thermal excitation at $T = 0$, carriers at sites with energy E_{max} must be excited by the electric field. Therefore, sites at E_{max} must participate in bonds of length $r_{da} > 0$. It follows that, for short bonds, the maximum acceptor energy cannot be less than E_{max} (see Figure 5-1). The maximum acceptor energy is for bonds formed parallel to the electric field. Therefore, for carriers at sites close to energy E_{max}, the critical energy at the percolation threshold is:

$$E_c = E_{max} - q r_{da} F \tag{5.9}$$

Eqs. (5.8) and (5.9) yield an occupational probability function $f(E_c)$ of the form $C\exp[-E_c/kT_F]$, where $kT_F = qF/2\alpha$, identical to the result of Shklovskii.[127] The constant C is approximated by extrapolating the exponential distribution to the Fermi energy (i.e., $f(E_F) \to 1$):

$$f(E_c) = \exp[-(E_c - E_F)/kT_F] \tag{5.10}$$

Therefore, in the zero-temperature limit, the critical energy is given by:

$$E_c = E_F + (s_c - 2\alpha r_{da})kT_F \tag{5.11}$$

The maximum donor energy is obtained in the limit $r_{da} \to 0$, $E_{max} = E_F + s_c kT_F$. At the maximum bond distance, $r_{max} = s_c/2\alpha$, $E_c = E_F$.

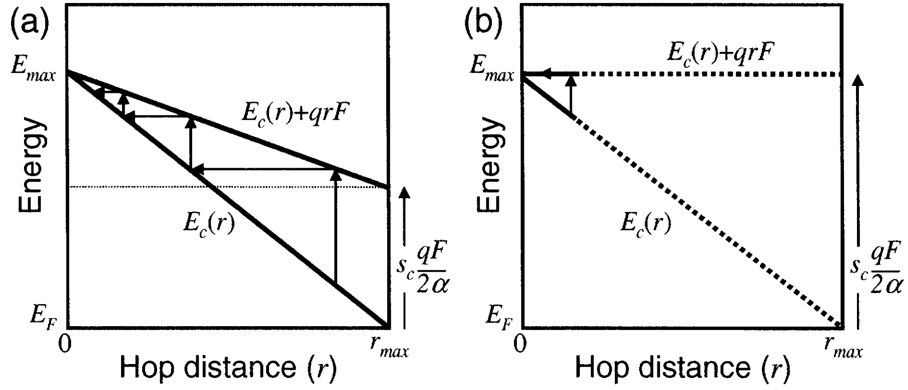

Figure 5-1:[80] Plots of maximum donor and acceptor energies to form bonds as a function of intersite hopping distance r. Vertical transitions represent hops from a donor to acceptor. Once a charge-carrier hops into an acceptor site, a horizontal transition is made so that the acceptor becomes a donor for a subsequent hop. At $T = 0$, the maximum acceptor energy for bond formation is $E_c(r)+qrF$. In (a), the donor distribution $f(E_c) \sim \exp[-E_c/kT_F]$ is assumed with $kT_F > qF/2\alpha$. Since the maximum acceptor energy to form a bond decreases with r, it takes an infinite number of hops for a carrier to reach E_{max}. Since the occupation fraction at E_{max} is non-zero, it follows that $E_c(r)+qrF = E_{max}$ and $kT_F = qF/2\alpha$ for small r, as shown in (b). Extrapolating to E_F, the distribution is $f(E_c) = \exp[-(E_c - E_F)/kT_F]$. From Limketkai, Jadhav, and Baldo (2007).[80]

5.2.4 Non-Zero Temperature and Electric Field

For non-zero temperature and electric field, the thermal energy is added to the energy supplied by the electric field:[87]

$$E_c = E_F + (s_c - 2\alpha r_{da})k(T + T_F) \tag{5.12}$$

The conductance between donor and acceptor sites is $G = G_0 \exp[-s_{da}]$, where s_{da} has some form that describes the hopping conductivity between two sites at non-zero temperature and electric field. Although the exact function for s_{da} is unsure, only the maximum bond energy is needed to calculate the bond number (the percolation criterion). The maximum bond energy for both the zero-field and zero-temperature cases was found from s_{da}. For non-zero temperature and field, the maximum energy of a donor site that can participate in bond formation for a given intersite distance r_{da} (Eq. (5.12)) is found by

adding the maximum thermal and field energies in the two limiting cases of zero field and temperature, respectively.

From Eq. (5.12), the maximum energy is $E_{\max} = E_F + s_c k(T + T_F)$. Therefore, the total density of sites that participate in bond formation for non-zero temperature and field is:

$$N_s = \int dE g(E)\theta\left(s_c k(T+T_F) - |E - E_F|\right) \tag{5.13}$$

The density of bonds is given by:

$$N_b = \int d^3 r_{da} \int dE_d \int dE_a g(E_d) g(E_a + \Delta_{da}) \theta(s_c - s_{da}) \tag{5.14}$$

where Δ_{da} is the energy shift due to an applied electric field. The electric field distribution between donor and acceptor sites forming bonds is assumed to be approximately constant, i.e., $r_{\max} dF/dx \ll F(x)$. Using Eqs. (5.5) and (5.12) to solve Eqs. (5.13) and (5.14), the critical average number of bonds is given by:

$$B_c = \frac{N_b}{N_s} \approx 16\pi \frac{T_0^3}{(2\alpha)^3} \frac{T+T_F}{(2T+T_F)^2 (2T+3T_F)^2} n(x) \exp\left[s_c (T+T_F)/T_0\right] \tag{5.15}$$

where the DOS is assumed to increase strongly with energy such that $|E_{\max} - E_F| \gg kT_0$ and $n(x) \simeq N_0 e^{E_F/kT_0}$ is the density of charge carriers for $|E_F| \gg kT_0$ and $T + T_F < T_0$. Solving Eq. (5.15) to obtain s_c, an analytic expression for the conductivity is:

$$\sigma = \sigma_0 e^{-s_c} = \sigma_0 \left[\frac{16\pi}{B_c} \frac{T_0^3}{(2\alpha)^3} \frac{T+T_F}{(2T+T_F)^2 (2T+3T_F)^2} n(x) \right]^{T_0/(T+T_F)} \tag{5.16}$$

The charge-carrier mobility, $\mu = \sigma/qn$, as a function of charge density, electric field, and temperature is then:

$$\mu = \frac{\sigma_0}{q} \left[\frac{16\pi}{B_c} \frac{T_0^3}{(2\alpha)^3} \frac{T+T_F}{(2T+T_F)^2 (2T+3T_F)^2} \right]^{\frac{T_0}{T+T_F}} n(x)^{\frac{T_0}{T+T_F}-1} \tag{5.17}$$

5.3 Experiment

Using the continuity equation ($dJ/dx = 0$) and Poisson's equation ($qn/\varepsilon = dF/dx$), the mobility expression in Eq. (5.17) is tested against the

comprehensive study by Brütting *et al.*[79] of charge transport in the archetype small-molecular weight electron transport molecule tris(8-hydroxyquinoline) aluminum (Alq_3). Figure 5-2 shows the theoretical fits to the current density versus voltage (*J-V*) characteristics for a range of temperatures for a 300-nm-thick film of Alq_3 with calcium cathode and aluminum anode. In Figure 5-2(a), the theoretical fit assumes a built-in potential of 0.4 V.[128] The parameters used to fit the experimental curves are the disorder temperature T_0 = 450K, the inverse decay length of the electronic wavefunctions $\alpha =$ 0.58 $Å^{-1}$, and the maximum conductivity prefactor $\sigma_0 = 1 \times 10^3$ S/m, which is dependent on the intermolecular orbital overlap. As expected, σ_0 is significantly smaller in amorphous Alq_3 than polycrystalline pentacene.[47] Note that there are only three parameters used to fit the data. The extension of the percolation model of Vissenberg and Matters[47] includes the effects of an applied electric field on the charge-carrier mobility but does not introduce any additional fit parameters.

The fit in Figure 5-2(a) is best at high electric fields (where the experimental data exhibits positive curvature with increasing field). However, the theory does not fit as well for the low electric field regime (where the experimental curves exhibit opposite curvature). The discrepancy between the theoretical fits and experimental curves may be attributed to uncertainty in the built-in potential and neglect of contact impedances (which must be considered at low bias). Indeed, Brütting *et al.*[79] assumed a built-in potential V_{bi} = 0.7 V in their fits, as compared to the measured value of 0.4 V by Campbell and Smith[128] and an expected Ca-Al work function difference of approximately 1.4V. Since the mobility expression is of bulk origin, any contact effects contributing to an interface impedance is lumped into a constant voltage offset, V_{off}. Figure 5-2(b) is a fit to the bulk-only *J-V* characteristics with a compensated voltage offset V_{off} = 2V. The conductivity prefactor σ_0 was increased to 2×10^3 S/m for the corresponding fits.

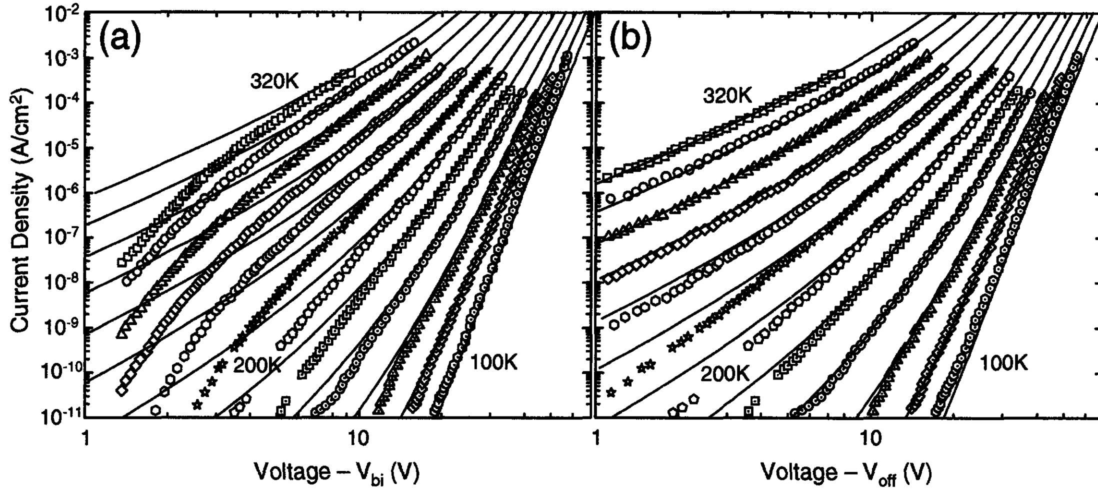

Figure 5-2:[80] Temperature dependence of the experimental *J-V* characteristics of an Al/Alq_3/Ca diode with an Alq_3 thickness of 300 nm. Data is from Brütting *et al.* (2001).[79] Solid lines are theoretical fits using Eq. (5.17). (a) The *J-V* curves were compensated by a built-in potential of V_{bi} = 0.4 V,[128] and fit to theory. (b) *J-V* curves were offset by a voltage V_{off} = 2 V to compensate for uncertainty in V_{bi} and the contact resistances, and then fit to theory. From Limketkai, Jadhav, and Baldo (2007).[80]

The fits to the experimental *J-V* curves demonstrates that Eq. (5.17) accurately models the bulk electron mobility in Alq_3. Equation (5.17), however, contains no explicit Poole-Frenkel field dependence. To examine the electric field dependence of mobility, the analytic expression for mobility is plotted against $\sqrt{F}$ in Figure 5-3 and compared against experimental data obtained from transient electroluminescence measurements.[79] Predictions from the steady-state model and transient measurements of drift velocity are not strictly comparable since mobility depends on the charge-carrier density. Since the charge density is uncertain in transient measurements, the measured mobility data is fit to theory assuming a charge density n = 2 x 10^{18} cm^{-3}. Both theory and experiment reproduce the 'Poole-Frenkel' behavior for a range of electric fields.

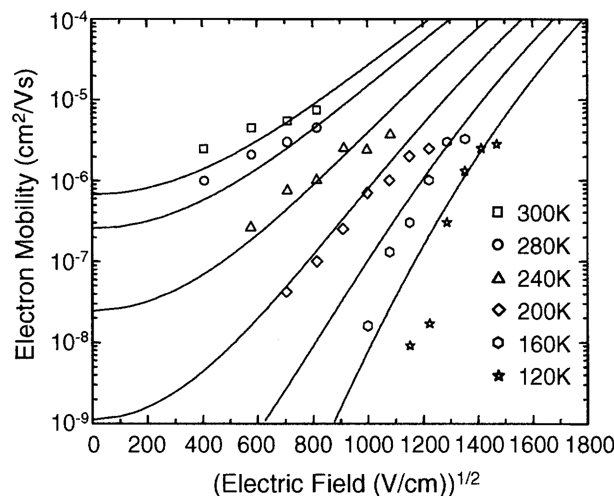

Figure 5-3:[80] Temperature and electric field dependence of charge-carrier mobility obtained from transient electroluminescence measurements.[79] Solid lines are theoretical fits using Eq. (5.17). From Limketkai, Jadhav, and Baldo (2007).[80]

5.4 Conclusion

In conclusion, an analytic theory for charge-carrier hopping transport has been formulated based on a percolation model. The theory is tested against bulk disordered amorphous organic semiconductors, which is believed to be a hopping system with completely localized states. The electric field dependence of the charge-carrier mobility is found to be well-modeled by an effective temperature. The dominant effect of the electric field is to increase the effective temperature, thereby generating a non-equilibrium charge distribution.

The bulk mechanism for transport was analyzed by reducing any contact impedances at the electrode-organic interface, thus making it negligible compared to the bulk resistance. This can be achieved with a device structure having a thick single layer organic with ohmic contacts. A theory for the bulk mechanism of electrical transport was then developed to characterize the bulk properties of organic semiconductors such as the charge-carrier mobility. With this description for the bulk transport, the injection mechanism can be extracted by subtracting any bulk effects from experiments that vary the contact materials. From this, it will be possible to develop a general theory that encompasses the mechanisms for transport (injection and bulk) in organic semiconductors.

5.5 Discussion

There has been previous work on the concept of field-induced effective temperature.[87, 127, 129-133] Shklovskii[127] derived a high-field conductivity expression by substituting temperature in the low-field conductivity expression $\sigma(T)$ with an effective temperature $T_{\text{eff}} = qF/2\alpha k$, $\sigma(T_{\text{eff}})$. Arkhipov *et al.*[133] derived an expression for effective temperature and used the analytical results to compare to experimental data of boron and phosphorous-doped *a*-Si:H. They pointed out that the effective temperature expression depends on the DOS function. The effective temperature $T_{\text{eff}}(T,F)$ as a function of field and temperature for an arbitrary algebraic DOS function, $g(E) = g_0\left[(E-E_F)/E_0\right]^{\lambda}$, $-1<\lambda<\infty$, is given by:[133]

$$T_{\text{eff}}(T,F) = T\left[\frac{4-(4+\lambda)f^{2+\lambda}-(5+\lambda)f^{3+\lambda}+(2+\lambda)f^{4+\lambda}+(3+\lambda)f^{5+\lambda}}{4\left(1-f^2\right)^2}\right]^{1/(1+\lambda)} \tag{5.18}$$

where $f = qF/2\alpha kT$. Field and temperature dependences of simulation results of transport in exponential DOS are found to be able to be parameterized by a single effective temperature expression given by:[130-132]

$$T_{\text{eff}}(T,F) = \sqrt{T^2 + \left(\beta\frac{qF}{2\alpha k}\right)^2} \tag{5.19}$$

Arkhipov *et al.*[133] pointed out that various values obtained for the parameter β for different DOS distributions and transport processes (dispersive and equilibrium hopping) suggests that there is no universal effective temperature that is applicable for all DOS and transport processes in disordered hopping systems.

Although the field and temperature dependence of conductivity in Eq. (5.16) cannot be parameterized entirely in terms of a single effective temperature T_{eff}, the temperature and field dependence is dominated by the exponent $T_0/(T+T_F)$. Therefore, the effective temperature derived from the percolation-based bulk theory gives a linear sum:

$$T_{\text{eff}} = T + \frac{qF}{2\alpha k} = T + T_F \tag{5.20}$$

This linear combination of T and T_F differs from previous work[130-133] which instead employed an effective temperature of the form:

$$T_{\text{eff}} = \sqrt{T^2 + \beta T_F^2} \tag{5.21}$$

To compare these approaches for the amorphous organic semiconductor material, Alq_3, the mobility data of Brütting *et al.*[79] is plotted under the two transformations of Eqs. (5.20) and (5.21) in Figure 5-4.

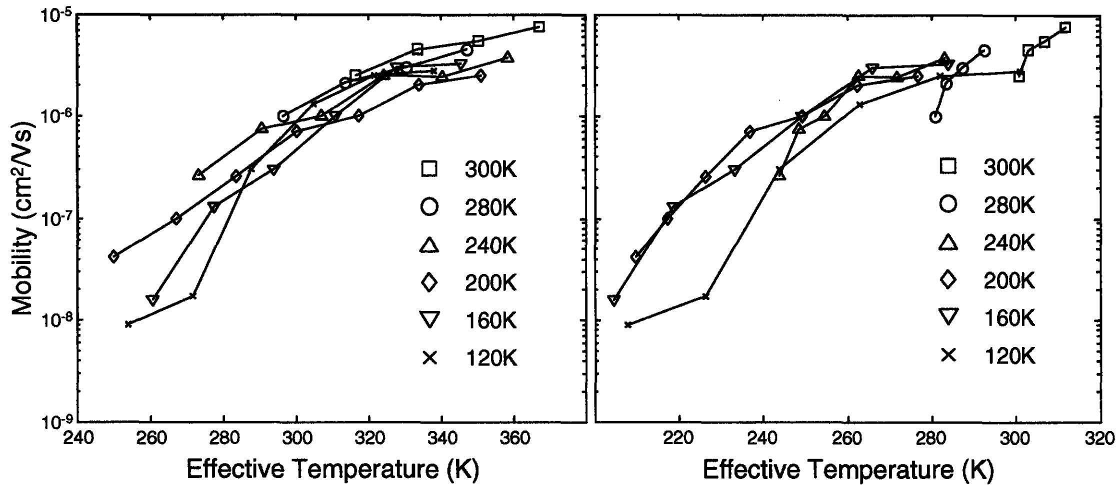

Figure 5-4: Mobility data[79] under two effective temperature transformations. In the left plot, the transformation employs Eq. (5.20), and the right plot employs Eq. (5.21). The parameter values are $\alpha \approx 0.58$ Å^{-1} and $\beta \approx 1.6$.

From Figure 5-4, it is shown that the linear combination transformation is more precise for the high temperature, low electric field data. When $T_F \ll T$, the sum of squares transformation deviates from the universal trend. Therefore, for the amorphous organic semiconductor material system, a linear sum of the effective temperature is a more accurate description.

Chapter 6 – Injection-limited Transport in Amorphous Organic Semiconductors

6.1 Introduction

Charge injection theories describe the physics of the injection of charge-carriers across the metal-semiconductor interface. If the injection interface is more resistive than the bulk of the film, then the current-voltage characteristics will be determined by injection theories. A lot of theories used to describe the injection current are based on two conventional charge injection models in covalently-bonded semiconductors, thermionic emission and tunneling. To properly model charge injection into organic semiconductors, the effects of disorder and localization are considered.

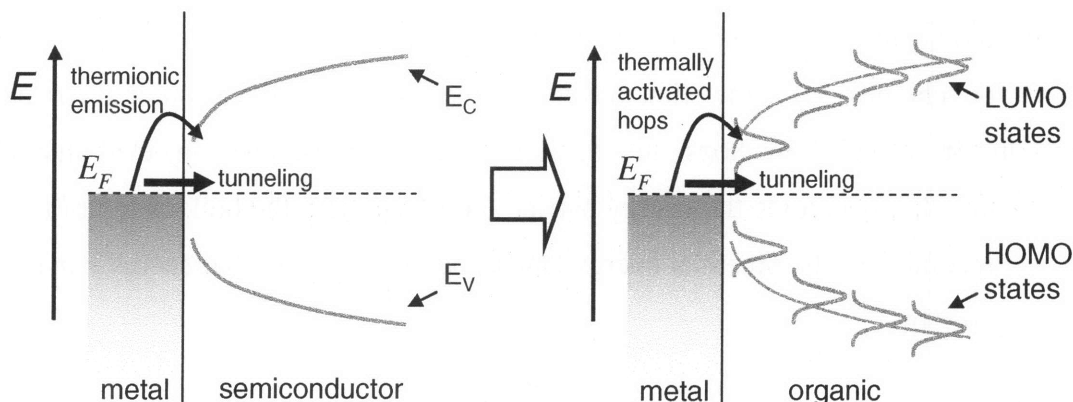

Figure 6-1: Left: Band diagram of metal-semiconductor device structure. Current injection occurs through thermionic emission and tunneling. Right: Energy diagram of metal-organic device structure when effects of disorder and localization are included. Current injection occurs through thermally activated hops and tunneling.

6.2 Modeling Localization and Disorder for Injection

Most models successfully explaining charge transport behavior in disordered organic semiconductors have been based on the formalism of a random walk of hopping charges within a Gaussian distribution of localized energy states.[3] The same principle of charge hopping into a distribution of localized states should also be considered for the

case of charge injection into disordered organic solids.[7, 9, 134] Abkowitz *et al.*[135] developed an injection model of thermally-assisted tunneling from carriers at the Fermi level of the metal to localized states in the semiconductor. Gartstein and Conwell[8] used Monte Carlo simulations to describe emission-limited injection into an energetically disordered insulator. Their model states that due to energetic disorder, most of the incoming charges will populate the tail of the DOS in the insulator layer close to the metal contact. The injection of charges further into the insulator is then determined by these charges jumping over an energy barrier created by the image-charge potential and energetic disorder. Their simulations calculate the probability for the charges in the interface layer to escape into the bulk and not return to the metal contact and recombine. From simulations, Gartstein and Conwell[8] demonstrated that energetic disorder increases the non-linearity of the thermal injection of carriers and enhances the field dependence of injection.[8, 136]

Arkhipov and coworkers[7, 9, 134] modeled the initial injection step from the Fermi level of the metal to the first layer of the energetically disordered material. Arkhipov *et al.*[7] presented an analytic theory for this model, where injection current is determined by injection of charges into the first layer of the energetically disordered organic semiconductor followed by hops into the bulk. The charges, once injected into the organic, can either overcome the energy barrier and escape into the bulk or return to the metal and recombine. The potential energy landscape that describes the energy barrier to escape is given by:[7]

$$U(x,E) = \Delta - \frac{q^2}{16\pi\varepsilon x} - qFx + E \qquad (6.1)$$

where x is the distance from the metal contact surface, E is the energy of the localized hopping sites (whose energy distribution is a Gaussian), F is the applied field, and Δ is the energy difference between the Fermi level of the metal contact and the center of the Gaussian DOS. After a charge injects into the Gaussian DOS in the interfacial layer, the escape probability into the bulk is determined by the drift and diffusion within the potential landscape described by Eq. (6.1). This probability is modeled with the one-dimensional Onsager escape probability[137] in the presence of disorder in energy E.[7] From their analytic theory, they solved for the injection current as a function of electric field, temperature, and energetic disorder width of the DOS:[7]

$$J = q\nu_0 \int_a^\infty dx_0 \exp[-2\gamma x_0] w_{esc}(x_0) \int_{-\infty}^\infty dE' \,\mathrm{Bol}(E') g[U_0(x_0) - E'] \qquad (6.2)$$

where w_{esc} is the escape probability for a charge to avoid surface recombination, a is the distance from the electrode surface to the first hopping site in the semiconductor interfacial layer, γ is the inverse localization radius, $\mathrm{Bol}(E)$ is the Boltzmann occupation statistics, $\nu_0 \exp[-2\gamma x_0]$ is the tunneling rate, $g(E)$ is the Gaussian DOS, and the electrostatic potential energy (energy barrier from electrode Fermi level to center of Gaussian DOS lowered by field F and image potential) a distance x_0 from the electrode surface is:[7]

$$U_0(x_0) = \Delta - \frac{q^2}{16\pi\varepsilon x_0} - qFx_0 \qquad (6.3)$$

Wolf *et al.*[9] conducted Monte Carlo simulations of this model of charge-carrier hopping injection from a metal into a random organic solid. In their simulations, the organic dielectric is modeled as a cubic lattice of 170 x 170 x 20 hopping sites, where the site energies are randomly chosen from a Gaussian distribution with standard deviation σ. They included the effect of image charges and an applied field on the site energy distributions in the organic semiconductor. Miller-Abrahams[13] rates are used to describe hopping of charges between sites in the organic and also from the Fermi level in the metal into a site in the organic. After the initial hop from the metal Fermi level to the organic, the charges are simulated to hop within a 5 x 5 x 5 surrounding lattice. The energy levels of metal sites are assigned to the Fermi energy of the metal, E_F. The charge will hop somewhere within this lattice, and can either recombine back into the metal or hop farther layer into the bulk. The process is repeated in the simulation for all these charges; for charges that have reached the ninth layer, they are considered to be dissociated. Simulation results of Wolf *et al.*[9] yielded similar temperature dependence as experimentally measured charge injection currents for amorphous Alq_3 film with Mg:Ag cathodes by Barth *et al.*[138]. The Monte Carlo simulations and analytical results of this model are compared by Arkhipov *et al.*[134]

Therefore, with the inclusion of the two main properties (localization of hopping sites and energetic disorder) in amorphous organic semiconductors, the temperature and

field dependence of charge injection can be understood from the analytic theory and the Monte Carlo simulations of this model.[7, 9, 134]

6.3 Interfacial Trap Model for Charge Injection

6.3.1 Introduction

The current-voltage characteristics of electron injection from metals into organic semiconductors have often been observed to follow a power law, $J \sim V^m$.[11, 139] To explain this power-law behavior for the injection current, Baldo *et al.*[139, 140] proposed an injection model shown in Figure 6-2. In this model, there is a spatial dependence of the energetic disorder width, where the strongest disorder is near the interface because of the additional interfacial disorder contributions (additional disorder contributions from interface dipoles and image potential that get randomized from the rough metal-organic interface morphology).

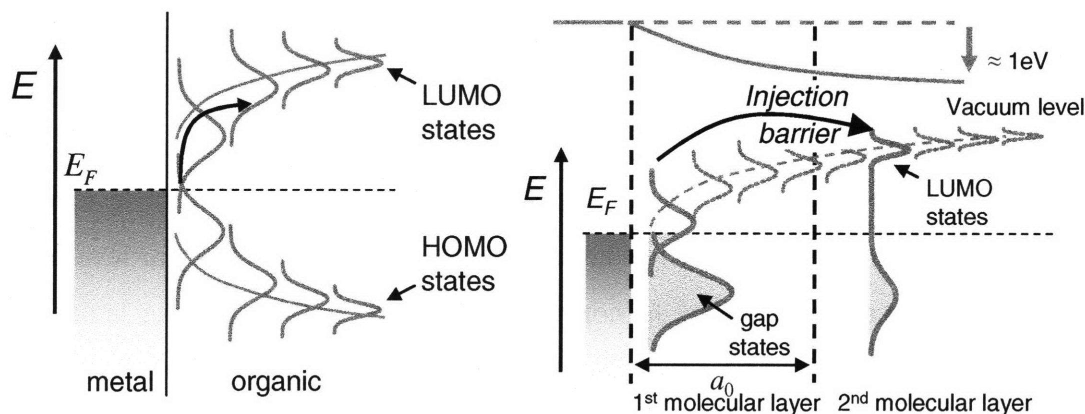

Figure 6-2: Left:[1] Simple picture of broadened interface DOS. The bulk disorder is narrower than the interfacial disorder. From Baldo (2004).[1] Right:[140] Model of interface between metal contact and doped organic semiconductor. The metal-organic chemistry dopes the organic semiconductor and form filled gap states (between LUMO and HOMO levels). Inhomogeneous image potential and dipoles at the interface broaden the interfacial DOS. From Limketkai and Baldo (2005).[140]

Therefore, the broad interfacial DOS effectively form traps for injected charge. Similarly to TCL model, current is limited by traps, except these traps do not limit bulk conduction but are interfacial traps limiting injection current. The model assumes that the most difficult and relevant hop to the injection current is the hop from the first molecular

layer to the second. Since the interface disorder contribution diminishes very quickly (falls off like the dipole and polarization energy), the second molecular layer is practically only bulk disorder. The interfacial DOS is broadened to form deep trap states, and current is limited by charges escaping these deep states into the second layer. After the charges are in the second layer (assumed to be empty since most injected charges are trapped at interface), they are assumed to move freely into the bulk. At high biases, when the deep interfacial traps are filled, the interface barrier is small and current transitions to a bulk SCL limit. In this interfacial trap model, the cathode dependence of current is mainly explained by cathode doping filling the interface traps.

6.3.2 Metal-Organic Interface

Since electronic states in amorphous organic semiconductors are highly localized and charge-carriers are limited to intersite hopping along molecular distances, the environment at the interface boundary has a significant effect on the injection of carriers. Several interfacial properties that have been experimentally confirmed to affect the injection currents include the interface barrier (work function difference between injecting electrode and organic semiconductor), interfacial chemistry (reactions between metal electrode and organic molecules can lower interface barrier, form interface and midgap states, add dopants, and etc), and interfacial morphology (depends on chemistry of materials and growth conditions: substrate temperature, deposition rate, pressure, etc.).[128, 139-145] Scott[146] summarizes the electronic environment at the metal-organic interface contacts and the consequent effect on the injection current.

Detailed ultraviolet photoelectron spectroscopy (UPS) of interfaces[147] between reactive metal cathodes and the electron transporting material tris(8-hydroxyquinoline) aluminum (Alq_3) has been thoroughly investigated by groups including that of Kahn *et al.*[143] Studies have highlighted four important characteristics of these interfaces. First, there is a large, material-dependent barrier to electron injection from the metal into the organic semiconductor. Second, UPS detects filled states in the energy gap between the highest occupied molecular orbital (HOMO) and the lowest unoccupied molecular orbital (LUMO) of the deposited Alq_3,[143, 148] confirming charge transfer from the reactive metal to Alq_3 molecules. Third, there is a large interfacial dipole, likely due to depletion of the

doped interface with an associated shift in the vacuum level. Finally, x-ray photoelectron spectroscopy (XPS) studies have observed that the C1*s* energy levels of Alq_3 molecules deposited on a metal surface are broadened.[143] The broadening has been attributed in part to inhomogeneous polarization at the disordered metal-organic interface.[143]

Despite UPS observations of a material-dependent metal-organic injection barrier, there is surprising evidence of *material-independent* charge injection at these complex interfaces. For example, the low-temperature *I-V* characteristics of interfaces between Alq_3 and the reactive metals Al and Mg are nearly identical[139] even though the electron injection barrier is thought to be 0.3 eV smaller at the Mg/Alq_3 interface.[143] The similarity in *I-V* characteristics suggests that—at least at low temperature—the injection mechanism may be independent of the metal-organic injection barrier. In another example, Kahn *et al.* [143, 149] have shown that the *I-V* characteristics of metal-on-Alq_3 interfaces are identical to inverted Alq_3-on-metal interfaces. Yet UPS studies find differences in the spatial extent of the chemical reaction[150] between Mg or Al cathodes and Alq_3 in these devices.[143] The contrast suggests that electron injection may be independent of interfacial morphology.

6.3.3 Interface Roughness and Polarization

In thermionic emission models of metal-semiconductor interfaces,[5] the mean energy of charge transport states is lowered by the image potential, defined as the potential due to polarization of the metal surface adjacent to a charge. Near a *flat* metal interface, the polarization energy is[146] $E_P(z) = -q^2/16\pi\varepsilon z$, where q is the electron charge, ε is the permittivity of the organic medium, and z is the distance from the metal. But XPS studies have highlighted the possible importance of inhomogeneous polarization at the interface.[143] Indeed, the C1*s* energy levels of Alq_3 molecules adjacent to a metal surface are observed to be broadened by approximately 0.5 eV at full width at half maximum.[143]

Roughness at the metal-organic interface contributes to disorder in the polarization potential. The potential ϕ due to a point charge located at $\vec{r}_0 = (x_0, y_0, z_0)$ in the molecular semiconductor is calculated using Poisson's equation:

$$\nabla^2\phi = \frac{-q}{\varepsilon}\delta(\vec{r}-\vec{r}_0). \tag{6.4}$$

Following previous studies,[151] the disordered metal interface is represented as a zero-mean random surface, with mean surface parallel to the *x-y* plane, satisfying the scaling relation $h(x,y) \simeq \gamma^{-H} h(\gamma x, \gamma y)$, where $h(x,y)$ is a single-valued stochastic self-affine function, γ is a scaling parameter, and H is the roughness exponent. Within the self-affine regime, we consider length scales tangential to the metal surface above the cutoff corresponding to the interatomic spacing, ≈1 Å, and bounded by length scales, ξ, where h is on the order of the intermolecular spacing. At ξ, we define w as the root mean square (RMS) displacement perpendicular to the metal surface. The metal surface is weakly rough, i.e., $w \ll \xi$.

The boundary conditions for the calculation of ϕ are $\phi\left[x,y,z=h(x,y)\right]=0$ and $\phi=0$ at $|\vec{r}|\to\infty$. Using perturbation analysis,[151] we expand the potential $\phi(z)$ in powers of $h(x,y)$:

$$\phi = \phi_0 + \phi_1 + \phi_2 + \ldots \tag{6.5}$$

We transfer the second boundary condition from $z=h(x,y)$ to $z=0$ using the following Taylor series expansion:

$$\phi(x,y,h) = \phi(x,y,0) + \frac{\partial\phi}{\partial z}(x,y,0)h(x,y) + \frac{\partial^2\phi}{\partial z^2}(x,y,0)h^2(x,y) + \ldots \tag{6.6}$$

The boundary condition is rewritten as:

$$\phi(x,y,0) + \frac{\partial\phi}{\partial z}(x,y,0)h(x,y) + \frac{\partial^2\phi}{\partial z^2}(x,y,0)h^2(x,y) + \cdots = 0 \tag{6.7}$$

Substituting Eq. (6.5) into Eq. (6.4) and Eq. (6.7), and equating coefficients of equal order in $h(x,y)$, we have for first order:

$$\begin{cases} \nabla^2\phi_1 = 0 \\ \phi_1(x,y,z=0) = -h(x,y)\left.\dfrac{\partial\phi_0}{\partial z}\right|_{z=0} \\ \phi_1(x,y,z\to\infty) = 0 \end{cases} \tag{6.8}$$

The zeroth-order solution, ϕ_0, is obtained using the method of images: [152]

$$\phi_0 = -\frac{q}{4\pi\varepsilon_r\varepsilon_0\left|\vec{r}-\vec{r}_0\right|} + \frac{q}{4\pi\varepsilon_r\varepsilon_0\left|\vec{r}+\vec{r}_0\right|}, \tag{6.9}$$

where the first term in Eq. (6.9) is the potential of the charge and the latter term is the image potential. The first-order solution of the image potential can be solved by rewriting Eq. (6.8) as:

$$\begin{cases} \dfrac{\partial^2}{\partial z^2}\Phi_1 - k^2\Phi_1 = 0 \\ \Phi_1\left(\vec{k}, z=0\right) = \Im\left\{-h(x,y)\dfrac{\partial\phi_0}{\partial z}\bigg|_{z=0}\right\}, \\ \Phi_1\left(\vec{k}, z\to\infty\right) = 0 \end{cases} \tag{6.10}$$

where $\Phi\left(\vec{k},z\right)$ is the 2d Fourier transform of the potential $\phi(x,y,z)$, $\Im\{\ \}$ is the Fourier transform operator, and $\vec{k}$ is the wave vector. The potential must decay as $z \to \infty$, thus the solution to Eq. (6.10) is

$$\Phi_1(\mathbf{k},z) = \Phi_1(\mathbf{k},0)e^{-kz} \tag{6.11}$$

From Eq. (6.9)

$$\phi_1(x,y,0) = -h(x,y)\frac{\partial\phi_0}{\partial z}\bigg|_{z=0} = \frac{-qz_0h(x,y)}{2\pi\varepsilon_r\varepsilon_0\left((x-x_0)^2+(y-y_0)^2+z_0^2\right)^{3/2}} \tag{6.12}$$

We take the inverse Fourier transform of Eq. (6.11) with a convolution of Eq. (6.12) to obtain the expression for the first order correction to the image potential in real space:

$$\phi_1(x_0,y_0,z_0) = \frac{-qz_0^2}{4\pi^2\varepsilon_r\varepsilon_0}\int_{-\infty}^{\infty}\frac{h(x'+x_0,y'+y_0)}{\left[x'^2+y'^2+z_0^2\right]^3}\,dx'\,dy' \tag{6.13}$$

We can simplify Eq. (6.13) by considering the numerator and denominator separately. $h(x',y')$ is slow varying relative to the denominator of Eq. (6.13), which peaks at $\sqrt{x'^2+y'^2} = z_0/\sqrt{5}$. For charges close to a self affine metal interface, i.e. $z_0/\sqrt{5} \ll \xi$, we can make the approximation $h(x'+x_0,y'+y_0) \approx h(x_0,y_0)$ and approximate Eq. (6.13) as:

$$\phi_1(x_0, y_0, z_0) \approx \frac{-q}{8\pi\varepsilon_r\varepsilon_0} \frac{h(x_0, y_0)}{z_0^2} \tag{6.14}$$

To first order then, the standard deviation in the $z = z_0$ plane is:

$$\sigma(z_0) \approx \frac{q^2}{8\pi\varepsilon_r\varepsilon_0} \frac{w}{z_0^2} \tag{6.15}$$

XPS measurements[143] of $\sigma(a_0) = 0.7$ eV are consistent with Eq. (6.15) for $a_0 = 6$Å,[7] $w = 3.5$Å, and $\varepsilon_r = 1$, confirming that the roughness of metal interfaces significantly influences energetic disorder in the adjacent semiconductor.

It is also notable that the ratio of standard deviations in the first and second molecular layers is:

$$\frac{\sigma_1}{\sigma_2} = 4 \tag{6.16}$$

independent of material parameters such as the surface roughness, where σ_1 and σ_2 is the standard deviation of transport states in the first and second layers, respectively. The first layer is defined to contain all molecules within one hopping distance, a_0, from the rough interface; the second layer is spaced by a further a_0; see Figure 6-2. Equation (6.16) is expected to be a general characteristic of metal-organic interfaces; its significance will be discussed in the following section.

Note that the effect of surface roughness on the mean image potential has been calculated by Rahman and Maradudin[153] for a generalized dielectric interface with Gaussian correlation statistics. Our treatment concentrates on the dependence of energetic disorder on distance from a self-affine metal surface.

Using a perturbation expansion in powers of $h(x,y)$,[151] the self-affine rough metal/organic interface height function, and equating coefficients of equal order (see Eqs. (6.5) through (6.7)), we find that the higher order terms of the image potential satisfy the differential equation:

$$\begin{cases} \nabla^2\phi_n = 0 \\ \phi_n(x, y, z = 0) = -\frac{1}{m!}\sum_{m=1}^{n} h^m \left.\frac{\partial^m \phi_{n-m}}{\partial z^m}\right|_{z=0} = \sum_{m=1}^{n} A_m \\ \phi_n(x, y, z \to \infty) = 0 \end{cases} \tag{6.17}$$

In k-space, the potential solutions ϕ_n for $n \geq 1$ follow an exponential z-dependence e^{-kz} with k-values limited by the interatomic spacing in the metal surface (≈ 1Å). The frequency spectrum of the self-affine surface $h(x,y)$ follows a power-law behavior that peaks at ξ. For weakly rough surfaces $\xi \gg \max\{h(x,y)\}$, the lower order contributions A_m in the boundary condition are negligible compared to A_n. Consequently, the dominant term of the potential solutions is: $\phi_n \sim h^n / z_0^{n+1}$. Hence, the higher order terms in the perturbation expansion of Eq. (6.5) approach zero as $n \rightarrow \infty$ if $w < z_0$.

6.3.4 Calculation of Current

As discussed in the introduction, UPS studies of Mg/Alq_3 and Al/Alq_3 interfaces detect filled states in the Alq_3 energy gap that are formed by chemical reactions between Alq_3 and low work function metals.[143, 148] Filled gap states are indicative of cathode-induced doping of the interfacial organic semiconductor. At equilibrium, charge diffusion back to the metal establishes an interfacial dipole that minimizes the energy barrier between the cathode and the organic semiconductor.

The first molecular layer at the interface contains both reacted molecules, characterized by filled gap states, and unreacted molecules, characterized by the intrinsic LUMO for Alq_3, albeit broadened by inhomogeneous polarization. There are two important consequences of disorder and doping at the interface. Firstly, the transition from the energetically disordered broad DOS at the interface to a narrow DOS in the next layer forms an injection barrier between the first and second layers. Secondly, doping enhances the interfacial dipole. Together with the broad DOS at the interface, the interfacial dipole may minimize any charge injection barrier between the metal and the organic semiconductor. Consequently, we assert that injection-limited I-V characteristics at cathode-doped interfaces are determined by the rate of charge hopping from the first to the second layer, not the rate of charge hopping from the metal to the first layer; see Figure 6-2. The current density, J, is given by:[139]

$$J(E_F) = a_0 q \int_{-\infty}^{\infty} \int_{-\infty}^{\infty} f_1(E_1, E_F) g_1(E_1) R(E_2 - E_1) g_2(E_2 + \Delta) \, dE_1 dE_2 \qquad (6.18)$$

where $g_i(E_i)=\left(N/\sqrt{2\pi\sigma_i^2}\right)\exp\left[-1/2(E_i/\sigma_i)^2\right]$ is the density of intrinsic LUMO states in the ith layer and $f_1(E_1,E_F)$ is the energy distribution of charges in the depletion region. Because its DOS is broad, the charge distribution in the first layer is assumed to be degenerate. The quasi Fermi level for electrons in the first layer is E_F, a_0 is the intermolecular spacing, and the molecular density is $N = 10^{21}$ cm^{-3}. $\Delta = -a_0qF + \Delta E_P$ is the shift in energy in the second layer due to the applied electric field, F, and the change in mean polarization energy, ΔE_P. We describe the hopping rate, R, with the Marcus formula:

$$R(E) = \kappa \exp\left[-(E+\lambda)^2/4\lambda kT\right] \tag{6.19}$$

where E is the energy difference between hopping sites, and κ is the transmission coefficient, and λ is the molecular reorganization energy. From Eqns. (6.18) and (6.19), and making the approximation that f_1 is degenerate, we get:

$$J(E_F) \approx \frac{\kappa a_0 qN}{\sigma_1\sqrt{\pi\left(2+\sigma_2^2/\lambda kT\right)}} \int_{-\infty}^{E_F} \exp\left[-\tfrac{1}{2}m(E_1/\sigma_1)^2\right]dE_1 \tag{6.20}$$

where $m = 1+\sigma_1^2/\left(\sigma_2^2+2\lambda kT\right)$ is the power law slope and we have assumed that $|E_F| \gg |\lambda-\Delta|$. At low temperatures the decay of energetic disorder in Eq. (6.16) gives $m = 1+\sigma_1^2/\sigma_2^2 \approx 17$.

The current density in Eq. (6.20) is related to the applied voltage, V, by the quasi Fermi energy, E_F, in the LUMO states. Calculating the total charge (injected + doped) in the first layer using an asymptotic approximation in the integration of the Gaussian distribution $f_1(E_1,E_F)g_1(E_1)$ gives:

$$V+\Delta V = V_0 \exp\left[-\tfrac{1}{2}(E_F/\sigma_1)^2\right] \tag{6.21}$$

where $V_0 = qa_0N\sigma_1 d/\sqrt{2\pi}\varepsilon|E_F|$ and d is the thickness of the electron-transport layer. The approximation is valid for $|E_F| >\sim \sigma_1$, when the Fermi level at least one standard deviation away from the mean of the Gaussian DOS. For high biases, where the interfacial DOS fills up to within one standard deviation, the injection step from first to second layers may no longer be the limiting factor for current. The applied voltage, V, is

calculated from the injected space charge trapped in the first layer. But free charge that has diffused from filled gap states due to doping of the interface also affects the density of charge in the LUMO states. To account for the effects of doping, Eq. (6.21) defines a doping-dependent voltage shift, ΔV, equivalent to the additional voltage required to inject an amount of charge equal to the doped free charge present in the LUMO states in the first layer.

Approximating Eq. (6.20) under the assumption that $|E_F| \gg \lambda, \Delta$, and substituting for the Fermi energy using Eq. (6.21), gives the analytic model for charge injection into cathode-doped amorphous organic semiconductors:

$$J = J_0 (V + \Delta V)^m / V_0^m \quad (6.22)$$

where ΔV is the doping-dependent voltage shift and $J_0 \approx q\kappa a_0 N (\lambda kT/\sigma_1 |E_F|) \sqrt{(2 + \sigma_2^2/\lambda kT)/\pi}$. Note that J_0 and V_0 are approximately constant since E_F is slowly-varying in the broad DOS $g_1(E_1)$. The assumption that $|E_F| \gg \lambda, \Delta$ is valid in the range of applied electric fields used in this study. For typical molecular reorganization energies, and applied electric fields $\approx 10^6$ V/cm, both λ and Δ are << $\sigma_1 \approx 0.7$ eV.

6.3.5 Current-Voltage Measurements

In this section we compare the model of Eq. (6.22) with *I-V* data for five organic semiconductors: tris(8-hydroxyquinoline) aluminum (Alq_3),[154] 9-dimethyl-4,7 diphenyl-1,10-phenanthroline (bathocuproine, or BCP),[155] 4,4'-N,N'-dicarbazole-biphenyl (CBP),[156] 3-phenyl-4-(1'-naphthyl)-5-phenyl-1,2,4-triazole (TAZ),[157] and copper phthalocyanine (CuPC).[158] Each material was incorporated in a device fabricated on a UV-ozone treated glass substrate precoated with an indium tin oxide (ITO) anode with a sheet resistance of ≈ 20 Ω/sq. The ITO was coated with a layer of poly(3,4-ethylenedioxythiophene):poly(4-styrenesulphonate) (PEDOT:PSS) to minimize leakage current in the finished devices. This layer was prepared by spin coating onto the ITO substrate followed by baking at $T \approx 120$ °C for at least 1 hour in an oxygen-free environment. All devices were fabricated with a hole blocking layer of BCP deposited on

the PEDOT:PSS. The deep HOMO of BCP[159] minimized the hole current in each device. Organic semiconductors to be tested were deposited on the BCP. All small molecular weight materials were deposited by high-vacuum ($< 10^{-6}$ Torr) thermal evaporation. The cathode materials employed in this study were Au, Ag, Al, a 1:50 mixture of Mg and Ag (Mg:Ag),[7] and Al with a 5Å-thick interfacial layer of LiF deposited between the Al and the organic material (Al/LiF).[160] All cathodes were deposited through 1-mm-diameter shadow masks and were 1000Å-thick, except Mg:Ag, which had an additional 300Å-thick film of Ag for protection from oxidation. Lithium doping at the interface was investigated at Al-BCP contacts (Al/BCP:Li) and Au contacts to Alq_3 (Au/Alq_3:Li) and BCP (Au/BCP:Li) by co deposition of 10% Li into a 200Å-thick organic layer adjacent to the cathode. All devices were tested immediately after fabrication and measured in an inert He atmosphere.

At T = 10K and high applied bias, the *I-V* characteristics of each interface exhibited power law behavior with $m = (20 \pm 1)$, as shown in Figure 6-3.

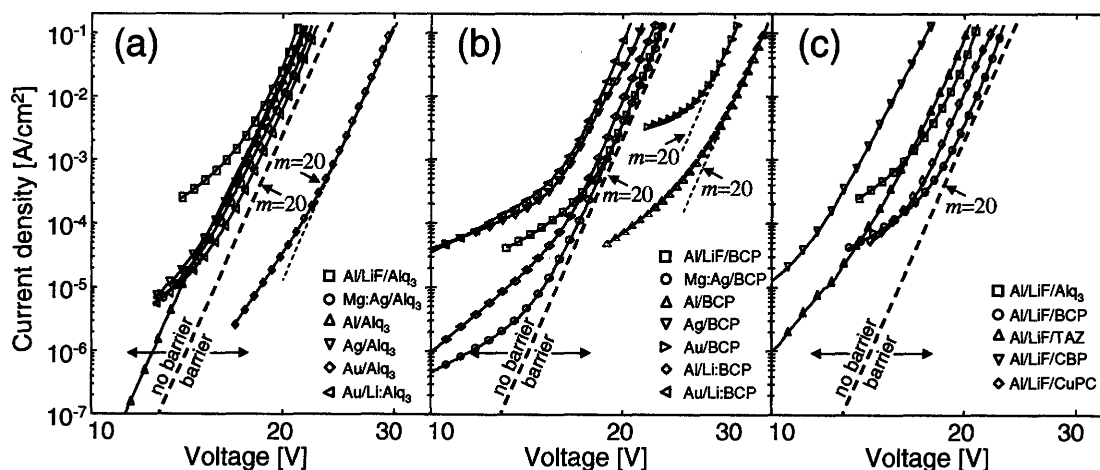

Figure 6-3:[140] The *I-V* characteristics at T = 10K for (a) Alq_3 interfaces, (b) BCP interfaces, and (c), a comparison of Al/LiF contacts to Alq_3, BCP, TAZ, CBP, and CuPC. All cathodes exhibit similar power law behavior, i.e. $J \sim V^m$, where $m = (20 \pm 1)$, and the IV characteristics of all but three contacts: Au/Alq_3, Au/BCP and Al/BCP are clustered together and controlled by an energy barrier between the first and second molecular layers. The heavy dotted line with power law slope $m = 20$ marks the approximate transition between contacts controlled by an energy barrier in the organic semiconductor and the three high voltage contacts limited by an additional energy barrier between the metal and organic semiconductor. From Limketkai and Baldo (2005).[140]

The power law slope for each device is summarized in Table 6-1. The *I-V* characteristics are remarkably similar at low temperature with the exception of Au/Alq_3, Au/BCP and Al/BCP interfaces, which require much higher voltages.

Device structure	Interface doping (N_D/N) [%]	Activation energy (E_A) [meV]	Power law slope m
$Al/LiF/Alq_3$	15±3	34±1	19±1
$Mg:Ag/Alq_3$	13±3	34±2	20±1
Al/Alq_3	8±3	35±2	21±1
Ag/Alq_3	3±1	22±1	21±1
Au/Alq_3	-	-	20±1
$Au/Li:Alq_3$	7±2	26±2	21±1
Al/LiF/BCP	17±4	32±3	21±2
Mg:Ag/BCP	10±4	40±5	21±1
Al/BCP	-	-	20±1
Ag/BCP	0	-	18±1
Au/BCP	-	-	20±2
Al/Li:BCP	13±4	42±3	22±1
Au/Li:BCP	12±4	47±3	21±2
Al/LiF/TAZ	12±4	28±3	19±2
Al/LiF/CBP	4±1	20±2	19±1
Al/LiF/CuPC	14±4	34±4	21±1

Table 6-1:[140] Doping and power law characteristics of all the interfaces studied in this work. The power law slope, m, where $J \sim V^m$, was determined at $J = 0.1$ A/cm^2 and T = 10K and found to be a conserved property of these interfaces, with $m = (20\pm1)$. Three of the interfaces: Au/Alq_3, Au/BCP and Al/BCP were significantly more resistive than the rest and injection at these interfaces was assumed to be limited by a large energy barrier between the metal and organic semiconductor. Of the remaining interfaces, the doping fraction, N_D/N, at the contact, and the doping activation energy, E_A, were determined by comparing *I-V* characteristics to extrapolations of low temperature (T < 50K) data. For example, the Ag/BCP *I-V* characteristic is aligned with the extrapolation of low temperature data, and is consequently found to be undoped. From Limketkai and Baldo (2005).[140]

Excluding the Au/Alq_3, Au/BCP and Al/BCP interfaces, the temperature dependencies of the remaining *I-V* characteristics are plotted in Figure 6-4 for (a) Alq_3 (b)

BCP and (c) a comparison of Al/LiF contacts. At high temperature, the IV characteristics vary significantly for the different interfaces. But the differences are diminished at low temperature. Since cathode-induced doping is expected to vary significantly among the various interfaces studied, the similarity at low temperature between the various *I-V* characteristics suggests that doping is thermally activated, i.e. $\Delta V\left(T \rightarrow 0\mathrm{K}\right) \approx 0$.

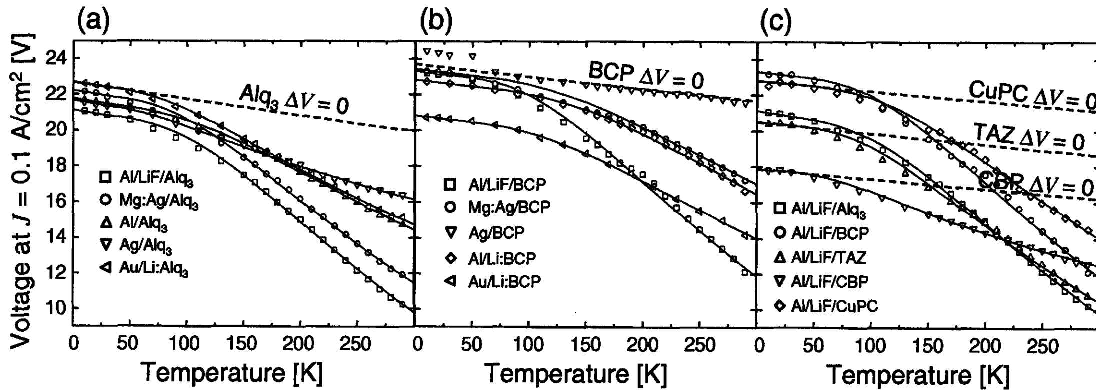

Figure 6-4:[140] The temperature dependence of the operating voltage at $J = 0.1$ A/cm^2 for (a) Alq$_3$ interfaces, (b) BCP interfaces, and (c), a comparison of Al/LiF contacts to Alq$_3$, BCP, TAZ, CBP, and CuPC. At high temperatures, differences in doping at the various cathode interfaces cause the characteristics to diverge. The estimated behavior of each organic semiconductor in the absence of doping is shown with dotted lines, and obtained by extrapolation from the low temperature data (T < 50K). Solid lines are the sum of the low temperature extrapolation and fits to $\Delta V(T)$ in Figure 6-5. From Limketkai and Baldo (2005).[140]

To quantify the temperature dependence of ΔV, we first fit Eq. (6.22) with $\Delta V = 0$ to the low temperature ($T < 50$K) data for each organic semiconductor, yielding the dotted lines in Figure 6-4. The $\Delta V(T)$ values for each cathode were then obtained by subtracting these fits from the applied voltage at $J = 0.1$ A/cm^2. As shown in Figure 6-5, the temperature dependencies of the doping-induced voltage shifts, ΔV, accurately fit a simple Arrhenius law. This is discussed further in the next section. The measured activation energies for the various contact interfaces are summarized in Table 6-1.

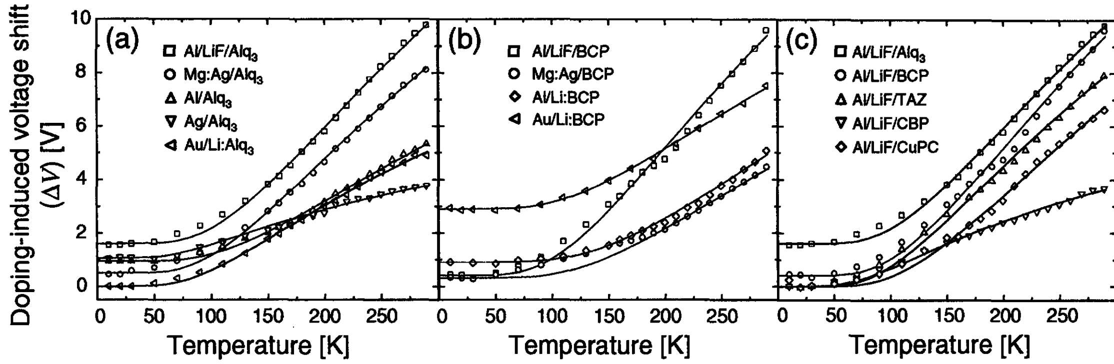

Figure 6-5:[140] The temperature dependence of doping for (a) Alq_3 interfaces, (b) BCP interfaces, and (c), a comparison of Al/LiF contacts to Alq_3, BCP, TAZ, CBP, and CuPC. The doping-induced voltage shift, ΔV, is obtained by subtracting an extrapolation of the low temperature data in Figure 6-4 from the actual voltage. Fits to Eq. (6.23) are shown in solid lines and used to determine the various doping fractions and activation energies summarized in Table 6-1. From Limketkai and Baldo (2005).[140]

We confirm in Figure 6-6 that ΔV is independent of current density at high bias, i.e. the *I-V* characteristics of all interfaces except Au/Alq_3, Au/BCP and Al/BCP interfaces are related by a temperature-dependent *rigid* shift in voltage. Thus, Eq. (6.22) provides a general description for charge injection at these interfaces. Except at low temperature, the Au/Alq_3, Au/BCP and Al/BCP interfaces are not related to the other IV characteristics by rigid shifts in voltage.

Application of the theory of Eq. (6.22) allows us to determine the various material parameters summarized in Table 6-2. In particular, from the fits for $\Delta V = 0$ and the power law slope at low temperature, we can determine σ_1 and σ_2. We obtain $\sigma_1 = 0.63\pm0.08$ eV for Alq_3, consistent with XPS measurements of broadening of the C1s energy level of Alq_3 at metal-Alq_3 interfaces.[143]

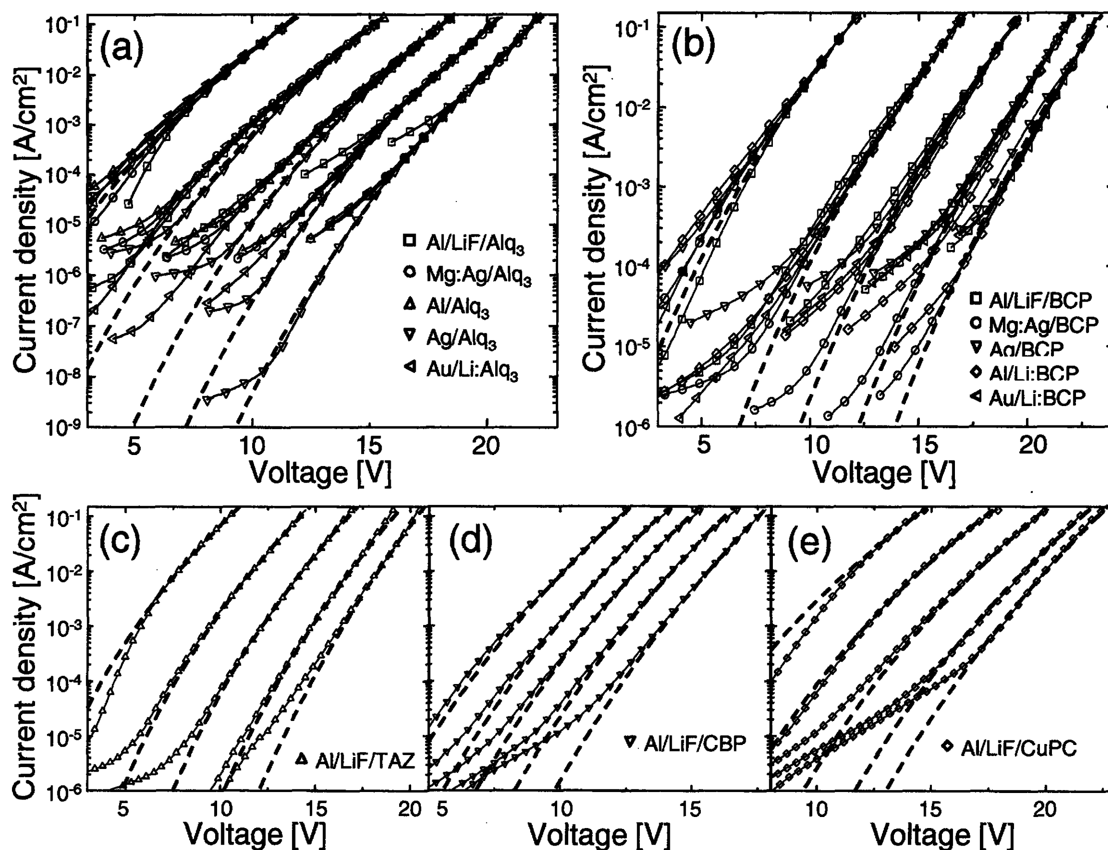

Figure 6-6:[140] Temperature dependence of *J-V* characteristics of (a) Alq_3 interfaces, (b) BCP interfaces, (c) Al/LiF/TAZ, (d) Al/LiF/CBP, and (e) Al/LiF/CuPC. A rigid voltage shift was applied to Alq_3 and BCP curves to overlap with Mg:Ag/Alq_3 data and Al/LiF/BCP data, respectively. All the measured Alq_3 and BCP data share the same characteristics, except for a cathode-dependent rigid voltage shift. From Limketkai and Baldo (2005).[140]

	Alq_3	BCP	TAZ	CBP	CuPC
σ_1 [eV]	0.63±0.08	0.74±0.09	0.64±0.07	0.59±0.08	0.69±0.09
σ_2 [eV]	0.14±0.02	0.16±0.02	0.14±0.02	0.13±0.02	0.15±0.02
λ [eV]	0.16±0.04	0.16±0.04	0.12±0.02	0.11±0.03	0.13±0.03
J_0 [A/cm^2]	84±12	74±10	74±9	69±13	74±8
V_0 [V]	30.39±0.20	31.50±0.22	27.30±0.14	23.73±0.21	30.38±0.15

Table 6-2:[140] Parameters for the five organic semiconductors studied in this work, as determined by the low temperature power law slope and fits to extrapolated *I-V* characteristics for $\Delta V = 0$. The standard deviation of the density of states in the first and second molecular layers is σ_1 and σ_2,

respectively. λ is the molecular reorganization energy. J_0 and V_0 are constants from Eq. (6.22). J_0 was determined at $T = 10K$. The extracted values of σ_1 are consistent with XPS measurements of Alq_3 interfacial energy level broadening of approximately 0.7 eV.[143] From Limketkai and Baldo (2005).[140]

6.3.6 Discussion

(i) Energy barriers at the metal/organic interface and in the organic semiconductor

From the *I-V* characteristics at T = 10K, we divide the various cathode interfaces into two categories. In the first category, the *I-V* characteristics are controlled by an energy barrier in the organic semiconductor. The similarity of *I-V* characteristics at T = 10K demonstrates unequivocally that electron injection at these interfaces is not controlled by an energy barrier between the metal and organic semiconductor. In this work, cathode interfaces in this category were typically either cathode-doped or deliberately doped with Li during fabrication.

The second category consists of interfaces with large energy barriers between the metal and organic semiconductor. The transition to power law behavior with $m = (20\pm1)$ is only observed in this category at extremely high biases, since the energy barrier at the metal-organic interface must be overcome before the energy barrier within the organic semiconductor is significant. But even for a high work function cathode such as Au, the metal-organic barrier can be minimized by doping. Indeed, Au/Li:Alq_3, Au/Li:BCP and Al/Li:BCP contacts exhibit *I-V* characteristics consistent with the first category of contacts.

(ii) Common characteristics of metal/organic interfaces

Two common properties are observed in the interfaces studied here: Firstly, the power law slope is $m = (20\pm1)$ at 10K, independent of the choice of cathode or organic material. Secondly, at a given temperature, the *I-V* characteristics of all contacts controlled by an energy barrier in the organic semiconductor are related by a rigid linear shift in voltage.

Several possible explanations for the common properties in the *I-V* data may be excluded. Firstly, the low temperature behavior is not due to a transition to bulk-limited conduction. Five different organic semiconductors were employed in this study, and

despite their different bulk charge transport properties all exhibited similar power law behavior at low temperature. Moreover, the thickness dependence of the IV characteristics for Alq_3 contacts is linear at low temperature, consistent with injection-limited charge transport.[139] Secondly, the similarities in *I-V* characteristics are not due to the common BCP/PEDOT:PSS/ITO anode. Nearly identical data has been obtained for the Alq_3 devices using Mg anodes[139] and varying the thickness of BCP.

Rather, calculations of polarization induced energetic disorder approximately match XPS measurements of energy level broadening at the metal surface.[143] And the invariance of the power-law slope at low temperature is consistent with predictions of the effect of interface roughness[153] on the image potential. Energetic perturbations decay rapidly with distance from the disordered interface, but only the decay rate – *which is independent of interface roughness* – affects σ_1/σ_2 and the injection theory. Hence the low temperature power law is preserved irrespective of the metal cathode, or the organic semiconductor employed. And hence the *I-V* characteristics of metal-on-organic and organic-on-metal interfaces are similar despite the morphological differences.[143] The discrepancy between the theoretical prediction of $m = 17$ and the observations of $m = (20\pm1)$ is likely due to the neglect of higher order terms in the calculation of m, and the assumption of a constant dielectric constant for charges in the first and second layers of the organic semiconductor, thereby ignoring the polarization of molecules in the first interfacial layer.

(iii) The temperature dependence of ΔV

The temperature dependence of the rigid doping induced voltage shift ΔV is observed to fit:

$$\Delta V = \Delta V_0 + \left(q a_0 d / \varepsilon_r \varepsilon_0\right) N_D \exp\left[-E_A / kT\right] \tag{6.23}$$

where E_A is the activation energy, N_D is the effective doping density, and ΔV_0 is a temperature-independent constant determined by the equilibrium density of charge in the LUMO states at zero temperature.

Since the activation energy of ΔV is observed to be much less than the energetic disorder at the interface, we speculate that E_A is determined by the temperature

dependence of charge diffusion. From the Marcus charge hopping expression, the temperature dependence of the isoenergetic diffusion constant, D, is described by:

$$D \propto \kappa \exp\left[-\lambda/4kT\right] \tag{6.24}$$

The activation energies and calculated doping densities, N_D, for the various cathode interfaces are listed in Table 6-1. For fitted values of the molecular reorganization energy $\lambda \approx 160$ meV, $E_A \approx \lambda/4$, consistent with Eq. (6.24).

(iv) Discrepancies at low bias

At low current densities the *I-V* characteristics of many of the contacts studied diverge significantly from power law behavior. There are two origins for the divergence. Firstly, we note that the power law theory of Eq. (6.22) is valid only in the high electric field limit. When $V = 0$, Eq. (6.22) reduces to $J = J_0\left(\Delta V/V_0\right)^m \neq 0$. Thus, power law behavior is not expected to hold at $V = 0$. Secondly, for low applied voltages, 'additional' current is observed (*i.e.* current exceeding the power law prediction). At high temperatures, it is likely that the additional current is thermally activated leakage associated with device imperfections. As confirmation, we note that many *I-V* characteristics are not repeatable for $J < 10^{-5}$ A/cm^2. At lower temperatures, several weakly doped contacts exhibit nearly pure power law behavior. But reproducible deviations at low currents are also observed, especially for heavily doped contacts such as Al/LiF/Alq_3, suggesting that doping may alter the density of states in the first few molecular layers. Indeed, depletion of heavily doped interfaces alters the DOS by generating a strong electric field at the interface that is affected by spatial disorder. Our calculations suggest that this effect could contribute several tenths of an eV to the variances σ_1 and σ_2 at heavily doped interfaces, significantly altering the *I-V* characteristics.

(v) Trapped charge limited conduction

Finally, we note that *I-V* characteristics following the power law form $J \propto V^m$ have been previously attributed to trap charge limited (TCL) conduction with an exponential distribution of traps.[11] TCL theories apply to bulk semiconductors and do not

usually consider the electric field and temperature dependence of charge carrier mobilities.[161] Yet, TCL theories fit aspects of the *I-V* characteristics of *injection-limited* devices because the broad DOS at the metal-organic interface forms traps for injected charge. The injection model presented in this work is empirically similar to TCL theories, suggesting that *I-V* characteristics previously attributed to TCL be reconsidered for the possibility of injection limited charge transport.

6.3.7 Conclusion

In conclusion, the theory of Eq. (6.22) agrees with experimental data for the injection characteristics at disordered, cathode-doped organic semiconductor interfaces. Common properties of disparate contacts are identified, notably: (i) a power law slope of $m = (20\pm1)$ at low temperature, independent of the choice of cathode or organic material; and (ii) relation of IV characteristics of contacts at a given temperature by a rigid linear shift in voltage. The similarity between *I-V* characteristics for disparate organic semiconductors at low temperatures highlights the important effect of interface roughness on the image potential. At higher temperatures, the effects of doping are more pronounced. Indeed, all contacts improve with doping, and doping technologies may be more significant than the choice of the bulk semiconductor in the engineering of low resistance contacts. This work also suggests that to minimize disorder and obtain consistent results from single-molecule electronic devices sandwiched between metal contacts, both the molecules and the metal interfaces must be fabricated with atomic precision.

6.4 Injection and/or Bulk Limited Conduction

To determine whether the measured current in an organic semiconductor diode is injection or bulk limited, the dependence of voltage on diode thickness at constant current is often used to discriminate between the two.[9, 79] From injection-limited models, at a given current density, the voltage should scale linearly with the thickness of the device. Bulk-limited models, however, predict a non-linear voltage dependence with thickness. For SCL current, the voltage is predicted to scale to the power 3/2 with thickness (see Eq. (3.3)).

However, Scott[146] commented that it is difficult to straightforwardly extract parameters from just the field and temperature dependences of the measured currents because the contributions from different processes have similar behaviors. For example, the field dependence of the Schottky effect and the mobility are both 'Poole-Frenkel' $\exp\left[\sqrt{F}\right]$, and the injection and hopping processes are both thermally-activated.[146] Scott[146] pointed out that many studies have looked at the temperature dependence of the measured current to extract the barrier height while ignoring the possible mobility contribution, which could have the same thermally-activated dependence. Indeed, the charge injection model developed by Scott and Malliaras[146, 162] predict a dependence on the mobility of the organic semiconductor. To experimentally verify this prediction, Shen *et al.*[163] measured the injected current from indium-tin oxide (ITO) into tetraphenyl diamine (TPD) doped in polycarbonate (PC). They found that the measured current was indeed proportional to the bulk hole mobility, which was varied by changing the concentration of the hole transport dopant TPD in the PC host matrix and measured by time-of-flight technique.[163]

Obtaining correct physical parameter values from the measured current density versus voltage (*J-V*) characteristics relies on the use of an accurate model. Difficulty arises for amorphous organic semiconductors because the measured current behavior with field is similar for predictions from both injection and bulk limited current models. Wolf *et al.*[9] demonstrated that over a limited field range, their simulations of charge injection into a disordered hopping system featured behavior resembling bulk transport with an exponential distribution of traps. They further remarked that with a Gaussian distribution of traps, the field dependence of the bulk-limited current looks even more like injection-limited current. Therefore, the field dependence of the current may be indistinguishable between injection and bulk limited conduction.[9]

Therefore, in order to describe transport in organic semiconductor diodes over a broad range of currents and parameters, both mechanisms for transport (injection and bulk), influenced by many factors (built-in potential, injection barriers, diode thickness, traps, etc), must be understood.[79, 164-167]

Chapter 7 – Cathode-Doping of Organic Semiconductors

7.1 Introduction

Frequency and bias-dependent capacitance measurements on hetero-layer organic devices composed of a N,N'-diphenyl-N,N'-bis(1-naphtyl)-1,1-biphenyl-4,4 diamine (NPD) hole transport layer (HTL) and tris(8-hydroxyquinoline)aluminum (Alq_3) electron transport layer (ETL) have shown evidence of the presence of fixed negative charges at the NPD-Alq_3 interface under reverse bias.[79, 168-171] To analyze the capacitance measurements, a circuit element model (Figure 7-1) for the double heterostructure is employed. Here, the resistors of the organic layers are dependent on the temperature, charge density, and applied field across the material; and the capacitors have parallel-plate capacitance, $C = A\varepsilon_r\varepsilon_0/d$, where A is the area of the metal contact, ε_r the relative permittivity, ε_0 the vacuum permittivity, and d the thickness of the individual layers. Brütting and coworkers[79, 168-170] studied the bias and frequency dependent capacitances of this structure in two regimes. One regime is when the resistances of both the Alq_3 and NPD are large enough such that $\omega\tau = \omega RC \gg 1$ is satisfied in both layers, where ω is the measurement frequency of the small-signal AC bias. In this case, the induced differential charge from the small AC voltage will collect at the parallel capacitors, and the measured value of total capacitance should be the series sum of the two capacitances, $C_{\mathrm{Alq_3}}$ and C_{NPD}. The second regime studied is when the NPD resistance, R_{NPB}, is small enough such that $\omega\tau_{\mathrm{NPD}} = \omega R_{\mathrm{NPD}}C_{\mathrm{NPD}} \ll 1$, but $R_{\mathrm{Alq_3}}$ is still large with $\omega\tau_{\mathrm{Alq_3}} = \omega R_{\mathrm{Alq_3}}C_{\mathrm{Alq_3}} \gg 1$. In this case, the charges will short C_{NPD} (by going through R_{NPD}), and the measured value of total capacitance should simply be the Alq_3 capacitance alone, $C_{\mathrm{Alq_3}}$.

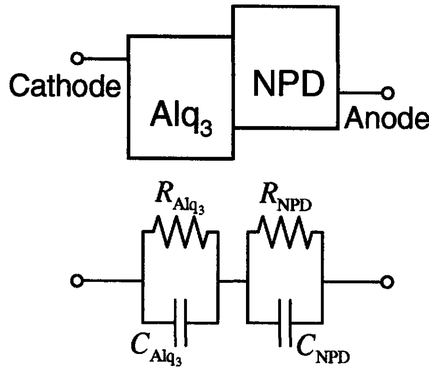

Figure 7-1:[79, 168, 169] Circuit element model of organic light-emitting diode composed of Alq_3 as the ETL and NPD as the HTL. Adapted from Berleb *et al.*[79, 168, 169]

Under forward bias, the voltage will be dropped predominantly across the Alq_3 layer.[168-173] since the NPD hole mobility is much larger than the Alq_3 electron mobility,[79, 118, 174, 175] the holes can easily inject from the anode to collect at the NPD-Alq_3 heterojunction, while the electrons will accumulate at the metal cathode-Alq_3 interface (assuming the forward bias is still small that electrons do not readily inject and transport across the Alq_3 layer). This is the regime when R_{NPD} is small, and for the appropriate measurement frequency, the measured capacitance for the whole hetero-layer device should be $C_{TOT} = A\varepsilon_r\varepsilon_0/t$, where t is the thickness of the Alq_3 layer alone. Under reverse bias, the resistances of the Alq_3 and NPD layers will be both very large. Charges will not easily transport across either organic layers, and they will pile up at the metal contact interfaces. This is the regime when R_{NPD} and R_{Alq_3} are both large, and for the appropriate frequency, the measured capacitance should then be the series sum of the individual Alq_3 and NPD capacitances. Therefore, the capacitance transition between the two regimes from $C_{TOT}^{-1} = C_{NPD}^{-1} + C_{Alq_3}^{-1}$ to $C_{TOT} = C_{Alq_3}$ occurs during the transition from reverse bias to forward bias voltage, which is expected to occur at an applied voltage equal to the built-in potential, V_{BI}.[79, 168-171] This is the point when the device reaches the flatband condition. The capacitance transition is an indication when R_{NPD} becomes small, which occurs when NPD reaches flatband. See Figure 7-2 below.

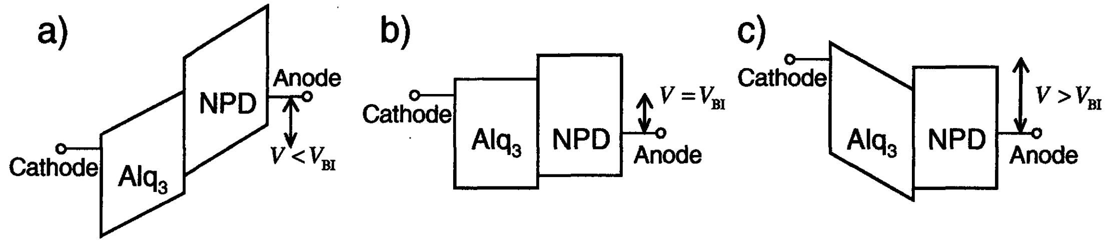

Figure 7-2: Band-diagrams for different biases. (a) At reverse bias, both organic layers are reverse biased, so $R_{\mathrm{Alq_3}}$ and R_{NPD} are both large. Charges will collect at metal contacts. Measured capacitance at the appropriate frequency should be $C_{\mathrm{TOT}}^{-1} = C_{\mathrm{NPD}}^{-1} + C_{\mathrm{Alq_3}}^{-1}$. (b) At $V = V_{BI}$, the organic layers become flatband, which is the transition point from reverse to forward bias. NPD is now flatband and begins to conduct holes well. This is the transition point and at the appropriate measurement frequency, the measured capacitance should be $C_{\mathrm{TOT}} = C_{\mathrm{Alq_3}}$. (c) At forward bias, NPD mobility is relatively large such that R_{NPD} is small enough to let holes inject and collect at Alq_3-NPD junction. Electrons collect at cathode contact since $R_{\mathrm{Alq_3}}$ is somewhat large. Therefore, the forward bias field drop is mostly across Alq_3. The measured capacitance at the appropriate frequeny should be $C_{\mathrm{TOT}} = C_{\mathrm{Alq_3}}$.

However, capacitance measurements reveal that the capacitance transition voltage, V_T, is not equal to V_{BI}, but some higher reverse bias.[79, 168-171] It was explained that this observed NPD flatband voltage shift, ΔV_{T}, away from the predicted $V_T = V_{BI}$ is the result of negative charges residing at the Alq_3-NPD interface in the reverse biased condition.[79, 168-171] Although $V_T < V < V_{BI}$ is a reverse bias voltage, NPD is still in the flatband condition because negative charges at the hetero-organic interface are contributing to the field drop in the Alq_3 layer. From Poisson's equation, the electric field, F_{i}, due to the surface density of negative charges at the hetero-organic interface, σ_{i}, is related to the change in transition voltage ΔV_{T} by:[79, 168-171]

$$\sigma_{\mathrm{i}} / \varepsilon_{\mathrm{r}} \varepsilon_0 = F_{\mathrm{i}} = F_{\mathrm{Alq_3}} = \Delta V_{\mathrm{T}} / t, \tag{7.1}$$

where t is the Alq_3 layer thickness. When large reverse bias $V < V_i$ is applied, where V_i is the voltage drop across the Alq_3 layer due to these interfacial negative charges, the Alq_3 and NPD layers are both in the reverse biased condition. (Figure 7-3(a)) However, when

the applied reverse bias reaches $V = V_T$, the NPD layer already reaches the flatband condition, but the Alq_3 layer is still reverse biased, accommodated by the negative interfacial charges. (Figure 7-3(b)) Note that the interfacial charge density is still equal to σ_i. As the reverse bias is decreased within the range, $V_T < V < V_{BI}$, holes inject from the anode to gradually compensate the negative interfacial charges. The density of charges at the hetero-interface decreases from σ_i. The NPD layer is still in the flatband condition while the Alq_3 layer is decreasing it's reverse biased potential slope. When the applied bias equals the built-in voltage ($V = V_{BI}$), all the interfacial charges are fully compensated and Alq_3 finally becomes flatband. (Figure 7-3(c)) Note that the amount of extra voltage needed to fully compensate the interface charge density σ_i is $V_i = V_{BI} + V_T$. At applied voltages past the built-in voltage ($V > V_{BI}$), the device becomes forward biased. Injected holes from the anode travel through the NPD because of its relatively high mobility (R_{NPD} small), but electrons collect at the cathode interface. (Figure 7-3(d))

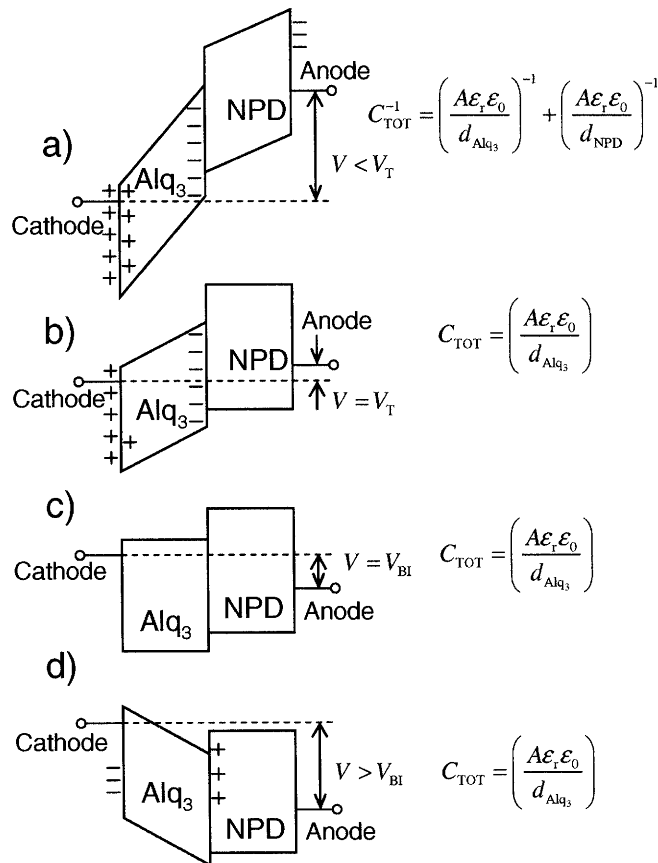

Figure 7-3:[168] Potential landscape of ITO/NPD/Alq_3/Ca OLED device under different bias conditions. (a) For large reverse biases, $V < V_T$, the amount of negative charges at the interface is equal to the total NPD-Alq_3 interfacial charges Q_i. The presence of these charges incurs a change in potential slope from across NPD to across Alq_3. (b) At $V = V_T$, NPD reaches the flatband condition. And the amount of interfacial charges is still equal to Q_i. With decreasing reverse bias within the range, $V_T < V < V_{BI}$, NPD remains in the flatband condition, but interfacial charge becomes less than Q_i as they are compensated by injected holes from the anode. (c) At $V = V_{BI}$, there is full compensation, and there are no more interfacial charges. Alq_3 reaches the flatband condition. (d) For forward bias, $V > V_{BI}$, holes are easily injected at the anode and travel across NPD to collect at the hetero-organic interface. Adapted from Berleb *et al.* (2000).[168]

In this chapter, the doping density is extracted from quasi-static capacitance-voltage (QSCV) measurements of hetero-layer devices with varying cathodes and Alq_3 thicknesses. The cathode and thickness dependence of the change in capacitance transition voltage, ΔV_T, is correlated to a negative interfacial charge density. The accumulation of this negative charge may be due to acceptor-like traps,[79, 168-171] formed at the interface from the reaction of thermally evaporated cathode metal atoms that may have diffused[143, 171, 176-179] through the organic semiconductor layer. Not only does the cathode metal disrupt the organic-organic interface in the OLED, but the cathode metal atoms in the bulk of the layer react with some surrounding organic molecules to form low-lying midgap states[143, 176] that partially dope the unreacted molecules (Figure 6-2 (right)). This cathode doping introduces a density of available charge-carriers in the device. The cathode dependence of the density of free charge is one contributing factor to the cathode dependence of the current-voltage characteristics. Fits to the temperature dependence of the *J-V* curves are done using a bulk percolation transport model (Chapter 5), with a cathode-dependent bulk doping density in the organic semiconductor.

7.2 Experimental Results

Organic hetero-layer devices were fabricated on UV-ozone treated glass substrates precoated with an indium tin oxide (ITO) anode with sheet resistance of ≈20Ω/sq. The hole transport layer was N,N'-Bis(3-methylphenyl)-N,N'-diphenylbenzidine (TPD) and electron transport layer was Alq_3. The cathodes employed in this study were Ag, Al, Mg (with a 40-nm-thick Ag cap to protect from oxidation), and

Al with a 5-Å-thick interfacial layer of LiF deposited between the Al and the organic material (Al/LiF).[160] The 100-nm-thick cathodes were thermally evaporated on top of the organic semiconductor layer through a 1-mm-diameter shadow mask. Materials were deposited by high-vacuum ($<10^{-6}$ Torr) thermal evaporation.

The device structure was an ITO anode underneath a fixed 60-nm-thick TPD layer, followed by an Alq_3 layer, and then a top cathode. The Alq_3 layer thickness was varied, but the TPD layer was fixed at 60 nm because the transition voltages have been previously observed to be independent of the higher mobility HTL thickness.[168] The quasi-static *C-V* plot of an aluminum device (ITO/60nm TPD/60nm Alq_3/Al) is shown in Figure 7-4(a). The Alq_3 thickness, t, dependence of V_T for the aluminum cathode devices is shown in Figure 7-4(b). Using Eq. (7.1), the interfacial surface charge density can be calculated from the change in V_T for each device thickness. From measurements of V_T vs t, the calculated surface charge densities as a function of t for each cathode are shown in Figure 7-5. Solid lines in Figure 7-4(b) and Figure 7-5 are fits assuming the charge density decays like an exponential function with thickness, $\sigma_i = A\exp[-t/B]$. The parameter A is 7.1 x 10^{15}, 6.7 x 10^{15}, 6.7 x 10^{15}, and 4.9 x 10^{15} e^{-}/m^2 for LiF/Al, Al, Mg, and Ag cathodes, respectively. The decay parameter B is 14286, 935, 361, and 231 nm for LiF/Al, Al, Mg, and Ag cathodes, respectively.

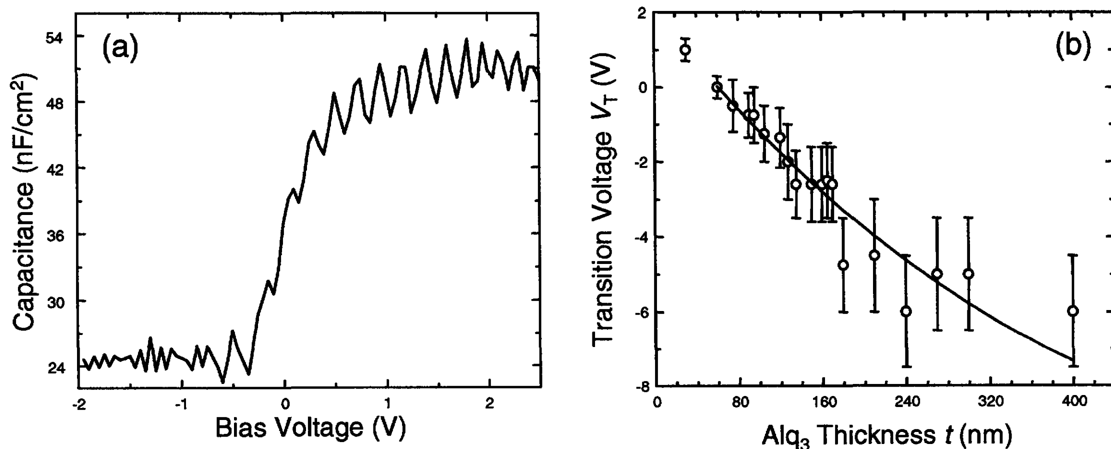

Figure 7-4: (a) Transition voltage, V_T, as a function of Alq_3 thickness, t, for the hetero-layer device ITO/60nm TPD/Alq_3/100nm Al. (b) QSCV plot of ITO/60nm TPD/60nm Alq_3/100nm Al.

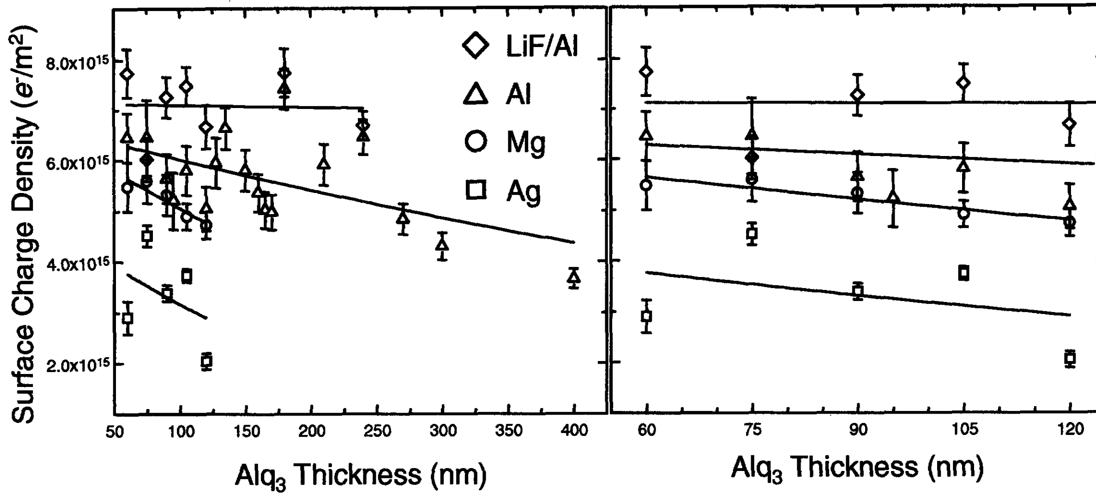

Figure 7-5: (left) Calculated surface charge density at TPD-Alq_3 interface as a function of Alq_3 thickness for different cathodes. (right) Same plot but for thicknesses up to 120 nm.

7.3 Discussion

7.3.1 Cathode Metal Forms Interface Traps

Similarly to what has been previously observed,[79, 168-171] the shift in capacitance transition voltage ΔV_T (or equivalently, TPD flatband voltage) is shown to be dependent on Alq_3 thickness, t. A voltage shift towards higher reverse bias and the capacitance values in Figure 7-4(a) (for relative permittivity $\varepsilon_R \approx 3.5$), confirm that the shift is caused by the presence of negative charges collecting at the hetero-organic junction. Figure 7-5 shows that the magnitude of interfacial charge density is decreasing with increasing Alq_3 thickness. The fixed negative charge that accumulates at the interface at reverse bias is thought to be caused by the presence of interfacial acceptor-like trap states.[79, 168-171] Thermally evaporated cathode metal atoms diffuse into the semiconductor layer and react with the organic molecules to form filled midgap states.[143, 176] At the hetero-organic interface, the reacted TPD midgap states will donate some charge to the Alq_3 side, leaving empty states that fill and become negatively charged when the device is under reverse bias. Charge transfer will take place if there are lower-lying empty Alq_3 midgap states, which would be present if these states donated their charge to the LUMO states of the unreacted Alq_3 molecules. If this is assumed, the magnitude of the density of mobile negative charge in the Alq_3 LUMO states at the hetero-organic interface will be

proportional to the magnitude of the density of empty TPD states. Note that for large t, it is predicted that there will be less interfacial charges because the cathode metal is not able to penetrate that far to the Alq_3-TPD boundary to form these empty traps. Therefore, the cathode doping density profile in an Alq_3 bulk can be probed by varying the Alq_3 thickness in C-V measurements of Alq_3-HTL hetero-layer devices.

7.3.2 Effect of Cathode-doped Charge on *J-V* Characteristics

The density of mobile negative charges in the Alq_3 LUMO transport states at the hetero-organic interface is proportional to the measured accumulated negative charge density at reverse bias voltage V = V_T. Therefore, the interfacial charge density σ_i profile, shown in Figure 7-5, is directly related to the doping density ρ profile.

The doped charge distribution, arising from cathode metal-organic reactions in the organic semiconductor bulk, is assumed to be approximately uniform for small thicknesses. The effect of these doped charges is to increase the available mobile charge-carriers, and hence the charge-density-dependent mobility, without the additional applied field of injected space charge. A uniform volume density of the bulk doped charge is $\rho = \sigma_i/2a_0$ cm^{-3}, where $a_0 = 1$ nm is the average intermolecular spacing. σ_i is taken to be the measured fixed interfacial surface charge density in the Alq_3-TPD devices for small t. From Figure 7-5 , σ_i is approximately equal to 7 x 10^{15} and 5.5 x 10^{15} e^-/m^2 for the LiF/Al and Mg cathodes at 70 nm. Fits to the current-voltage curves for a single 70-nm-thick Alq_3 layer diode device with a Mg cathode is shown in Figure 7-6. The current-voltage relation is calculated using the percolation-based bulk charge transport model[80] with compensated built-in potential offset of 1V and with the inclusion of uniformly bulk doped free charge. The parameters used in the percolation model are: $\alpha = 0.5$ Å^{-1}, $\sigma_0 = 2$ x 10^4 S/m, and $T_0 = 1000$K.

To study the cathode dependence of the *J-V* characteristics, note that from previous studies the effect of the cathode on the current-voltage relation is a voltage shift.[140] Fits to plots of voltage versus temperature at constant current density $J = 10^{-2}$ A/cm^2 with different cathodes and ITO/poly(3,4-ethylene-dioxythiophene):poly(4-styrenesulphonate) (PEDOT:PSS) anode are shown in Figure 7-7. The LiF/Al cathode

device is also calculated with the percolation-based bulk charge transport model with built-in potential offset of 0.5V.[80]

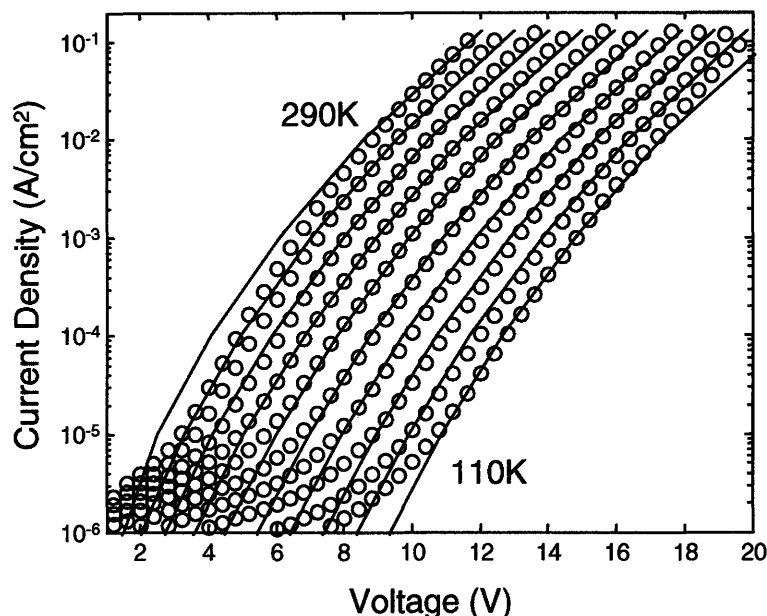

Figure 7-6: Temperature dependence of *J-V* characteristics for ITO/PEDOT:PSS/70nm Alq_3/Mg device at 20K intervals from 290K to 110K. Theoretical fits are shown in solid lines. Symbols are data from Limketkai and Baldo (2005).[140]

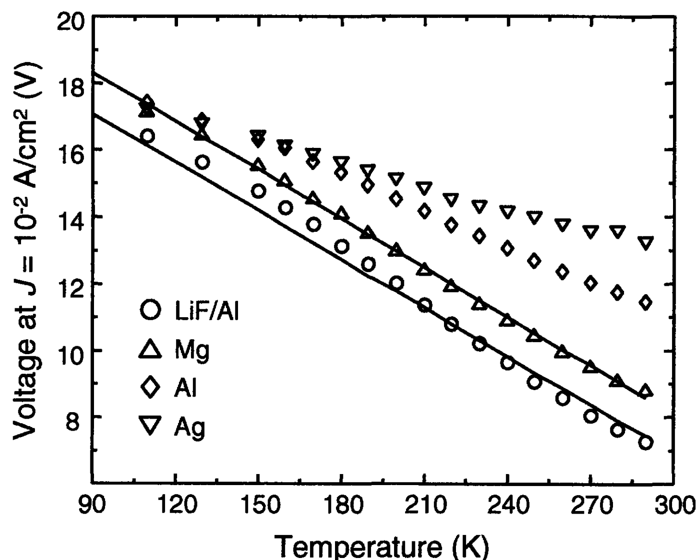

Figure 7-7: Temperature dependence of voltage at a constant current density for different cathodes. Solid lines are fits to the LiF/Al and Mg cathode devices. Symbols of circles (○), triangles (Δ), diamonds (◊), and inverted triangles (∇) are data from Limketkai and Baldo (2005)[140] for LiF/Al, Mg, Al, and Ag contacts, respectively, at $J = 10^{-2}$ A/cm^2.

It is interesting to note that the Al/LiF and Mg devices follow the bulk model prediction and only differ by a rigid voltage shift, which is attributed to the difference in cathode doping density and built-in potentials. The other two cathodes, Al and Ag, cannot be fit to a pure bulk transport theory. Although Al dopes Alq_3 particularly well, its high work function introduces an additional injection barrier. Note that an Al cathode for a BCP organic semiconductor diode exhibits a lot higher operating voltages compared to an Al/Alq_3 diode because aluminum does not react with BCP as well to dope the material with free charge-carriers.[140]

Transport is determined by the injection and bulk current. Initially, the applied field has to be large enough to overcome the injection barrier. At high electrical biases, when the field is large and injection current is non-limiting, the injected space charge in the bulk limits the current. Note that the bulk transport percolation model does not include injection effects, which would become more dominant for low-doped interfaces and higher work function cathodes and at low biases. The deviation from a near linear theoretical bulk voltage versus temperature for Ag and Al in Figure 7-7 indicates the non-negligible effects of contact impedances for these cathodes.

The thickness dependence of the operating voltage at constant current density, $J = 10^{-1}$ A/cm^2, for Mg/Alq_3/Mg devices is plotted in Figure 7-8. The solid line is the percolation model prediction, assuming zero built-in potential and half the uniform volume density used in the fits for the ITO/PEDOT:PSS/Alq_3/Mg device in Figure 7-6. Note that the presence of mobile charge-carriers in a bulk-limited conduction model gives an approximately linear thickness dependence of the voltage. This suggests that the voltage dependence on thickness alone is insufficient to distinguish between injection and bulk-limited current.

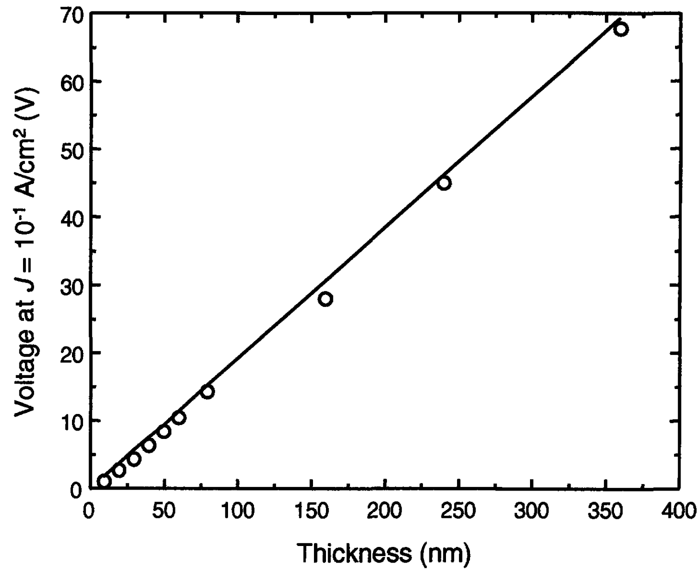

Figure 7-8: Thickness dependence of voltage at constant current density, J = 10^{-1} A/cm^2, for Mg/Alq$_3$/Mg devices at room temperature. Symbols are experimental data. The solid line is the bulk percolation model prediction.

7.4 Conclusion

In conclusion, cathode metal diffuse into the organic semiconductor upon evaporation to react/dope the material. The disruption of an organic-organic interface by cathode metal reaction explains the transition voltage shift of capacitance measurements in hetero-layer organic devices, such as OLEDs. The cathode metal introduces unfilled states at the hetero-organic junction that collect interfacial negative charge-carriers under reverse bias. The cathode has been shown to directly dope the organic material, introducing a distribution of free charge to effectively increase the charge-density-dependent mobility. For organic semiconductor diodes with low contact impedances, the current-voltage behavior can be assumed to be determined by the bulk mobility, and differences in doping density from the cathodes contributes to the operating voltage shifts. Any deviations from a bulk fit may be explained by neglected contact effects that become significant for low-doped, high work function cathodes, and low electrical biases.

Chapter 8 – Conclusion

8.1 Summary and Future Work

In conclusion, this thesis presents a model for charge-carrier transport in amorphous organic semiconductors. The model (Chapter 5) derives an expression for the charge-carrier mobility and the current-voltage relation. It unifies the material, temperature, electric field, and charge density dependences of transport and is compared to experimental measurements. In Chapter 7, the current-voltage characteristics for single-layer organic devices with different cathodes are found to be well-described by the percolation-based bulk conduction model with a cathode-dependent mobile charge distribution arising from diffusion of cathode metal atoms doping the organic semiconductor layer. However, higher work function metals like silver (Ag) and aluminum (Al) cannot be fully explained by bulk conduction alone, and it is hypothesized that injection mechanisms become more significant for organic diodes employing these cathodes.

Possible future work for this research is to explore the concept of the field-dependent effective temperature, such as how it adds to the actual temperature in different materials and to find an accurate description in the regime where this current effective temperature model fails, at high fields and low temperatures. In addition, it will be useful to have a model for the injection mechanism that can be combined with the bulk conduction theory that will give an overall and general model for transport spanning between these two rate-limiting cases. Future research will hopefully provide a complete understanding of charge-carrier transport enabling predictive models for the electrical behavior of arbitrary organic semiconductor device architectures.

References

1 M. A. Baldo, *6.729 Molecular Electronics Course Notes* (Massachusetts Institute of Technology, 2004).

2 H. Bässler, Philosophical Magazine B **50**, 347 (1984).

3 H. Bässler, Physica Status Solidi B **175**, 15 (1993).

4 E. A. Silinsh and V. Capek, *Organic Molecular Crystals: Interaction, Localization, and Transport Phenomena* (AIP Press, New York, 1994).

5 S. M. Sze, *Physics of Semiconductor Devices* (John Wiley & sons, New York, 1981).

6 I. D. Parker, Journal of Applied Physics **75**, 1656 (1994).

7 V. I. Arkhipov, E. V. Emelianova, Y. H. Tak, et al., Journal of Applied Physics **84**, 848 (1998).

8 Y. N. Gartstein and E. M. Conwell, Chemical Physics Letters **255**, 93 (1996).

9 U. Wolf, V. I. Arkhipov, and H. Bässler, Physical Review B **59**, 7507 (1999).

10 M. A. Lampert and P. Mark, *Current Injection in Solids* (Academic Press, NY, 1970).

11 P. E. Burrows, Z. Shen, V. Bulovic, et al., Journal of Applied Physics **79**, 7991 (1996).

12 H. J. Snaith and M. Grätzel, Physical Review Letters **98**, 177402 (2007).

13 A. Miller and E. Abrahams, Physical Review **120**, 745 (1960).

14 B. Kramer and A. MacKinnon, Reports on Progress in Physics **56**, 1469 (1993).

15 H. Overhof, Journal of Non-Crystalline Solids **227-230**, 15 (1998).

16 N. F. Mott, Journal of Non-Crystalline Solids **1**, 1 (1968).

17 P. W. Anderson, Physical Review **109**, 1492 (1958).

18 R. H. Young, Philosophical Magazine B **72**, 435 (1995).

19 D. H. Dunlap, P. E. Parris, and V. M. Kenkre, Physical Review Letters **77**, 542 (1996).

20 A. Dieckmann, H. Bässler, and P. M. Borsenberger, Journal of Chemical Physics **99**, 8136 (1993).

21 S. V. Novikov, D. H. Dunlap, V. M. Kenkre, et al., Physical Review Letters **81**, 4472 (1998).

22 S. V. Novikov and A. V. Vannikov, Journal of Physical Chemistry **99**, 14573 (1995).

23 M. Pope and C. Swenberg, *Electronic Processes in Organic Crystals* (Oxford University Press, Oxford, 1982).

24 T. Holstein, Annals of Physics **8**, 325 (1959).

25 T. Holstein, Annals of Physics **8**, 343 (1959).

26 L. B. Schein, Philosophical Magazine B **65**, 795 (1992).

27 R. A. Marcus, Journal of Chemical Physics **24**, 966 (1955).

28 G. L. Closs and J. R. Miller, Science **240**, 440 (1988).

29 C. S. Hung and J. R. Gliessman, Physical Review **79**, 726 (1950).

30 N. F. Mott, Canadian Journal of Physics **34**, 1356 (1956).

31 E. M. Conwell, Physical Review **103**, 51 (1956).

32 B. Movaghar and W. Schirmacher, Journal of Physics C: Solid State Physics **14**, 859 (1981).

[33] M. C. J. M. Vissenberg, (University of Leiden, 1999), Vol. PhD.
[34] V. Ambegaokar, B. I. Halperin, and J. S. Langer, Physical Review B **4**, 2612 (1971).
[35] S. Kirkpatrick, Reviews of Modern Physics **45**, 574 (1973).
[36] H. Scher and E. W. Montroll, Physical Review B **12**, 2455 (1975).
[37] D. Emin, Physica Status Solidi B **205**, 69 (1998).
[38] M. Sahimi, *Applications of Percolation Theory* (Taylor & Francis, London, 1994).
[39] N. F. Mott, Philosophical Magazine **19**, 835 (1969).
[40] A. H. Clark, Physical Review **154**, 750 (1967).
[41] P. A. Walley and A. K. Jonscher, Thin Solid Films **1**, 367 (1968).
[42] P. A. Walley, Thin Solid Films **2**, 327 (1968).
[43] A. H. Clark, Journal of Non-Crystalline Solids **2**, 52 (1970).
[44] K. L. Chopra and S. K. Bahl, Physical Review B **1**, 2545 (1970).
[45] B. I. Shklovskii and A. L. Efros, Soviet Physics - JETP **33**, 468 (1971).
[46] M. Pollak, Journal of Non-Crystalline Solids **11**, 1 (1972).
[47] M. C. J. M. Vissenberg and M. Matters, Physical Review B **57**, 12964 (1998).
[48] G. E. Pike and C. H. Seager, Physical Review B **10**, 1421 (1974).
[49] M. Grünewald, P. Thomas, and D. Würtz, Physica Status Solidi B **94**, K1 (1979).
[50] M. Grünewald and P. Thomas, Physica Status Solidi B **94**, 125 (1979).
[51] F. R. Shapiro and D. Adler, Journal of Non-Crystalline Solids **74**, 189 (1985).
[52] D. Monroe, Physical Review Letters **54**, 146 (1985).
[53] S. D. Baranovskii, P. Thomas, and G. J. Adriaenssens, Journal of Non-Crystalline Solids **190**, 283 (1995).
[54] S. D. Baranovskii, T. Faber, F. Hensel, et al., Journal of Physics: Condensed Matter **9**, 2699 (1997).
[55] S. D. Baranovskii, H. Cordes, F. Hensel, et al., Physical Review B **62**, 7934 (2000).
[56] S. D. Baranovskii, O. Rubel, and P. Thomas, Journal of Non-Crystalline Solids **352**, 1644 (2006).
[57] O. Rubel, S. D. Baranovskii, P. Thomas, et al., Physical Review B **69**, 014206 (2004).
[58] M. Pope, H. P. Kallmann, and P. Magnante, Journal of Chemical Physics **38**, 2042 (1963).
[59] W. Helfrich and W. G. Schneider, Physical Review Letters **14**, 229 (1965).
[60] N. Karl, Synthetic Metals **133-134**, 649 (2003).
[61] W. Shockley and R. C. Prim, Physical Review **90**, 753 (1953).
[62] G. C. Dacey, Physical Review **90**, 759 (1953).
[63] A. Rose and R. W. Smith, Physical Review **97**, 1531 (1955).
[64] A. Rose, Physical Review **97**, 1538 (1955).
[65] M. A. Lampert, Physical Review **103**, 1648 (1956).
[66] N. F. Mott and R. W. Gurney, *Electronic Processes in Ionic Crystals* (Clarendon Press, Oxford, 1940).
[67] A. Rose, Physical Review **97**, 322 (1955).
[68] H. Bässler, G. Herrmann, N. Riehl, et al., Journal of Physics and Chemistry of Solids **30**, 1579 (1969).
[69] J. Steiger, R. Schmechel, and H. von Seggern, Synthetic Metals **129**, 1 (2002).

[70] M. van der Auweraer, F. C. de Schryver, P. M. Borsenberger, et al., Advanced Materials **6**, 199 (1994).
[71] B. Hartenstein, H. Bässler, S. Heun, et al., Chemical Physics **191**, 321 (1995).
[72] L. B. Schein, A. Rosenberg, and S. L. Rice, Journal of Applied Physics **60**, 4287 (1986).
[73] M. Abkowitz, H. Bässler, and M. Stolka, Philosophical Magazine B **63**, 201 (1991).
[74] L. Pautmeier, R. Richert, and H. Bässler, Synthetic Metals **37**, 271 (1990).
[75] P. W. M. Blom, M. J. M. d. Jong, and M. G. v. Munster, Physical Review B **55**, 656 (1997).
[76] I. H. Campbell, D. L. Smith, C. J. Neef, et al., Applied Physics Letters **74**, 2809 (1999).
[77] H. C. F. Martens, P. W. M. Blom, and H. F. M. Schoo, Physical Review B **61**, 7489 (2000).
[78] L. B. Schein, A. Peled, and D. Glatz, Journal of Applied Physics **66**, 686 (1989).
[79] W. Brütting, S. Berleb, and A. G. Mückl, Organic Electronics **2**, 1 (2001).
[80] B. N. Limketkai, P. Jadhav, and M. A. Baldo, Physical Review B **75**, 113203 (2007).
[81] W. D. Gill, Journal of Applied Physics **43**, 5033 (1972).
[82] G. Pfister, Physical Review B **16**, 3676 (1977).
[83] L. Onsager, Physical Review **54**, 554 (1938).
[84] S. V. Novikov and A. V. Vannikov, Journal of Physics: Condensed Matter **6**, 10519 (1994).
[85] S. V. Novikov and A. V. Vannikov, Chemical Physics Letters **182**, 598 (1991).
[86] S. V. Novikov and A. V. Vannikov, Chemical Physics **169**, 21 (1993).
[87] B. Movaghar, A. Yelon, and M. Meunier, Chemical Physics **146**, 389 (1990).
[88] P. M. Borsenberger, L. Pautmeier, and H. Bässler, Journal of Chemical Physics **94**, 5447 (1991).
[89] P. M. Borsenberger and H. Bässler, Physica Status Solidi B **170**, 291 (1992).
[90] Y. N. Gartstein and E. M. Conwell, Chemical Physics Letters **245**, 351 (1995).
[91] Z. G. Yu, D. L. Smith, A. Saxena, et al., Physical Review Letters **84**, 721 (2000).
[92] J. M. Sin and Z. G. Soos, Philosophical Magazine **83**, 901 (2003).
[93] Z. G. Yu, D. L. Smith, A. Saxena, et al., Physical Review B **63**, 085202 (2001).
[94] D. Emin, C. H. Seager, and R. K. Quinn, Physical Review Letters **28**, 813 (1972).
[95] V. M. Kenkre and D. H. Dunlap, Philosophical Magazine B **65**, 831 (1992).
[96] D. H. Dunlap and V. M. Kenkre, Chemical Physics **178**, 67 (1993).
[97] K. Seki and M. Tachiya, Physical Review B **65**, 014305 (2001).
[98] Y. N. Gartstein and E. M. Conwell, Chemical Physics Letters **217**, 41 (1994).
[99] Z. G. Soos, S. Bao, J. M. Sin, et al., Chemical Physics Letters **319**, 631 (2000).
[100] P. E. Parris, V. M. Kenkre, and D. D.H., Physical Review Letters **87**, 126601 (2001).
[101] C. Tanase, E. J. Meijer, P. W. M. Blom, et al., Physical Review Letters **91**, 216601 (2003).
[102] C. M. Ramsdale and N. C. Greenham, Advanced Materials **14**, 212 (2002).
[103] A. R. Brown, C. P. Jarrett, D. M. de Leeuw, et al., Synthetic Metals **88**, 37 (1997).

[104] V. I. Arkhipov, E. V. Emelianova, P. Heremans, et al., Physical Review B **72**, 235202 (2005).

[105] R. Coehoorn, W. F. Pasveer, P. A. Bobbert, et al., Physical Review B **72**, 155206 (2005).

[106] W. F. Pasveer, J. Cottaar, C. Tanase, et al., Physical Review Letters **94**, 206601 (2005).

[107] V. I. Arkhipov, P. Heremans, E. V. Emelianova, et al., Journal of Physics: Condensed Matter **14**, 9899 (2002).

[108] H. C. F. Martens, I. N. Hulea, I. Romijn, et al., Physical Review B **67**, 121203(R) (2003).

[109] Y. Roichman and N. Tessler, Synthetic Metals **135**, 443 (2003).

[110] Y. Roichman, Y. Preezant, and N. Tessler, Physica Status Solidi A **201**, 1246 (2004).

[111] H. Shimotani, G. Diguet, and Y. Iwasa, Applied Physics Letters **86**, 022104 (2005).

[112] X. Jiang, Y. Harima, K. Yamashita, et al., Chemical Physics Letters **364**, 616 (2002).

[113] V. I. Arkhipov, E. V. Emelianova, and G. J. Adriaenssens, Physical Review B **63**, 081202(R) (2001).

[114] V. I. Arkhipov, P. Heremans, E. V. Emelianova, et al., Physical Review B **71**, 045214 (2005).

[115] W. Weise, T. Keith, N. von Malm, et al., Journal of Applied Physics **98**, 043511 (2005).

[116] R. G. Kepler, P. M. Beeson, S. J. Jakobs, et al., Applied Physics Letters **66**, 3618 (1995).

[117] B. J. Chen, W. Y. Lai, Z. Q. Gao, et al., Applied Physics Letters **75**, 4010 (1999).

[118] A. G. Mückl, S. Berleb, W. Brütting, et al., Synthetic Metals **111-112**, 91 (2000).

[119] I. H. Campbell, D. L. Smith, C. J. Neef, et al., Applied Physics Letters **75**, 841 (1999).

[120] P. N. Murgatroyd, Journal of Physics D: Applied Physics **3**, 151 (1970).

[121] M. Abkowitz, J. S. Facci, and M. Stolka, Chemical Physics **177**, 783 (1993).

[122] A. J. Campbell, M. S. Weaver, D. G. Lidzey, et al., Journal of Applied Physics **84**, 6737 (1998).

[123] C. Tanase, P. W. M. Blom, and D. M. de Leeuw, Physical Review B **70**, 193202 (2004).

[124] B. Ramachandhran, H. G. A. Huizing, and R. Coehoorn, Physical Review B **73**, 233306 (2006).

[125] L. Li, G. Meller, and H. Kosina, Solid-State Electronics **51**, 445 (2007).

[126] O. Tal, Y. Rosenwaks, Y. Preezant, et al., Physical Review Letters **95**, 256405 (2005).

[127] B. I. Shklovskii, Soviet Physics Semiconductor **6**, 1964 (1973).

[128] I. H. Campbell and D. L. Smith, Applied Physics Letters **74**, 561 (1999).

[129] M. Grünewald and B. Movaghar, Journal of Physics C: Condensed Matter **1**, 2521 (1989).

[130] S. Marianer and B. I. Shklovskii, Physical Review B **46**, 13100 (1992).

[131] S. D. Baranovskii, B. Cleve, R. Hess, et al., Journal of Non-Crystalline Solids **164-166**, 437 (1993).
[132] B. Cleve, B. Hartenstein, S. D. Baranovskii, et al., Physical Review B **51**, 16705 (1995).
[133] V. I. Arkhipov, E. V. Emelianova, and G. J. Adriaenssens, Journal of Applied Physics **93**, 6150 (2003).
[134] V. I. Arkhipov, U. Wolf, and H. Bässler, Physical Review B **59**, 7514 (1999).
[135] M. A. Abkowitz, H. A. Mizes, and J. S. Facci, Applied Physics Letters **66**, 1288 (1995).
[136] E. M. Conwell and M. W. Wu, Applied Physics Letters **70**, 1867 (1997).
[137] D. F. Blossey, Physical Review B **9**, 5183 (1974).
[138] S. Barth, U. Wolf, H. Bässler, et al., Physical Review B **60**, 8791 (1999).
[139] M. A. Baldo and S. R. Forrest, Physical Review B **64**, 085201 (2001).
[140] B. N. Limketkai and M. A. Baldo, Physical Review B **71**, 085207 (2005).
[141] M. Abkowitz, J. S. Facci, and J. Rehm, Journal of Applied Physics **83**, 2670 (1998).
[142] I. H. Campbell, P. S. Davids, D. L. Smith, et al., Applied Physics Letters **72**, 1863 (1998).
[143] C. Shen, A. Kahn, and J. Schwartz, Journal of Applied Physics **89**, 449 (2001).
[144] N. Koch, A. Elschner, J. Schwartz, et al., Applied Physics Letters **82**, 2281 (2003).
[145] T. A. Beierlein, W. Brütting, H. Riel, et al., Synthetic Metals **111-112**, 295 (2000).
[146] J. C. Scott, Journal of Vacuum Science and Technology A **21**, 521 (2003).
[147] H. Ishii, K. Sugiyama, E. Ito, et al., Advanced Materials **11**, 605 (1999).
[148] M. G. Mason, C. W. Tang, L.-S. Hung, et al., Journal of Applied Physics **89**, 2756 (2001).
[149] C. Shen, I. G. Hill, and A. Kahn, Advanced Materials **11**, 1523 (1999).
[150] C. Shen, I. G. Hill, A. Khan, et al., Journal of the American Chemical Society **122**, 5391 (2000).
[151] Y.-P. Zhao, G.-C. Wang, T.-M. Lu, et al., Physical Review B **60**, 9157 (1999).
[152] J. D. Jackson, *Classical Electrodynamics* (John Wiley & Sons, New York, 1975).
[153] T. S. Rahman and A. A. Maradudin, Physical Review B **21**, 504 (1980).
[154] C. W. Tang and S. A. VanSlyke, Applied Physics Letters **51**, 913 (1987).
[155] H. Nakada, S. Kawami, K. Nagayama, et al., Polymer Preprints Japan **43**, 2450 (1994).
[156] H. Kanai, S. Ichinosawa, and Y. Sato, Synthetic Metals **91**, 195 (1997).
[157] J. Kido, C. Ohtaki, K. Hongawa, et al., Japanese Journal of Applied Physics **32**, L917 (1993).
[158] C. W. Tang, Applied Physics Letters **48**, 183 (1985).
[159] I. G. Hill and A. Kahn, Journal of Applied Physics **86**, 4515 (1999).
[160] L. S. Hung, C. W. Tang, and M. G. Mason, Applied Physics Letters **70**, 152 (1997).
[161] A. Ioannidis, E. Forsythe, Y. Gao, et al., Applied Physics Letters **72**, 3038 (1998).
[162] J. C. Scott and G. G. Malliaras, Chemical Physics Letters **299**, 115 (1999).
[163] Y. Shen, M. W. Klein, D. B. Jacobs, et al., Physical Review Letters **86**, 3867 (2001).
[164] S. Berleb, A. G. Mückl, W. Brütting, et al., Synthetic Metals **111-112**, 341 (2000).

[165] W. Brütting, S. Berleb, and A. G. Mückl, Synthetic Metals **122**, 99 (2001).
[166] G. G. Malliaras, J. R. Salem, P. J. Brock, et al., Physical Review B **58**, R13411 (1998).
[167] G. G. Malliaras, J. R. Salem, P. J. Brock, et al., Journal of Applied Physics **84**, 1583 (1998).
[168] S. Berleb, W. Brütting, and G. Paasch, Organic Electronics **1**, 41 (2000).
[169] S. Berleb, W. Brütting, and G. Paasch, Synthetic Metals **122**, 37 (2001).
[170] W. Brütting, H. Riel, T. Beierlein, et al., Journal of Applied Physics **89**, 1704 (2001).
[171] D. Y. Kondakov, J. R. Sandifer, C. W. Tang, et al., Journal of Applied Physics **93**, 1108 (2003).
[172] M. Matsumura, A. Ito, and Y. Miyamae, Applied Physics Letters **75**, 1042 (1999).
[173] F. Rohlfing, T. Yamada, and T. Tsutsui, Journal of Applied Physics **86**, 4978 (1999).
[174] T. Tsutsui, H. Tokuhisa, and M. Era, Proceedings of SPIE **3281**, 230 (1998).
[175] S. Naka, H. Okada, H. Onnagawa, et al., Japanese Journal of Applied Physics **38**, L1252 (1999).
[176] G. Parthasarthy, C. Shen, A. Kahn, et al., Journal of Applied Physics **89**, 4986 (2001).
[177] S. T. Lee, Z. Q. Gao, and L. S. Hung, Applied Physics Letters **75**, 1404 (1999).
[178] J. Shen, D. Wang, E. Langlois, et al., Synthetic Metals **111**, 233 (2000).
[179] D. Y. Kondakov, Journal of Applied Physics **99**, 024901 (2006).